8-2012

Experimental Studies of Vertical Mixing in an Open Channel Raceway for Algae Biofuel Production

Ram Sudheer Voleti
Utah State University

EXPERIMENTAL STUDIES OF VERTICAL MIXING IN AN OPEN CHANNEL

RACEWAY FOR ALGAE BIOFUEL PRODUCTION

by

Ram Sudheer Voleti

A thesis submitted in partial fulfillment
of the requirements for the degree

of

MASTER OF SCIENCE

in

Mechanical Engineering

Approved:

_____   _____
Dr. Byard D. Wood   Dr. Clair J. Batty
Major Professor   Committee Member

_____   _____
Dr. Leijun Li   Dr. Barton L. Smith
Committee Member   Committee Member

_____
Dr. Mark R. McLellan
Vice President for Research and
Dean of the School of Graduate Studies

UTAH STATE UNIVERSITY
Logan, Utah

2012

ABSTRACT

Experimental Studies of Vertical Mixing in an Open Channel

Raceway for Algae Biofuel Production

by

Ram Sudheer Voleti, Master of Science

Utah State University, 2012

Major Professor: Dr. Byard D. Wood
Department: Mechanical and Aerospace Engineering

Turbulent mixing plays an important role in the distribution of sunlight, carbon dioxide, and nutrients for algae in the raceway ponds. For large-scale raceway ponds the choice of mixing technology still needs to be evaluated in order to prevent algae sedimentation and to enhance light utilization efficiency. In open ponds, mixing the algae culture is of great significance in terms of input energy costs and particularly productivity. A very small amount of research has been performed previously using different vortex generators in the algal raceway ponds, but the quantification of mixing depth relationships is not defined well. By accepting the premise from the literature review that mixing increases algal production, delta wings were selected to study mixing characteristics in the raceway. The main objective of this research was to study algae-raceway hydrodynamics with an emphasis on increasing vertical mixing.

A clear acrylic raceway was designed and constructed for flow visualization studies. Experimental investigations were performed to quantify the vertical mixing with and without delta wings in a lab-scale raceway at approximately the same power input to the paddle wheel. Velocity vector profiles and turbulence parameters were measured using an Acoustic Doppler Velocimeter (ADV) at various locations along the entire length of the raceway. The results indicated that the addition of delta wings increases the vertical mixing intensity or circulation of algae cells over the raceway depth. Vortices were observed in the raceway up to a distance of around 3 m downstream of the delta wing. This sort of systematic vertical mixing plays an important role to produce the flashing light effect (light-dark cycles) on algae mass culture. In addition, turbulence dissipation rates were evaluated to compare them with the published literature and to estimate the microscales using the Kolmogorov hypothesis. Also, an energy model was developed to operate the paddlewheel-driven raceway with the delta wing.

(123 pages)

PUBLIC ABSTRACT

Experimental Studies of Vertical Mixing in an Open Channel

Raceway for Algae Biofuel Production

by

Ram Sudheer Voleti, Master of Science

Utah State University, 2012

Major Professor: Dr. Byard D. Wood
Department: Mechanical and Aerospace Engineering

The USU BioEnergy Center has been successful in developing algae feedstocks for renewable biofuels and bioproducts. The concept is to utilize and maximize algae feedstocks for liquid transportation fuels, biomass for burning and digestion, and high value co-products. It is theorized that increasing the mixing in open and closed algal production systems improves the productivity of the algae culture. A raceway cultivation system was chosen to examine the phenomena of mixing. Vertical mixing will provide more uniform exposure to sunlight for all of the algae in the raceway. The main focus of this research was to increase vertical mixing. Delta wing vortex generator was selected as a viable source of creating vertical mixing. A series of experiments were carried out to study the mixing characteristics in a lab-scale raceway that was designed specifically for raceway hydrodynamics. Finally, the results were discussed and appropriate conclusions drawn.

ACKNOWLEDGMENTS

I would like to express my highest regards and gratitude to my major professor and supervisor, Dr. Byard Wood, who continues to provide encouragement, guidance, support, and advice. I will be forever indebted to him for believing in me right from the beginning of my career as a research assistant at USU. I am thankful to Dr. Barton Smith for his class lectures, help, and input during the progress of my research. I would like to thank my committee members, Dr. Clair Batty, Dr. Leijun Li, and Dr. Barton Smith, for extending their service and support.

I am thankful to all the current and past Raceway Hydraulics Research Group members, including Aaron, Blake, Dan, Garrett, Jayson, Justin, and Pete, for the support given by them during my research. Also, I would like to thank all the people who were involved directly or indirectly and helped in the construction of the clear acrylic raceway at USU Algae Energy Systems lab. I feel grateful to the USU BioEnergy Center and the US Department of Energy (Grant Number DE-EE0003114) for all the financial support.

Finally, I am thankful to my wonderful family, teachers, relatives, and friends for their love and support, and for all the confidence and trust they put in me.

Ram Sudheer Voleti

CONTENTS

LIST OF TABLES

LIST OF FIGURES

ACRONYMS

ADV	Acoustic Doppler Velocimeter
CCD	Charge-Coupled Device
CFD	Computational Fluid Dynamics
COR	Correlation Coefficient
LDV	Laser Doppler Velocimetry
Nd: YAG	Neodymium-doped Yttrium Aluminum Garnet
PIV	Particle Image Velocimetry
PTV	Particle Tracking Velocimetry
RMS	Root Mean Square
SNR	Signal-to-Noise Ratio
TI	Turbulence Intensity
TKE	Turbulence Kinetic Energy
USU	Utah State University
VMI	Vertical Mixing Index

NOMENCLATURE

A	Cross-sectional area of flow, [m^2]
b	Width of a channel, [m]
b_A	Standard accuracy of the measured velocity, [m/s]
b_R	Standard resolution of the ADV velocity, [m/s]
$b_{\overline{U}}$	Systematic standard uncertainty of the mean velocity, [m/s]
C	Speed of sound, [m/s]
C_D	Drag coefficient
d	Water depth, [m]
D_h	Hydraulic diameter of a channel, [m]
$E(k)$	Wavenumber spectral density function
F_D	Change in received frequency (Doppler shift), [Hz]
F_S	Frequency of transmitted sound, [Hz]
f	Frequency, [Hz]
f_{max}	Maximum flow frequency, [Hz]
f_s	Sampling frequency, [Hz]
g	Acceleration due to gravity, [m/s^2]
h	Depth of a channel, [m]
h_K	Kinetic head loss, [m]
h_f	Frictional head loss, [m]
h_L	Total head loss, [m]

K	Kinetic loss coefficient for 180° bends
k	Wavenumber, [rad/m]
L	Length of a channel, [m]
l	Integral length scale, [m]
N	Number of samples
n	Roughness coefficient or factor (Manning's n)
P	Wetted perimeter of flow cross-section, [m]
p	Grid point
Q	Volumetric flow rate, [m^3/s]
R	Hydraulic radius of a channel, [m]
Re	Reynolds number
$S(f)$	Power spectral density, [cm^2/s^2/Hz]
S_U	Standard deviation of the mean velocity, [m/s]
$S_{\bar{U}}$	Random standard uncertainty of the mean velocity, [m/s]
s	Number of grid points
u, v, w	Instantaneous velocity in streamwise, lateral and vertical directions, [m/s]
u', v', w'	Instantaneous velocity fluctuation in streamwise, lateral and vertical directions, [m/s]
U, V, W	Mean velocity in streamwise, lateral and vertical directions, [m/s]
U_A	Average velocity of the streamwise velocity at a section, [m/s]
$U_{\bar{U}}$	Expanded uncertainty of the mean velocity, [m/s]
V_{avg}	Average velocity in a channel, [m/s]

V_{mag}	Magnitude of the resultant of the mean velocity components, [m/s]
V_p	In-plane velocity, [m/s]
V'	Magnitude of the resultant of the RMS values, [m/s]
x, y, z	Local coordinate system in streamwise, lateral and vertical directions, [m]
α	Angle of attack of the delta wing, [deg]
β	Kolmogorov constant
ε	Turbulence dissipation rate, [m²/s³]
η	Kolmogorov length scale or microscale, [μm]
γ	Rate-of-strain, [rad/s]
μ	Dynamic viscosity, [Pa.s]
ϑ	Kinematic viscosity, [m²/s]
ρ	Fluid density, [kg/m³]
τ	Shear stress, [N/m²]

CHAPTER 1

INTRODUCTION

Biofuels produced from vegetable oils and animal fats will never be able to replace fossil-based transport fuels, but algae-derived biofuels have the potential to displace liquid transport fuels derived from petroleum [1]. Microalgae grow in aqueous media and produce high energy output with minimum land use requirements. Microalgae (henceforth referred to as algae) as a source of biomass for liquid fuels production have a number of advantages like waste water treatment, reducing carbon dioxide emissions, etc. All of these factors combine to indicate that algae have the potential to be a viable feedstock for a full range of fuels including gasoline, biodiesel, and jet fuel.

Algae are photosynthetic microorganisms that convert sunlight, water, carbon dioxide, and supplemented nutrients to algal biomass. Turbulent mixing is necessary for uniform distribution of sunlight, carbon dioxide, and nutrients for algae cells. The advantages of keeping the algal suspension in movement are numerous. The continuous mixing prevents settling of the algal biomass and keeps the nutrients in active contact with the algal cell surface, and to a more effective utilization of incident light. Mixing of algae is also essential to prevent thermal stratification [2]. The extent of turbulence in the culture affects the light−dark cycles to which each algal cell is exposed and has a great effect on the growth rate in light limited systems.

Algae are grown in either open or closed photobioreactors. Raceway ponds have been the most common choice for outdoor algal production because they cost less to

build and operate although they have low algal productivity compared to engineered photobioreactors. Raceway ponds are generally mixed with paddle wheels and are the easiest to maintain. In raceway ponds, mixing can be achieved by increasing the liquid circulation velocity, but requires additional energy input for the paddle wheel. Thus, one of the challenges in a raceway pond is to maintain adequate mixing and circulation velocity with minimal energy input [3]. One of the major purposes for algae pond mixing is to move algae in and out of the light zone, thus improving distribution of light to the cells, for optimal photosynthesis. Hence, vertical mixing in the ponds is of primary interest. Usually raceway ponds are not deeper than 15−30 cm because of the need to keep the algae exposed to sunlight and the limited depth to which sunlight can penetrate the pond water (see Figure 1-1). Optimal pond mixing has been shown to be between 15 and 30 cm/s of channel velocity [4-6].
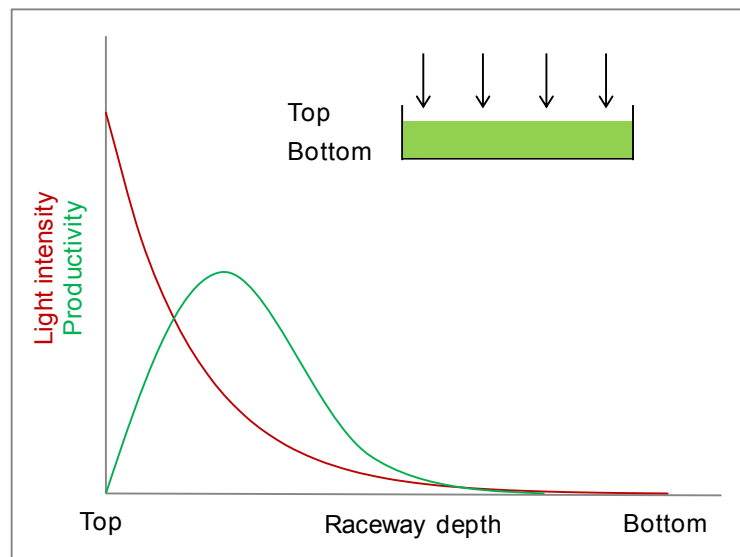
Figure 1-1.   A theoretical representation of algae productivity against light intensity in algal production systems

Researchers tried to increase cell density by increasing the raceway pond depth to 60 cm [4]. This resulted in lower cell densities than predicted, and the depth of the culture was again reduced to 30 cm. The flow rates and the depth of the raceway affect the distribution of sunlight, carbon dioxide, and nutrients, and these factors should be regulated to maintain algal suspension and mixing. For large-scale raceway ponds the choice of the mixing technology still needs to be evaluated. Vortex generating devices like air foils, cylinders, delta wings, etc., can be installed in the raceway pond to increase mixing. Vortices are produced in the raceway pond due to the pressure differential created as water flows over and under the devices. The system of vortices with rotational axes parallel to the direction of flow produces the sort of systematic vertical mixing necessary to produce the flashing light effect [7]. Previous research has shown that increasing the mixing in open and closed algal production systems improves the productivity of the algae culture. The main goal in this algal-based biofuel research is to increase vertical mixing using delta wings at the same energy consumption thereby anticipating increased algal production rates. However, the productivity also depends on the algae strains and their sensitivity to turbulence.

The aim of this research is to explore this problem more in depth and to try to quantify the vertical mixing in a raceway pond for algae biofuel production (to link biology to hydrodynamics), in view of a potential application at a larger outdoor scale. The main body of this thesis contains a list of specific objectives, an extensive literature review, approach and procedure, and a summary of the results of the research work performed.

CHAPTER 2

OBJECTIVES

The main objective of this work is to conduct experiments and characterize the fluid flow with and without delta wings in an open channel raceway for algae biofuel production. This main objective is broken down into the following specific objectives:

- Perform a literature review to study the effects of turbulent mixing on algae growth

- Design and construct an open channel acrylic raceway to visualize the flow

- Perform a quantitative flow visualization using an Acoustic Doppler Velocimeter (ADV). Measure the velocity vector profiles and turbulence parameters to aid in the understanding of vertical mixing at various sections of the raceway

- Compare the ADV data with Particle Image Velocimetry (PIV) data obtained for the raceway

- Develop an energy model to circulate the water in paddlewheel-driven raceways

- Suggest appropriate recommendations for the use of delta wings in enhancing the vertical mixing

CHAPTER 3

LITERATURE REVIEW

The literature review in this chapter focuses on the methods of turbulent mixing generation and its effect on algae sensitivity and productivity.

3.1. Effects of Turbulence on Algae Growth

Algae used for biofuel production are usually in the size range from 10 to 50 μm. At this small-scale, the direct effects of water turbulence on algae are of potential algal research importance. Turbulence has two major influences on algae, *i.e.* it facilitates fluctuating light regimes and decreases the boundary layer which results in an increased exchange rate between the algae and its environment [8]. Several studies have demonstrated the impact of turbulence on algae growth and sensitivity. Some of those findings are presented in this review.

Grobbelaar [8] in 1991 studied the influence of light/dark cycles in cultures using a photosynthetic chamber and concluded that mixing enhancement will increase productivity, but the synergistic effect pronounces within a certain range of turbulences. Conflicting results have been reported in the literature for *phytoplankton* cultures, where on the one hand it is suggested that turbulence enhances productivity, whilst on the other hand no evidence of such stimulatory effect could be found. Ogbonna et al. [9] in 1995 investigated the effects of cell movement on algal productivity by random mixing between the surface and bottom of photobioreactors using different culture depths and strains. Mixing was achieved by means of gas sparging through glass ball filters inserted

into the reactors and by means of magnetic stirrers. Movement of *Chlorella* cells between the surface and bottom of the reactor resulted in increased productivity for shallow reactor and decreased productivity for deep reactor. Higher cell growth and productivity were observed for *Spirulina* cells in the deep reactor. They concluded that reactor productivity will depend on the degree of mixing, the incident light intensity and the depth of the ponds as well as the light requirements of the algal strains. Unfortunately, many of these early theoretical and experimental studies lack the quantification of turbulence applied in many of the experiments.

Thomas and Gibson [10] in 1990 reported that various algae groups seem to have different sensitivities to growth inhibition by turbulence. The authors hypothesized on an ascending scale of inhibition of relative sensitivities to turbulence are *green algae < blue-green algae < diatoms < dinoflagellates*. They were claimed the first and discussed the turbulence flow parameters that may be most important to algal survival are the turbulence dissipation rate (ε), rate-of-strain ($\gamma \equiv (\varepsilon/\vartheta)^{1/2}$), and shear stress ($\tau \equiv \mu\gamma$). Experiments were conducted in a rotating cylinder (Couette) for a *dinoflagellate* species at different rotation speeds and the cell numbers and chlorophyll fluorescence were declined for $\varepsilon > 1.8\times10^{-5}$ m^{2}s^{-3}, $\tau > 0.002$ Nm^{-2}, $\gamma > 4.4$ rads^{-1}. The turbulence dissipation rate has been increasingly used as a meaningful scaling parameter to integrate growth rates with fluid flow motion in the algal production systems [11]. The reader is referred to an excellent amount of literature survey and experimental work on the effects of small-scale turbulence on the growth response of marine microalgae (*phytoplankton* and *dinoflagellates*) reported by Berdalet et al. [12, 13]. The authors concluded that the

growth response appears to be species-specific and dependent on the experimental design and setup used to generate small-scale turbulence.

Hondzo and Lyn [14] in 1999 conducted laboratory experiments to determine the effect of small-scale turbulence (comparable to the surface of lake turbulence) on the growth of freshwater algae *Scenedesmus quadricauda* in an oscillating grid apparatus. The only growth limiting factor in their laboratory cultures was the effect of small-scale fluid motion and all other factors were kept constant. Turbulence dissipation rates at different oscillation frequencies were estimated from the power spectra of the velocity time series data measured using Laser Doppler Velocimetry (LDV). They reported decreased algae growth rates due to high turbulence levels ($\varepsilon \sim 1.4 \times 10^{-4} \, m^2 s^{-3}$ to 1.9×10^{-5} $m^2 s^{-3}$). This study revealed the formation of aggregates of dead and living cells of algae in a turbulent flow due to high shear rates. It was hypothesized that the capacity of the algae to withstand shear varies with the type of algae.

Sullivan and Swift [15] in 2003 made a determined effort to test the paradigm that the algae growth is negatively affected by turbulence. This study differs from the past research in quantifying the three-dimensional turbulence exposure in hydrodynamic terms. Experiments were conducted in rectangular tanks where 10 species of autotrophic *dinoflagellates* were exposed to three-dimensional turbulence which resemble to ocean turbulence. Turbulence in each water column was generated by vertically oscillating a pair of rods. As the rods moved through the water, they shed turbulent vortices that interacted and decayed. Changing the vertical velocity of the rods provided different intensities of small-scale turbulence. The turbulence in each tank was quantified using

ADV. Turbulence dissipation rates were estimated using two different methods. Method 1 used the dimensional approximation ($\varepsilon \sim u'^3/l$, where u' is the root mean square velocity and l is the integral length scale of largest turbulent eddy and was set to the diameter of the stirring rod). Method 2 estimated the turbulence dissipation rate by an examination of the ADV velocities in the inertial subrange of the frequency spectrum (Method 2 was followed to calculate turbulence dissipation rates in this thesis). The species were exposed to two turbulence treatments: high turbulence ($\varepsilon \sim 10^{-4}$ m^2s^{-3}), low turbulence ($\varepsilon \sim 10^{-8}$ m^2s^{-3}), and a non turbulent (unstirred) control. It was found from their results that for high turbulence treatment levels, four species exhibited no significant change, three species were reduced, and three species were increased in the net growth rate. Two other species were also chosen for a comparison to previous research and the net growth of one species was unaffected while the other species was enhanced due to high turbulence treatment. They found contradictory results for these two species and assumed that the difference might be due to the methods under which turbulence was generated (Shakers or Couette flow).

Sullivan et al. [16] in 2003 examined another study on the effects of small-scale turbulence (much like in ocean) of two *dinoflagellates* cultures and followed the same methodology as described in previous paper [15]. They reported that the division rate of one species increased linearly as a function of the logarithmic increase in turbulence energy dissipation rate (ε) between $\sim 10^{-8}$ and 10^{-4} m^2s^{-3}. However, when ε increased to $\sim 10^{-3}$ m^2s^{-3}, division rate sharply decreased. Another species had fairly high division

rates even at high dissipation rate $\varepsilon \sim 10^{-3}$ m^{2}s^{-3}. They believed from their results that the paradigm small-scale turbulence negatively affects algae growth is too simplistic.

Warnaars and Hondzo [17] in 2006 investigated the impact of small-scale fluid motion on algae (*Selenastrum capricornutum*) growth rate and nutrient uptake subjected to a moving versus non-moving fluid. Turbulence was generated in a flow-flow reactor equipped with submersible speakers to generate low levels of energy dissipation ($\varepsilon \sim$ 1.25×10^{-6} m^{2}s^{-3} to 9.6×10^{-6} m^{2}s^{-3}). The turbulent flow was quantified by using a two-dimensional Particle Image Velocimetry (PIV) system. Turbulence dissipation rates were directly estimated from the spatial velocity gradients. It was found that the diffusive sublayer thickness surrounding a cell was decreased and facilitated nutrient uptake rates due to increase in fluid motion. The increase in growth rate was nearly 2-fold for a moving fluid with an energy dissipation rate of 10^{-7} m^{2}s^{-3}, a common turbulence found in lakes and oceans.

Experimental studies have introduced mixing using a variety of methods (Reactor tanks, Couette cylinders, stirrers, shakers, oscillating grids, bubbling, etc.) by the researchers and have reported a wide range of different conclusions as to the effect of small-scale fluid motion on algal growth rate [18]. However, it's now clear from the above studies that the significance of turbulence on algae growth is more related to the methods of turbulent generation and the type of algae species selected for the algal production. It is hypothesized that if mixing has a direct impact on algae growth enhancement than it will be a more valuable source to the algal biofuel producers in terms of areal and volume production yields.

3.2.   Mixing in Algal Raceway Ponds

Richmond and Vonshak [19] in 1978 reported a 50% increase in algae growth when doubling the flow rate in raceway from 15 to 30 cm/s. Researchers have claimed that utilization of the flashing light effect in algal ponds requires modulated mixing whereby cells are moved to the surface and bottom of the ponds at an optimum frequency. Weissman et al. in 1988 reported essentially no significant increase in algae productivity (Planktonic *Chlorella* Sp.,) as the flow speed in a 100 m^2 open raceway is changed from 1 to 30 cm/s [20].

Laws et al. [7] in 1983 emphasized the use of flashing light to enhance algal mass culture production in the simplest and least expensive means. The basic idea was that the "wing-shaped foil arrays" in the pond culture would generate vortices that would create organized pattern of vertical mixing in the ponds, expected to result in exposure of the cells to regular dark-light cycles. The mechanism used in their research to produce systematic vertical mixing in the flume is shown in Figure 3-1. The width of each foil and the gap between foils were equal to the depth of the culture. The vortex rotation rate was measured with the pivoted cylinder and an optimum angle of attack approximately 23° was found. Due to the addition of foils in 48 m^2 continuous flume culture system, a significant increase over 200% in algal productivity (3.3 g/m^2/day to 11 g/m^2/day) was reported in the experimental results. The authors claimed that this effect was attributed to a flashing light effect. They reported that the addition of foil arrays in a flume having a flow rate of 30 cm/s produced vortices with rotation rates of 0.5 to 1.0 Hz.
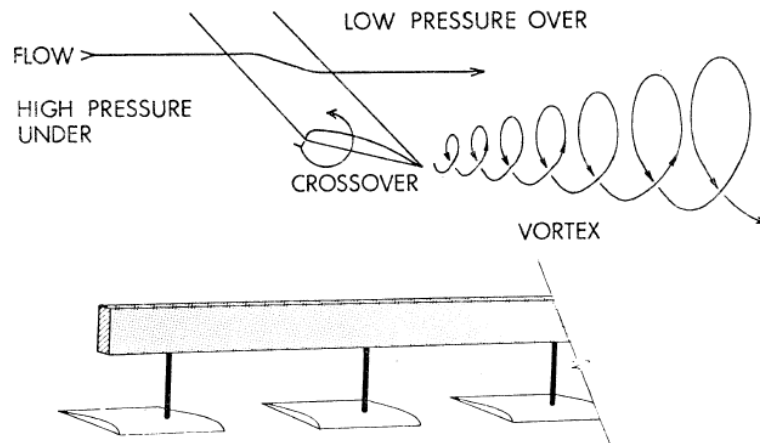
Figure 3-1.   Schematic of a single air foil indicating mechanism of vortex production (top) and positioning of individual foils in foil array (bottom) [7]

However, it is not clear if the improvement is due primarily to the light modulation experienced by the cells or whether other effects of mixing were involved.

Cheng et al. [21] in 1995 tested the use of a row of variously shaped and positioned submerged plates in the open channel subjected to shallow raceways, where cultures of marine algae were grown. This study was an extension to the previous research by Laws et al. [7] and focused on the mixing relationships and energy expenditures in an open channel flow rather than mixing versus algae production. The authors studied the mixing relationships with submerged plates (square and triangular) in the test flume (10 cm in depth) at a flow velocity of 30 cm/s measured with STREAMFLO miniature current flowmeter system. The 20° angled plates created a notably higher degree of mixing than those at 10°. The mean velocity profiles indicated that a series of test plates positioned at approximately 4.5 m intervals would be sufficient to promote the notable mixing conditions. They reported that the mean drag force on the

plates (0.0414 to 0.2082 N/plate) was relatively insignificant regardless of the plate shape or angles of attack. However, they were not able to study the fluctuating velocity, turbulence intensity, and vortices in the test flume due to lack of instrumentation and equipment.

Based upon this literature review, it is clear that there is a very limited amount of research performed on the quantification of turbulent mixing in an algal raceway pond. To the author's knowledge, only two research papers [7, 21] have used different vortex generators to create mixing in application for the algal raceway ponds. However, knowledge of the effects of vertical mixing is necessary in order to determine the hydraulic benefits of installing and operating mixing systems in algal raceway ponds. Based upon published research in the heat transfer enhancement studies, triangular plates are selected for this experimental research as most viable means of creating systematic longitudinal streamwise vortices in the algal raceway pond.

In this research, the principal objective is to quantify the vertical mixing with and without delta wings in the raceway and to compare the obtained results with the published literature. Finally, from the literature review and the lessons learned, it is hypothesized that two turbulent effects play a role in the mixing of algae:

1. Large-scale eddies move the algae cells between the surface and bottom of algal raceway pond thereby increasing light utilization efficiency, and

2. Small-scale fluid motion or small-scale eddies effect the exchange rate between the algae cells and its environment (carbon dioxide and nutrients).

CHAPTER 4

APPROACH AND PROCEDURE

The following sections provide an approach and procedure to meet the research objectives.

4.1.   Experimental Setup

A scaled model clear acrylic raceway was designed and constructed at USU Algae Energy Systems lab for flow visualization studies. The test flume cross-section is rectangular in shape with dimensions of 6.1 m in length, 0.44 m in width (width of a single channel), and 0.61 m in depth. An image of the experimental raceway setup and the detailed dimensions are shown in Figure 4-1 and Figure 4-2.
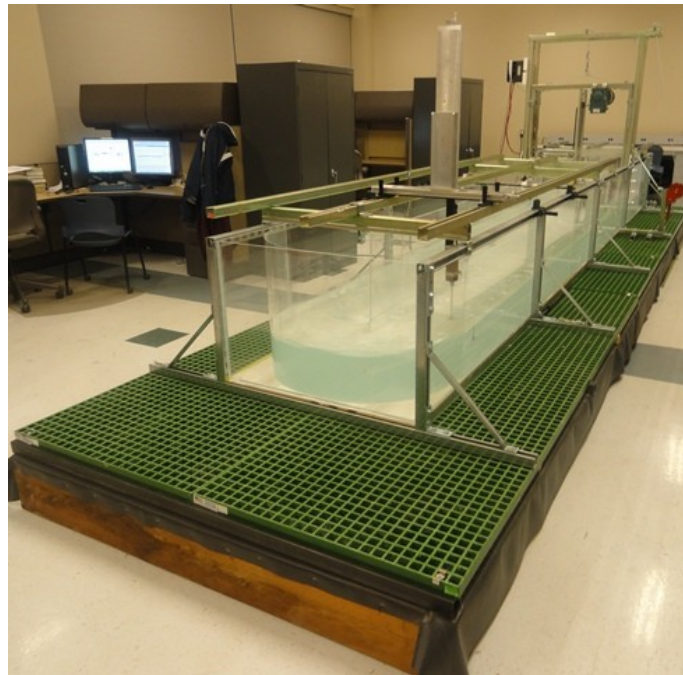
Figure 4-1.   Schematic view of the lab-scale raceway used for the experiments
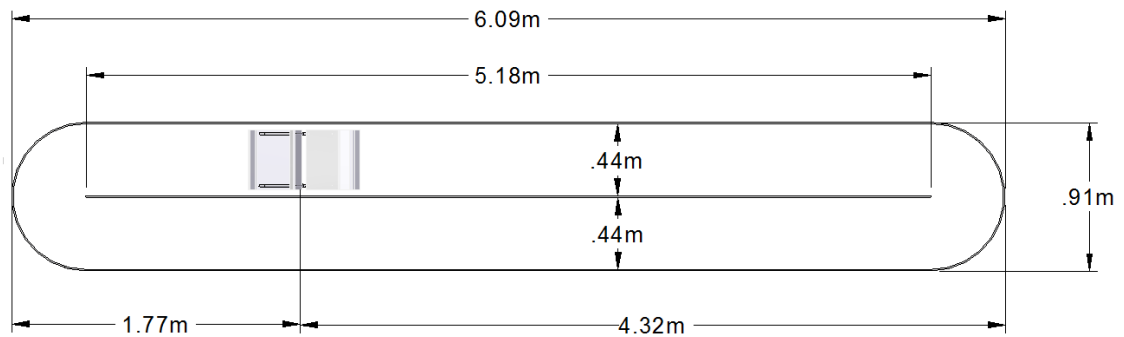
Figure 4-2. Experimental lab-scale raceway dimensions

4.1.1. Raceway Description

The raceway is divided into two channels by a divider running along the raceway channel and connected by two 180° bends at both ends with a bend radius of 0.44 m. The raceway walls are supported by a rigid frame structure. A six-blade paddle wheel is connected through a chain drive to a gear reducer shaft and three-phase motor assembly (gearmotor) which is mounted above the water surface. The gearmotor is equipped with a variable speed drive which controls the rotational speed of the paddle wheel. Finally, paddle wheel circulates the water around the raceway in a clockwise direction relative to the observer at far end. The raceway far end was defined as the end far away to the paddle wheel and the near end was the end near to the paddle wheel. The paddle wheel drive system and gearmotor are shown in Figure 4-3. The raceway is provided with a rail system and a two dimensional manual positioning slide (accuracy of 1 mm) that works as a carriage to hold the ADV probe and move along the entire length of the raceway. Due to the gearmotor mounting assembly on a frame structure at the paddle wheel location, the measurements at that location are not taken.
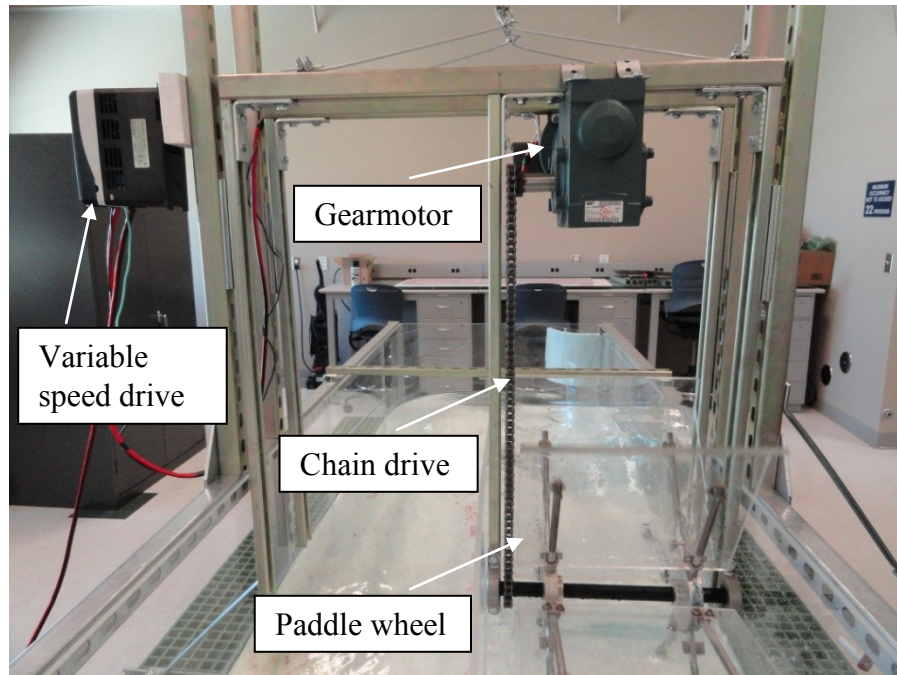
Figure 4-3.   Photograph showing different components of the raceway

4.1.2.   Delta Wing Setup

The delta wings in the shape of an equilateral triangle are made of aluminum sheets, cut to 0.3683 m on each side. The delta wings are held in position, with the lower edges 3.17 cm above the channel bed, by thin steel rods that extended above the water surface, where they are mounted with clamps onto a horizontal brace and equally spaced across the width of the flume. The entire delta wing setup is supported on the trolleys. This arrangement allowed flexibility in delta wing positioning. The delta wings are positioned in such a way that they oppose the incoming flow. Typical positioning of the delta wing is shown in Figure 4-4.
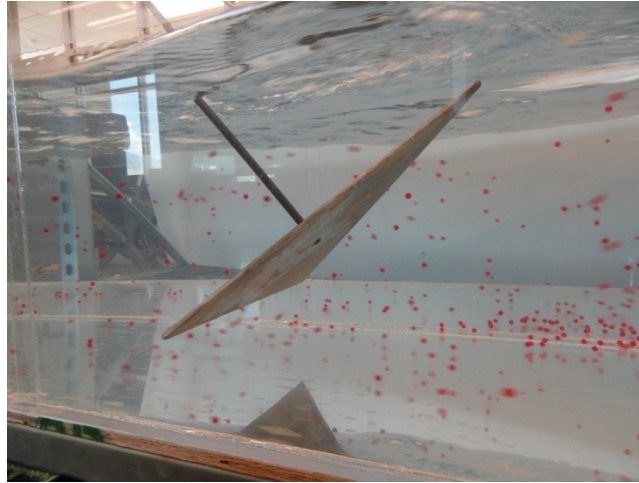
Figure 4-4.   Delta wing submerged in the raceway at an angle of attack α = 30 deg

4.2.   Preliminary Experiments

The reason for doing hydraulic tests in the raceway was to obtain vertical mixing characteristics without algae. Flow visualization techniques were performed on the raceway to obtain a qualitative picture of the vertical mixing using tracer particles and dye within the raceway. A food coloring dye (red colored, density close to that of water) was injected upstream of the delta wing with a syringe as a visual indicator of the flow field. The movement of the dye downstream of the delta wing was videotaped with a camcorder and a high speed camera (MotionXtra HG-100K, Redlake, USA). The dye mixed rapidly in the water and the circulation or flow patterns were not clearly detectable. Due to recirculating open channel flow colored water needs to be drained from the raceway for each run.

Neutrally buoyant fluorescent yellow spheres ranging in diameter from 850 μm to 1000 μm were used to mimic the flow of algae in the water. These fluorescent microspheres under ultraviolet light changed their color to green. An attempt was made to

capture these tracer particle pathline images. The particle pathlines are controlled by user-specified shutter speed using a high speed camera. The shutter speed determines the length of individual pathlines, such that long exposures produce longer pathlines. Slow shutter speeds are not possible on this high speed camera and the tests were not entirely successful. Dead zones were identified near the bends are close to the divider. Dye injections and photographs at various sections in the raceway supplemented some of the preliminary mixing results using delta wings by visual inspection and are not presented in this thesis. These techniques were useful for visualizing flow patterns but they are usually not adequate for measuring characteristic flow parameters. Finally, tests were performed to obtain quantitative information in the form of velocity vector profiles and turbulence measurements using ADV. Other flow measurement techniques are available as well in many studies, including Laser Doppler Velocimetry (LDV) and Particle Tracking Velocimetry (PTV), but they tend to be more expensive and are impractical for field environments. ADV is capable and advantageous over other systems to measure flow turbulence later in the field research.

4.3. Acoustic Doppler Velocimeter Measurements

The turbulence flow measurements were performed at different points of the raceway using an ADV tool.

4.3.1. ADV Description and Principle of Operation

The 16-MHz MicroADV (SonTek- a Xylem brand, San Diego, CA, USA) is a single-point, high-resolution instrument used to measure three-dimensional water

velocity components at specified frequencies. The ADV is used by various researchers for turbulence studies of water in both laboratory and field environments. A photograph of the SonTek MicroADV probe is shown in Figure 4-5. The ADV mainly consists of three modules: measuring probe, signal conditioning module, and the processing module. The down-looking acoustic sensor consists of three acoustic receivers and one acoustic transmitter. The acoustic sensor is mounted on a 25 cm long stainless steel stem. The probe (acoustic sensor and stainless steel stem) is attached to the signal conditioning module, which contains internal receiver electronics enclosed in a submersible housing. The probe is permanently mounted to the front end of the housing, while the other end cap is connected to a high-frequency cable using a 16-pin underwater mateable connector. The high-frequency cable is connected to the processing module which carries analog signals from the probe to the digital processing electronics. The processing module performs the digital signal processing required to measure Doppler shifts and is connected to a controlling computer running SonTek's powerful data acquisition software. The SonTek software package HorizonADV is used to configure ADV system, collect, review, and process data.
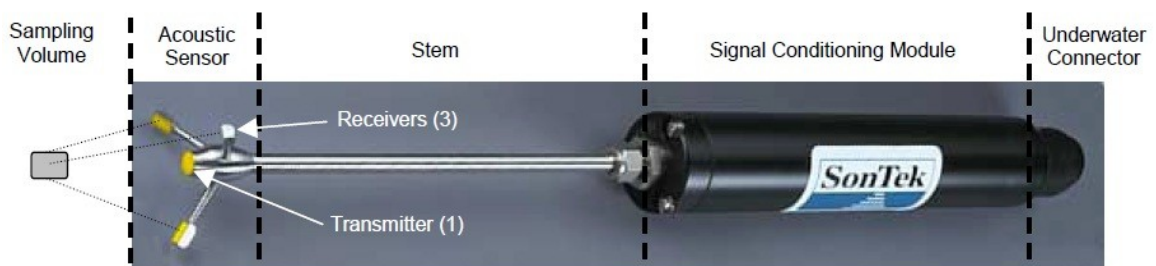
Figure 4-5.   Typical MicroADV field probe and its components [22]

The ADV operates by the principle of Doppler shift. If a source of sound is moving relative to the receiver, the frequency of the sound at the receiver is shifted from the transmit frequency by the amount [22]:

$$F_D = -F_S \left(\frac{V_S}{C} \right)$$
(4.1)

where

F_D = change in received frequency (Doppler shift)

F_S = frequency of transmitted sound

V_S = velocity of source relative to receiver

C = speed of sound

The pulses emitted from the transmitter are scattered by the tracer particles, and the receivers receive the reflected echoes. The receivers are positioned in 120° increments on a circle around the transmitter. The receivers are slanted at 30° from the axis of the transmitter and focus on a common sampling volume. The sampling volume (the volume of water in which measurements are made) of MicroADV is located 5 cm away from the transmitter to provide undisturbed measurements. The sampling location is specified as the vertical center of the sampling volume. For ADV in operation, the data acquisition software displays the distance from the tip of the probe to the boundary, the distance from the center of the sampling volume to that boundary, and the velocity range setting. The distance measurements are accurate to about ±1 mm. The illustration of beams and sampling volume of ADV is shown in Figure 4-6.
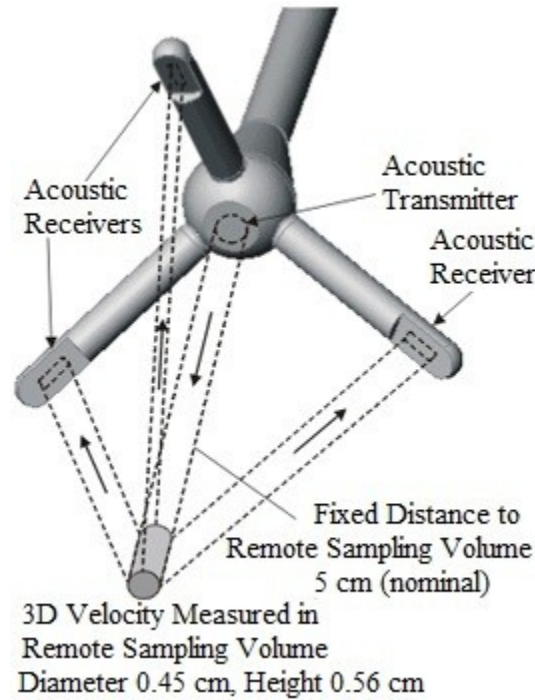
Figure 4-6. MicroADV beams and sampling volume geometry [23]

The positive X-axis for ADV is defined from the acoustic transmitter to acoustic
receiver 1 which is painted in red. The positive Y-axis is defined to give a right hand
coordinate system. The positive Z-axis is defined upwards along the mounting stem or
cable (from the sensor towards the signal conditioning module). The coordinate system
(XYZ) is based on the orientation of ADV when taking the measurements at any
specified location. Data can be acquired at sampling rates up to 50 Hz. The accuracy of
the probe, with factory calibration, is specified to ±1.0% of the measured velocity (i.e., an
accuracy of ±1.0 cm/s on a measured velocity of 100 cm/s). The factory calibration does
not change unless the probe has been physically damaged. The technical specifications
are shown in Table 4-1.

Table 4-1. Technical specifications of the MicroADV [23]

Parameter	Recommended value
Sampling rate	0.1 to 50 Hz
Sampling volume	0.09 cm^3
Distance to sampling volume	5 cm
Resolution	0.01 cm/s
Programmed velocity range	3, 10, 30, 100, 250 cm/s
Accuracy	1% of measured mean velocity, ±0.25 cm/s

4.3.2. Sampling Frequency and Time

The reliability of turbulence parameters or statistics depends on the sensor type, sampling frequency, and sampling time. Sampling frequency is the number of velocity samples to be recorded per second at the measuring point. Guidance is available in the literature for choosing the sampling frequency [24]. In order to resolve turbulent fluctuations of a certain frequency, a sampling frequency of at least twice our frequency of interest (Nyquist frequency) is needed. It has been suggested that the minimum sampling frequency of the instrument should be greater than the maximum flow frequency to analyze the spectral distribution down to the viscous subrange. The highest flow frequency for the open channel turbulence was proposed by Nezu and Nakagawa in 1993 [25] and is given by

$$f_{max} \geq \left(\frac{50}{\pi}\right)\left(\frac{U}{d}\right)$$

(4.2)

where U is the mean flow velocity in the streamwise direction and d is the flow depth.

The smallest turbulence scales are the Kolmogorov microscales, which governs the turbulence kinetic energy dissipation rate. For a mean streamwise velocity of 25 cm/s and a water level of 20 cm, the maximum flow frequency f_{max} is around 20 Hz. The ADV sampling frequency is capable of resolving this maximum flow frequency. Therefore, all the velocity measurements were conducted with a sampling frequency of 50 Hz.

Sampling time is defined as the period of time (seconds or minutes) over which the velocity is recorded at each of the measurement locations. A preliminary study was performed to choose the appropriate sampling time. Water was seeded with hollow glass spheres with a density close to that of water and a mean diameter around 10 μm (Potter Industries, USA) to increase the strength of the signal and reduce noise. The ADV was mounted on a fine adjustment traversing mechanism which slides on the raceway in streamwise, lateral and vertical directions. Velocity measurements were taken at the fixed location, near the bottom and in the main body of the flow, for the same flow conditions using number of samples ranging from 500 to 10,000 with a sampling frequency of 50 Hz. The near-bottom point is located at 5 cm and the main body of the flow point is located at 10 cm from the bottom. The instrument generated noise (Doppler noise) is random and averaging multiple data points will converge towards the true value without introducing bias. Instrument generated noise is purely random (white), and its signature is a flat power spectrum. Generally, under good operating conditions, the noise for data output at 50 Hz using MicroADV is about 1% of the velocity range setting (i.e., ±1 cm/s

when using the 100 cm/s velocity range). The effect of number of samples on the mean streamwise velocity component of the raceway is shown in Figure 4-7. The mean streamwise velocity converges towards a constant value after 6,000 samples. Therefore, each spatial point on the grid was sampled for 2 min, which corresponds to 6000 samples with a sampling frequency of 50 Hz.
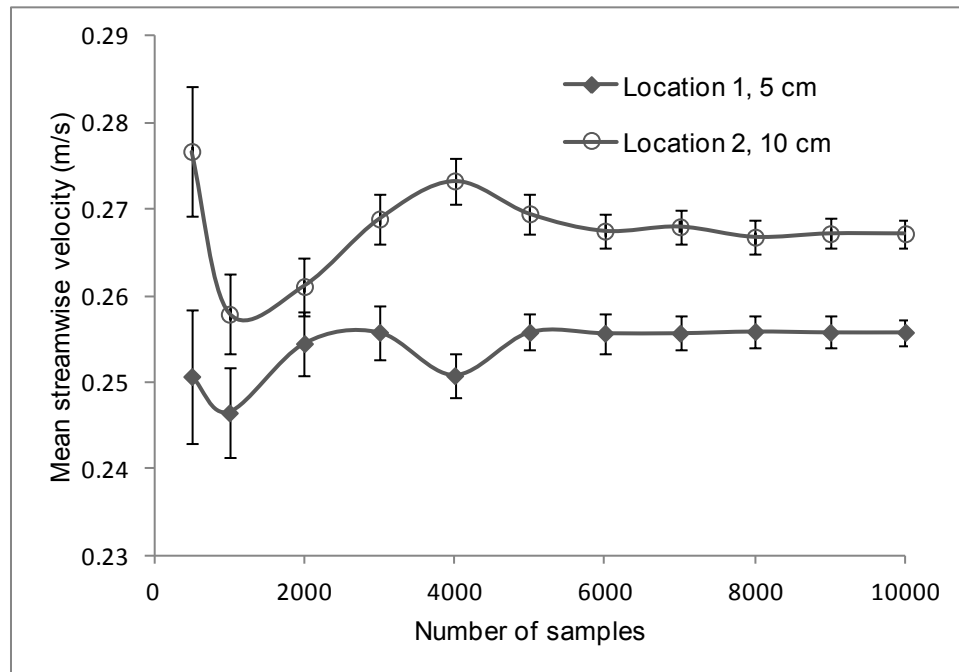
Figure 4-7.   Effect of number of samples on mean streamwise velocity

4.3.3. Section-wise Grid Measurements

Because the ADV measures velocity at a single point, it was placed at different points to collect the water velocities. The ADV sensor measures the velocity at a point located 5 cm under it and must stay submerged during measurements, so that it cannot measure in the top of the flow. Due to minimum flow depth requirements for the acoustic sensor, the upper 6 cm of the flow could not be measured. Due to the limitation of sensor radius and to avoid contact with the walls of the open channel, a flow width of 3.81 cm near to the divider and sidewall could not be measured. The average water depth in the raceway was maintained constant at 20 cm for all the experiments and an operating average velocity of around 25 cm/s. Grid-wise velocity measurements were taken in the y-z plane at different sections downstream of the delta wings as shown in Figure 4-8. A detailed comparison was also made by taking the measurements at the same locations without delta wings. For each section, 81 data points were collected. The period of data collection time for each section was around 4 hrs.
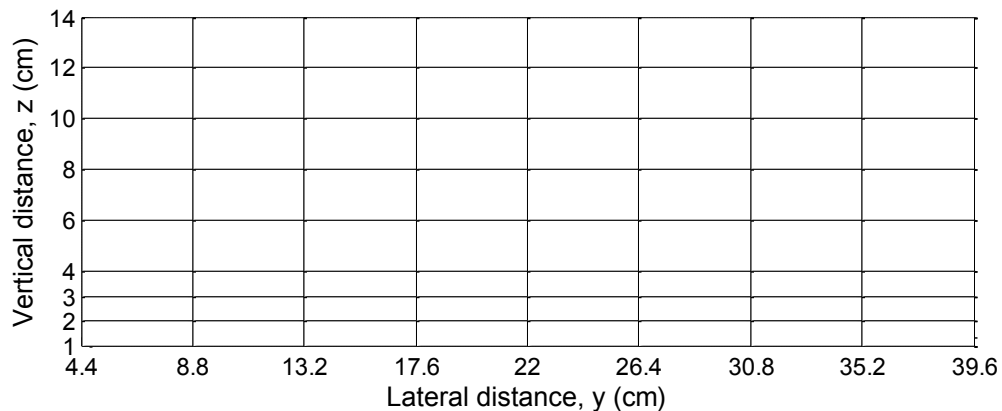
Figure 4-8.   Illustration of the measurement locations on a y-z plane

An arbitrary angle of attack of 30° (assumed from the literature review and CFD simulations) and arbitrary placement of delta wings were chosen (assumed from the preliminary experiments) for these vertical mixing studies. Optimization of the angle of attack of delta wings for vertical mixing may be performed using ADV which requires more data collection time. Alternatively, for the optimization of angle of attack and spacing of the delta wings, CFD and PIV can be powerful tools for a fast approach. The ADV in operation is shown in Figure 4-9. It is important to note that the addition of delta wings will impact the resistance felt by the paddle wheel in circulating the water. Power was considered as an important factor to ensure that the addition of delta wings will be economically equivalent way of mixing. Three sets of experiments were conducted by changing the position of delta wing as shown in Figure 4-10 to Figure 4-12.
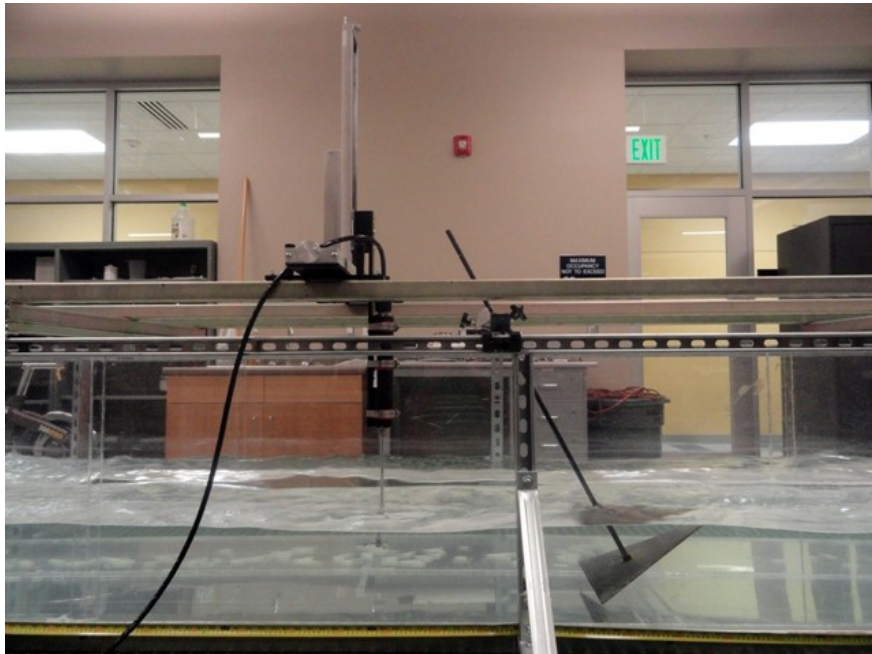
Figure 4-9.   Photograph of ADV taking measurements in the raceway
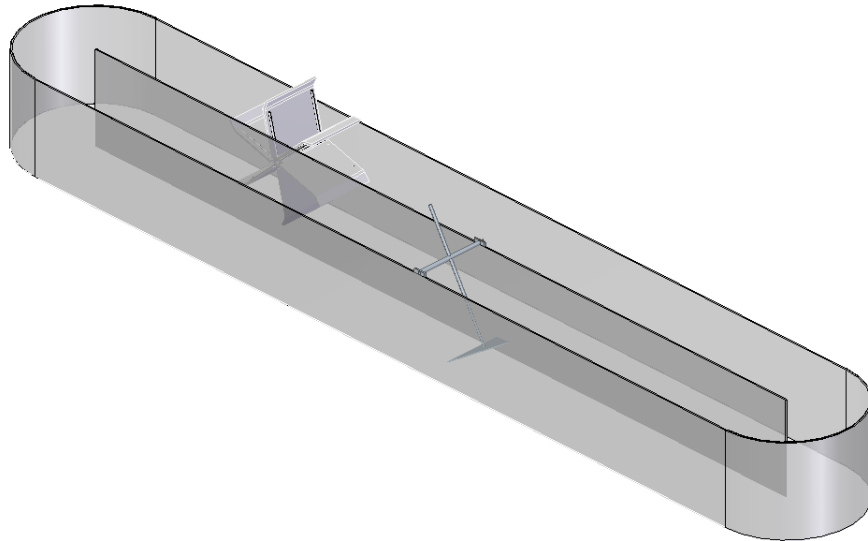
Figure 4-10. Solid model of the raceway showing delta wing position in open channel at a distance of 2.44 m from the far end for experiment set 1
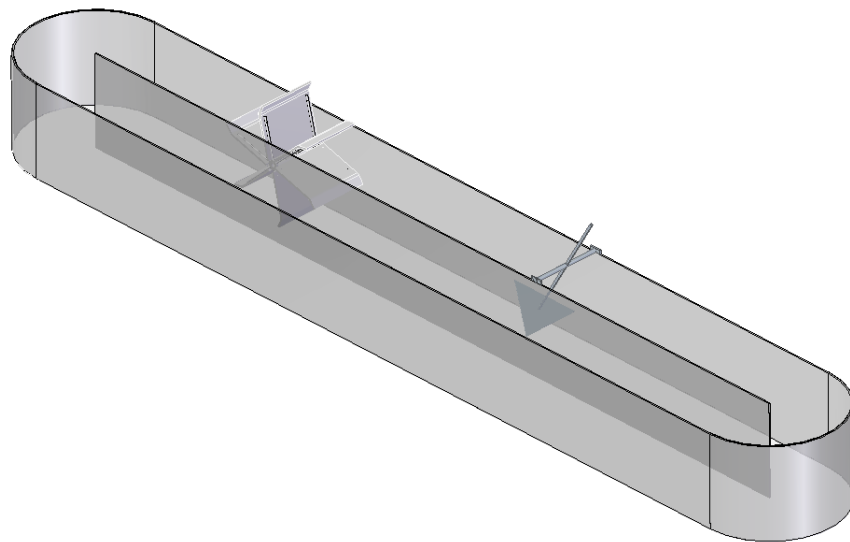
Figure 4-11. Solid model of the raceway showing delta wing position in open channel at a distance of 2.44 m from the far end for experiment set 2, delta wing is placed in the channel relative to paddle wheel
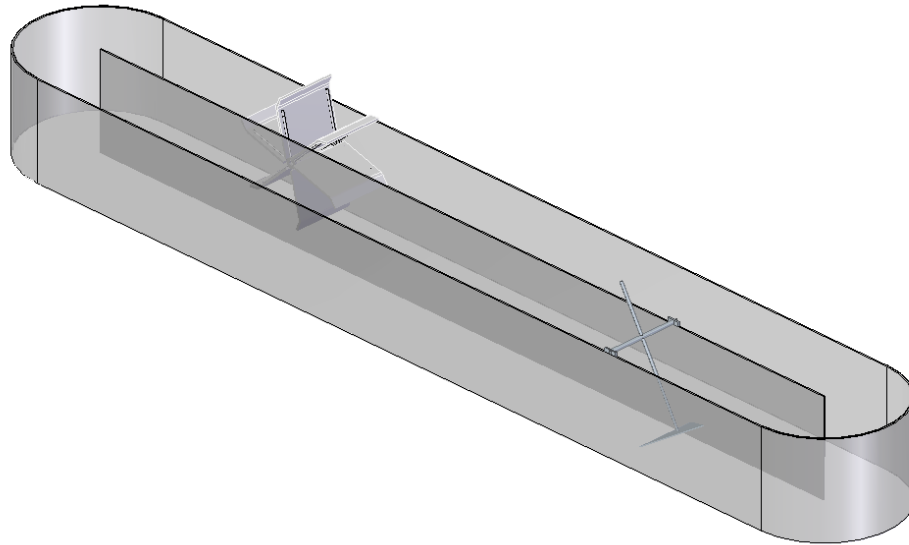
Figure 4-12. Solid model of the raceway showing delta wing position in open channel at a distance of 1.22 m from the far end for experiment set 3

4.4.   Data Analysis

The following subsections provide a description of the ADV data analysis.

4.4.1. Data Post Processing

The ADV records nine values with each sample: three velocity components, three signal strength values (one for each receiver) and three correlation values (one for each receiver). Signal strength, recorded for each ADV receiver, is a measure of the intensity of the reflected acoustic signal. The main function of signal strength data is to verify there is sufficient particulate matter in the water. To check if the water is properly seeded, the ADV provides a read-out of the Signal-to-Noise Ratio (SNR), an indicator of how well the flow is seeded: the higher the SNR, the better the seeding, and the more reliable the velocity measurements are. As SNR decreases, the noise in velocity measurements

will increase. For high-resolution velocity measurements, the manufacturer recommends maintaining SNR of at least 15 dB. The correlation coefficient (COR) is a data quality parameter that is a direct output of the Doppler velocity calculations. In general, correlation values above 70% are designed for good velocity data. To ensure that ADV measurements provide an accurate representation of the flow velocity, one should evaluate the SNR and the correlation values. Filtering the data using these parameters can improve the quality of the measurement. Figure 4-13 shows an example of ADV data containing spikes.
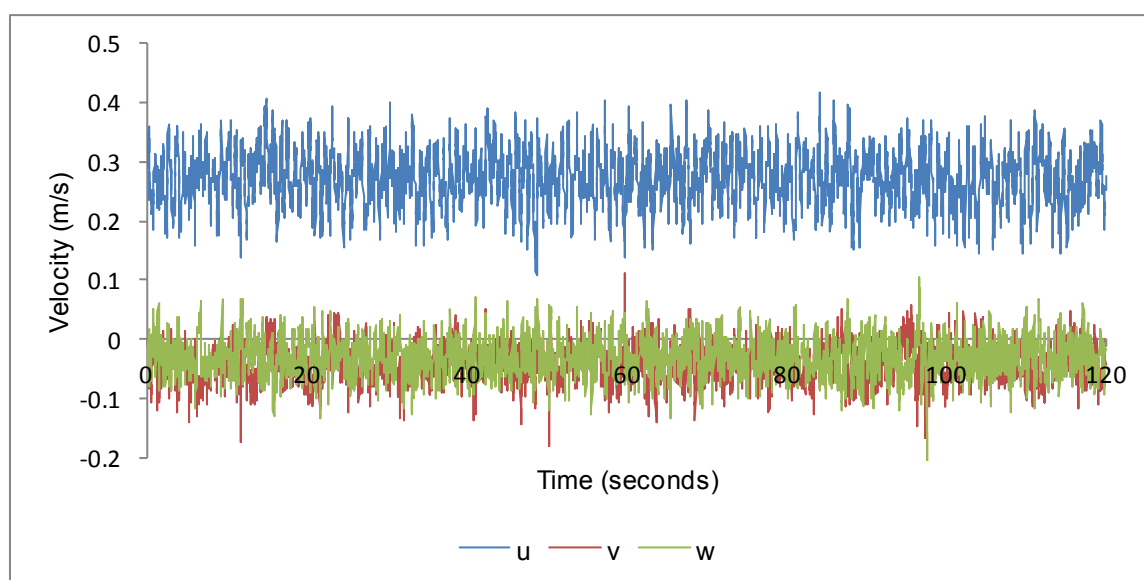
Figure 4-13.   Raw ADV velocity time series data

Data quality was monitored through SNR and COR during real-time as well as in recorded data. Data were filtered and analyzed using WinADV software which process batches of ADV generated data files [26]. The velocity range setting in ADV determines

the maximum velocity that can be measured. If the expected velocity range is set too low in the ADV system settings, aliasing of the velocity data may occur when velocities exceed the maximum range, causing occasional velocity "spikes" in data. Aliasing occurs when the measured phase difference between the two acoustic pulses transmitted and received by the ADV exceeds 180°. As the ADV cannot distinguish between a phase difference of 181° and -179°, the velocity recorded in the ADV file will change sign, producing a dramatic spike in the velocity data [26]. Goring and Nikora [27] developed a phase-space threshold method to eliminate these spikes and improved later by Wahl [28]. This technique uses the concept of a phase-space plot of the velocity data, and its first and second derivatives, and assumes that good data are located inside an ellipsoid in phase-space. The points outside the ellipsoid are considered as spikes and should be removed. The method iterates until the number of good data becomes constant. Finally, data post processing was done by filtering velocity data using SNR (>15 dB), COR (>70), and phase-space threshold despiking filters. Data obtained after applying filter methods for an example is shown in Figure 4-14. All the velocity time series datasets were checked for spikes and noise during post processing.
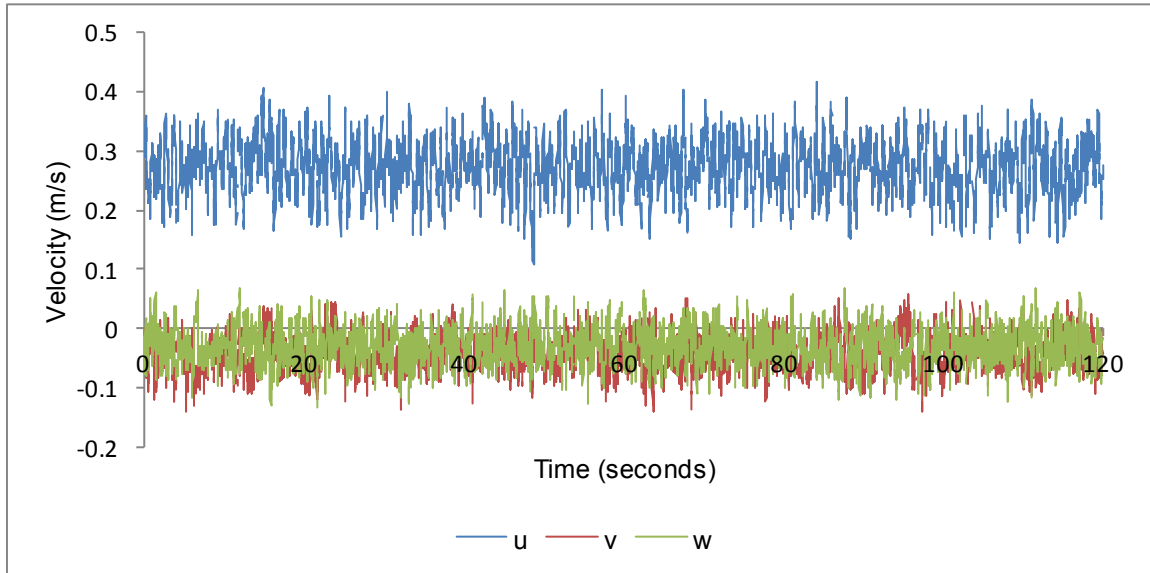
Figure 4-14. Filtered ADV velocity time series data

4.4.2. Measurement Uncertainty Analysis

The uncertainties in mean velocity and turbulence measurements reported using ADV are typically about 5% and 10% respectively [29]. However, the short term uncertainty (noise) of ADV depends on the acoustic scattering level of the fluid. The expanded uncertainties (with a 95% confidence level) of the measured velocity data were estimated through a detailed uncertainty analysis of all the uncertainty components associated with the ADV [30]. The mean and standard deviation of the sample population are calculated by using the following equations

$$U = \frac{1}{N} \sum_{i=1}^{N} u \tag{4.3}$$

$$S_U = \left[\frac{1}{N-1} \sum_{i=1}^{N} (u - U)^2 \right]^{1/2} \tag{4.4}$$

The random standard uncertainty of the mean velocity for large-sample approximation (95% confidence level) was found using the equation

$$S_{\bar{U}} = \frac{2S_U}{\sqrt{N}}$$

(4.5)

where u is the instantaneous velocity in streamwise direction and S_U is the standard deviation of the sample of N measurements from the filtered data.

The systematic standard uncertainty was considered from the instrument manufacturer's information. Accuracy for ADV velocity data refers to the presence of a bias in mean velocity measurements after removing instrument-generated noise. The accuracy of the probe, with factory calibration, is specified to ±1% of the measured velocity (b_A). The resolution of the ADV is 0.0001 m/s. For a digital output, the minimum 95% standard uncertainty (b_R) in the data was taken as ±1/2 the resolution. It was assumed that there are no correlated systematic or random errors for the measured quantity. The ADV specifications state a maximum zero offset velocity of ±0.0025 m/s. With Doppler processing, there is no potential for zero offset in velocity measurements; this specification is included because of the difficulty in generating calibrated velocities at low flows [22]. Hence, the systematic uncertainty due to zero offset was ignored.

The systematic standard uncertainty of the mean velocity ($b_{\bar{U}}$) was found using the equations

$$b_A = \frac{0.01U}{\sqrt{N}}$$

(4.6)

$$b_{\bar{U}}^2 = b_A^2 + b_R^2$$

(4.7)

The expanded uncertainty for the mean velocity at a 95% level of confidence was calculated using the equation

$$U_{\bar{U}} = 2\left(S_{\bar{U}}^2 + b_{\bar{U}}^2\right)^{1/2} \tag{4.8}$$

It was observed from the experimental data that the expanded uncertainty (95% level of confidence) for the mean velocities is within the range of 2 to 5%, which is in agreement with ADV literature [29]. The general uncertainty analysis was performed using Taylor Series Method. For the more general case where the result r is a function of several variables, $r = r(X_1, X_2, \ldots X_J)$, the overall uncertainty of the result is determined from [30]:

$$U_{95} = \left[\sum_{i=1}^{J}\left(\frac{\partial r}{\partial X_i}\right)^2 U_i^2\right]^{1/2} \tag{4.9}$$

where each U_i is the large-sample 95% expanded uncertainty for variable X_i.

4.4.3. Estimation of Turbulence Parameters

The parameters turbulence kinetic energy (TKE) and turbulence intensity (TI) were calculated using the mean and fluctuating velocity components of ADV time series data to make a comparison with PIV data. The magnitude of the resultant of the mean velocities components (V_{mag}) and magnitude of the resultant of the RMS values (V'), in-plane velocity (V_p), TKE, and TI were calculated using the following equations

$$V_{mag} = \sqrt{U^2 + V^2 + W^2} \tag{4.10}$$

$$V' = \sqrt{\overline{u'^2} + \overline{v'^2} + \overline{w'^2}} \tag{4.11}$$

$$V_p = \sqrt{\overline{v'^2} + \overline{w'^2}} \tag{4.12}$$

$$TKE = \frac{1}{2}(\overline{u'^2} + \overline{v'^2} + \overline{w'^2}) \tag{4.13}$$

$$TI = 100 \frac{\sqrt{\frac{2}{3}TKE}}{V_{mag}} \tag{4.14}$$

4.4.4. Estimation of Turbulence Dissipation Rates

The turbulence dissipation rate (ε) has been increasingly used as a scaling parameter to integrate microbiological organisms with fluid flow motion in natural and engineered aquatic ecosystems [11]. Also, this is an indicator of turbulence's ability to enhance mixing. ADV's have been shown to accurately measure the intermediate scales of turbulence by numerous researchers [31]. Turbulence dissipation rates were estimated using Kolmogorov hypothesis. Turbulence dissipation rate is the rate at which kinetic energy is transferred from the mean flow to large eddies, then to small eddies, and is finally dissipated by viscosity (energy cascade). Even though isotropy does not apply to the energy-containing eddies, it was assumed that local isotropic turbulent flow exists in the inertial subrange for small scale structure. Under these conditions, the turbulence dissipation rate can be estimated by the magnitude of the wave number spectra in the inertial subrange, which takes the form:

$$E(k) = \beta \varepsilon^{2/3} k^{-5/3} \tag{4.15}$$

where k is wave number, $E(k)$ is the wavenumber spectral density, and β is the Kolmogorov constant which is equal to 0.49 for the streamwise velocity component and

0.65 for the lateral and vertical velocity components. The inertial subrange extends from large eddies, the scale of which is typically determined by physical dimensions of the flow (e.g., depth) to the Kolmogorov microscale, which is determined by kinematic viscosity and dissipation rate [32]. The large-scales are very important from the point of view of transport, but direct effects on algae can be expected to occur at small-scales. An illustration of the turbulence energy spectrum is shown in Figure 4-15.
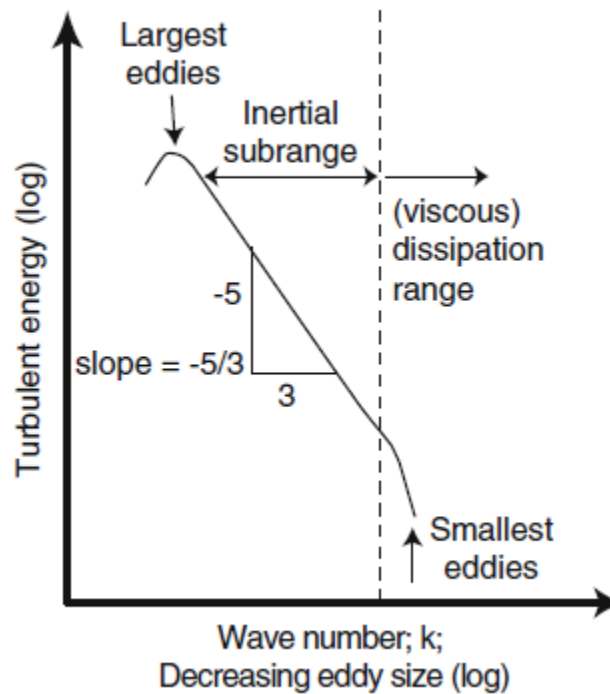

Figure 4-15.   Schematic representation of a typical turbulence energy spectrum [33]

Taylor's frozen turbulence hypothesis [31] is used to transform temporal spectra into spatial spectra ($k = 2\pi f/U$) which is valid when the velocity fluctuations are much smaller than the streamwise mean velocity ($u'/U \ll 1$). Then, the spectrum can be transferred from the frequency domain to the wave number domain by

$$E(k) = \frac{U}{2\pi} S(f) \qquad (4.16)$$

The velocity time series data at a fixed point were used to estimate the energy density spectrum as a function of frequency. The turbulence dissipation rate was calculated using the following equation

$$\varepsilon = c.\frac{2\pi}{U}\left[S(f)f^{5/3}\right]^{3/2} \qquad (4.17)$$

where c is a constant (2.9 or 1.9 depending on whether the direction of velocity component is inline with or normal to mean flow, U) and $\left[S(f)f^{5/3}\right]$ is the portion of the frequency spectra that exhibits a -5/3 slope in the inertial subrange. The vertical component of the ADV velocity signal was used to calculate dissipation rates because the Doppler noise level is less compared to the other two components. Spectral density plots were obtained and smoothed using 512-point Hamming windows with 50% overlap and ensemble-averaging (Welch) method. For each data run, the power spectral density plot was individually inspected and the magnitude of the spectra in the range over which the theoretical -5/3 slope was found and was used to estimate the dissipation rate. The Kolmogorov length scales or microscales, which corresponds to dissipative eddies were calculated using the Equation (4.18).

$$\eta = \left(\frac{\vartheta^3}{\varepsilon}\right)^{1/4} \tag{4.18}$$

where ϑ is the kinematic viscosity of water (10^{-6} m^2/s at a temperature of 22°C).

4.5. Comparison of ADV and PIV Measurements

Particle Image Velocimetry (PIV) is a powerful tool in fluid mechanics and aerodynamics for the quantification of the velocity vector field with high spatial and temporal resolution. PIV is an optical method of flow visualization in which the laser light sheet is pulsed twice, and images of tracer particles lying in the light sheet are recorded on a high speed camera separated by a known time increment. Image processing software is then used to determine the particle displacement, and hence the flow velocity, from the photographic images. A digital Stereo PIV system is used to capture high resolution spatial data of the instantaneous three-component velocity vector field in the planar region illuminated by a laser light sheet. In a stereoscopic arrangement, two cameras view the plane at different angles and capture tracer particle displacement images that contain the influence of the third velocity component.

Tests were conducted in an open channel flow with a state-of-the-art Stereo PIV system (LaVision Inc.) to make a comparison with ADV. The flow region of interest was illuminated with a double pulse Nd: YAG laser (New Wave Research, USA). The flow was seeded with 10 μm hollow glass sphere particles with a density close to that of water (Potter Industries, USA). Two Imager Intense 12 bit CCD cameras (LaVision Inc.) were used and set at 45o angle for the best resolution of streamwise velocity. Each data set was taken with 1000 images at a random frequency around 2 Hz. DaVis imaging software

was used to generate three-component velocity vector field from these images. The velocity vector field cannot be measured by PIV near the free surface because of fluctuations of the water depth.

4.6. Power Measurements and Raceway Energy Model

The total power required to mix the raceway at an operating average velocity was determined by measuring both the voltage and current to a gearmotor which drives the paddle wheel. At a given mixing speed, the voltage to the gearmotor armature remains nearly constant. The armature current, which is proportional to the torque, vary considerably throughout each revolution of the paddle wheel, producing a small peak as the blade enters the water and a larger peak as it lifts a slug of water to the downstream depth. CTScope real-time software oscilloscope was connected to a variable speed drive which measures the actual power waveform and the data was graphically averaged.

For raceway energy model, the average head loss across the paddle wheel was measured as a function of average channel velocity. From the measurements of head loss and velocity, the hydraulic power was calculated. The hydraulic power required for mixing is the product of volumetric flow rate, specific weight, and head loss. The total power includes the effects of drive train and mixer inefficiencies. Finally, an energy model was developed to operate the paddlewheel-driven raceways with different velocities and roughness factors. The raceway energy model was developed based on the well-known Bernoulli and energy equations. This includes the drag losses, frictional head losses and kinetic head losses associated with the delta wing, straight channel and bends respectively. The model was detailed in Appendix A.

Addition of delta wings in the raceway will impact the resistance felt by the paddle wheel due to drag losses. For basic comparisons, the raceway with and without delta wing was operated at the same paddle wheel rotational speed in experiment set 1. The addition of delta wings in the raceway should be economical *i.e.* the power consumption of the raceway with delta wings should be equal or less compared to the raceway without delta wings. Clearly, mixing speeds higher than 30 cm/s are impractical, at least for energy production systems [4]. It was assumed that the outdoor raceway with delta wings operate at lower circulation velocity than the normal raceway. Therefore for the addition of delta wing in the experimental raceway, the liquid circulation velocity was decreased by adjusting the paddle wheel rotational speed. The raceway with and without delta wing was operated at two different paddle wheel rotational speeds for experiment set 2 and 3. Power consumed by the paddle wheel for different set of experiments is shown in Table 4-2.

Table 4-2.   Power consumption by the paddle wheel at different conditions

Parameter	Paddle wheel speed (RPM)	Experiment set 1 Power consumption (W)	Paddle wheel speed (RPM)	Experiment set 2 & 3 Power consumption (W)
Without delta wing	11.5	62.07±8.31	11.5	62.07±8.31
Delta wing	11.5	63.91±8.09	11	60.46±7.19
Percent change (%)		2.96	–	-2.6

* ± bands indicate standard deviation of the mean power consumption

CHAPTER 5

EXPERIMENTAL RESULTS AND DISCUSSION

The results obtained from the experiments performed with and without delta wing in the raceway are presented and discussed in this chapter.

5.1.   Comparison of ADV Data with PIV Data

A comparison was made between ADV and PIV tools to know the measurement accuracy of data collected in the raceway. Both PIV and ADV were operated at the same location, water depth, and paddle wheel speed with and without delta wing in the open channel, opposite to the paddle wheel. Since the presence of ADV probe disturbs the flow measurements using PIV, the measurements were not simultaneous. The edges of high-spatial resolution PIV data in the plane was trimmed to exactly match with the ADV filtered grid data. Table 5-1 and Table 5-2 show a comparison of measured and calculated parameters using the two experimental tools. It was observed that the mean velocities measured using ADV and PIV were in good agreement within 4% and the difference were within the uncertainty of each measurement tool. The expanded uncertainty of the mean velocities measured using ADV was within the range of 2 to 5%. The RMS velocities measured by the two techniques were within 9%. The turbulence kinetic energy and turbulence intensity parameters will depend on the accuracy of mean and fluctuating components, and the instrument generated noise. The higher RMS values measured by the PIV were probably due to random uncertainty in the data. A side-by-side comparison between ADV and PIV contour plots was also shown in Appendix B.

Table 5-1.   Data obtained by ADV and PIV at 1.07 m downstream of the delta wing in the raceway

Parameter	ADV	PIV	Percent difference (%)
Mean velocity (m/s)	0.2493	0.2459	1.37
Root mean square velocity (m/s)	0.0904	0.0988	8.88
In-plane mean velocity (m/s)	0.0533	0.0549	2.96
Turbulence kinetic energy (m^2/s^2)	0.0041	0.0049	17.78
Turbulence intensity (%)	21.3985	23.73	10.33

Table 5-2.   Data obtained by ADV and PIV without delta wing in the raceway

Parameter	ADV	PIV	Percent difference (%)
Mean velocity (m/s)	0.238	0.2458	3.22
Root mean square velocity (m/s)	0.0887	0.0957	7.59
In-plane mean velocity (m/s)	0.0132	0.0152	14.08
Turbulence kinetic energy (m^2/s^2)	0.004	0.0046	13.95
Turbulence intensity (%)	22.6368	23.56	4

5.2.   Velocity Vector Profiles

Velocity vector profiles were generated to provide a qualitative and quantitative information of the impact of vertical mixing with and without delta wing in the raceway. Three sets of experiments were performed and the measurements were conducted along the entire length of the raceway. The angle of attack of the delta wing was set constant at 30° throughout these experiments.

5.2.1. Experiment Set 1

The delta wing was placed in the open channel opposite to the paddle wheel. For basic comparisons, measurements were conducted at a paddle wheel speed of 11.5 RPM with and without delta wing in the raceway. The measurement locations are shown in Figure 5-1. The arrow on the plot represents the direction of the fluid flow in the raceway. Due to the supporting frame structure for the paddle wheel drive train system, data was not collected near the paddle wheel location. The maximum vertical velocities were compared for both cases in order to determine the intensity of vertical motion at the measured locations and are shown in Table 5-3. It was found that there was a significant increase in vertical velocities with the addition of delta wing compared to the raceway without delta wing. This will be discussed in greater detail in Section 5.3 where a vertical mixing index is introduced.
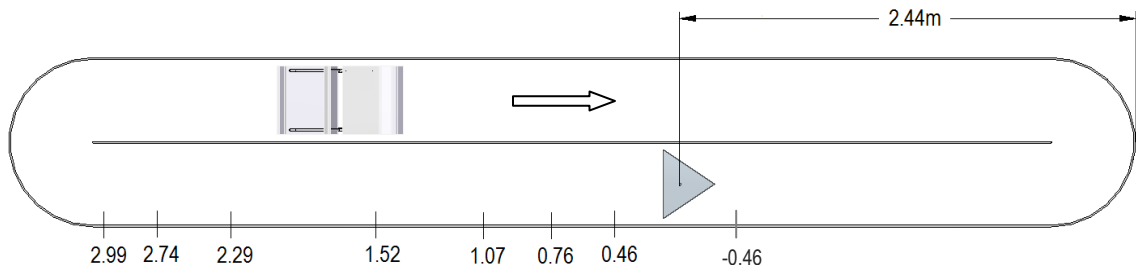

Figure 5-1. Position of the delta wing in open channel and measurement locations (in m) referenced from the centroid of the delta wing

Table 5-3. Comparison of maximum vertical velocities for experiment set 1

Distance (m)	Delta wing V_{max} (m/s)	Without delta wing V_{max} (m/s)
-0.46	0.0098	0.0108
0.46	0.108	0.0047
0.76	0.0915	0.0035
1.07	0.0729	0.0019
1.52	0.0468	0.0045
2.29	0.0232	-0.0008
2.74	0.019	-0.0003
2.99	0.0149	-0.0011

Figure 5-2 indicates the normal flow conditions before the water flows over the delta wing. Figures 5-2 to 5-9 show a comparison between velocity vector fields in y-z plane for the raceway with and without delta wing. The velocity vectors were scaled by a colored contour of the magnitude of in-plane velocities. It should be noted that the left side and right side of these plots indicate the divider and outer wall of the raceway respectively. It can be seen that the mixing created by the paddlewheel without delta wing was not sufficient to keep algae in vertical motion or circulation due to the absence of strong vortices. Secondary flows are commonly present in open channel flows. Lateral mixing (y direction - spanwise) was seen in this case due to the dominance of secondary flow structures postulated in the open channel. It was observed that the delta wing creates

two strong counter-rotating circular vortices that were sustained downstream of the delta wing. Hence, it was hypothesized that this sort of systematic vertical mixing in the raceway will produce the necessary flashing light effect (light-dark cycles) on algae mass culture. It was noticed that the shape of the vortices was elongated as they move downstream of the delta wing. Further downstream of the delta wing, the right side vortex move towards the side wall and broke down probably due to the effect of curved bend.

5.2.2. Experiment Set 2

To satisfy the power consumption limitations, raceway with delta wing was operated at a paddle wheel speed of 11 RPM and without delta wing was operated at 11.5 RPM. The measurement locations are shown in Figure 5-10. These experiments were conducted to study the vertical mixing phenomena in the open channel relative to the paddle wheel. Interestingly, the velocity vector fields revealed that the presence of paddle wheel in the normal raceway had less impact on the vertical mixing or circulation of algae compared to the raceway with delta wing. It was observed that the vortex core moves around the channel as the vortices stretch downstream of the delta wing and that represents the large-scale unsteadiness of the fluid motion. A significant difference in the maximum vertical velocities for both cases can be seen in Table 5-4. The velocity vector fields obtained at different locations are shown in Figures 5-11 to 5-17.
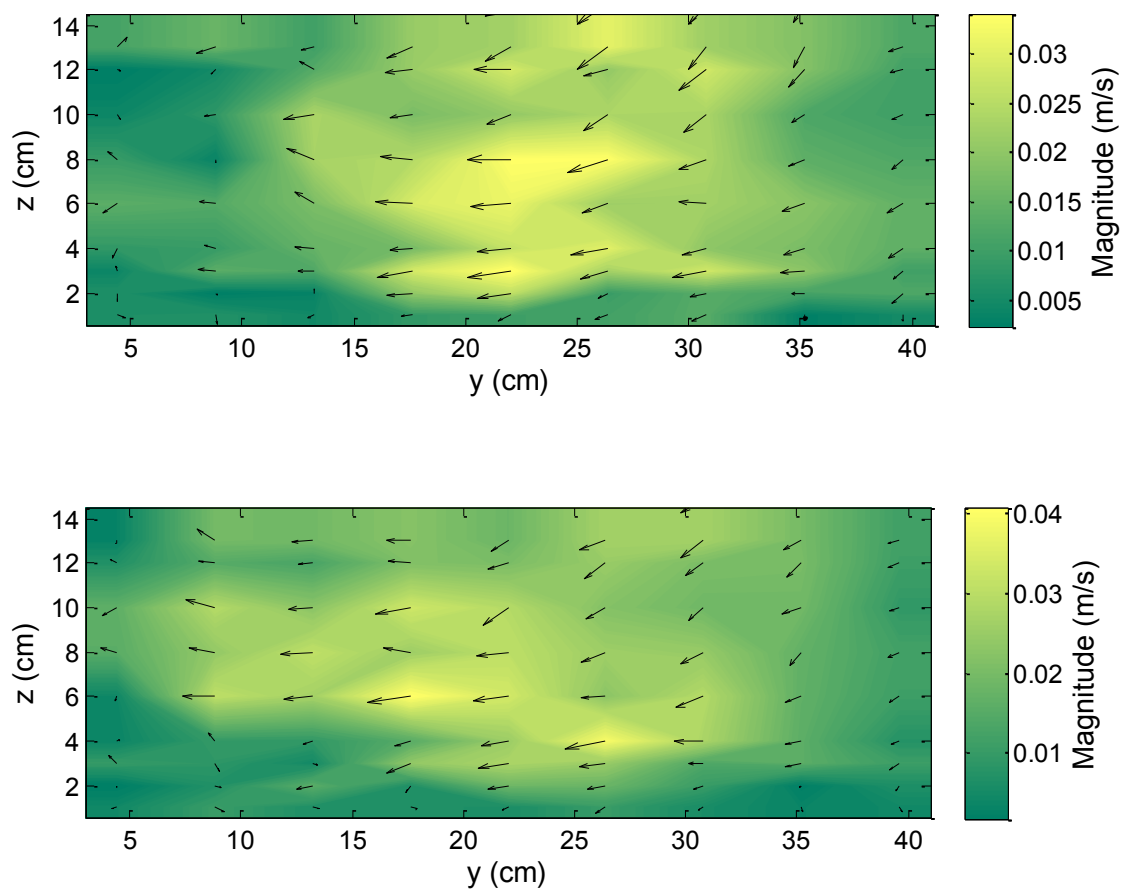
Figure 5-2.   Planar velocity vector fields obtained at 0.46 m upstream of the delta wing (top) and without delta wing (bottom) at the same location
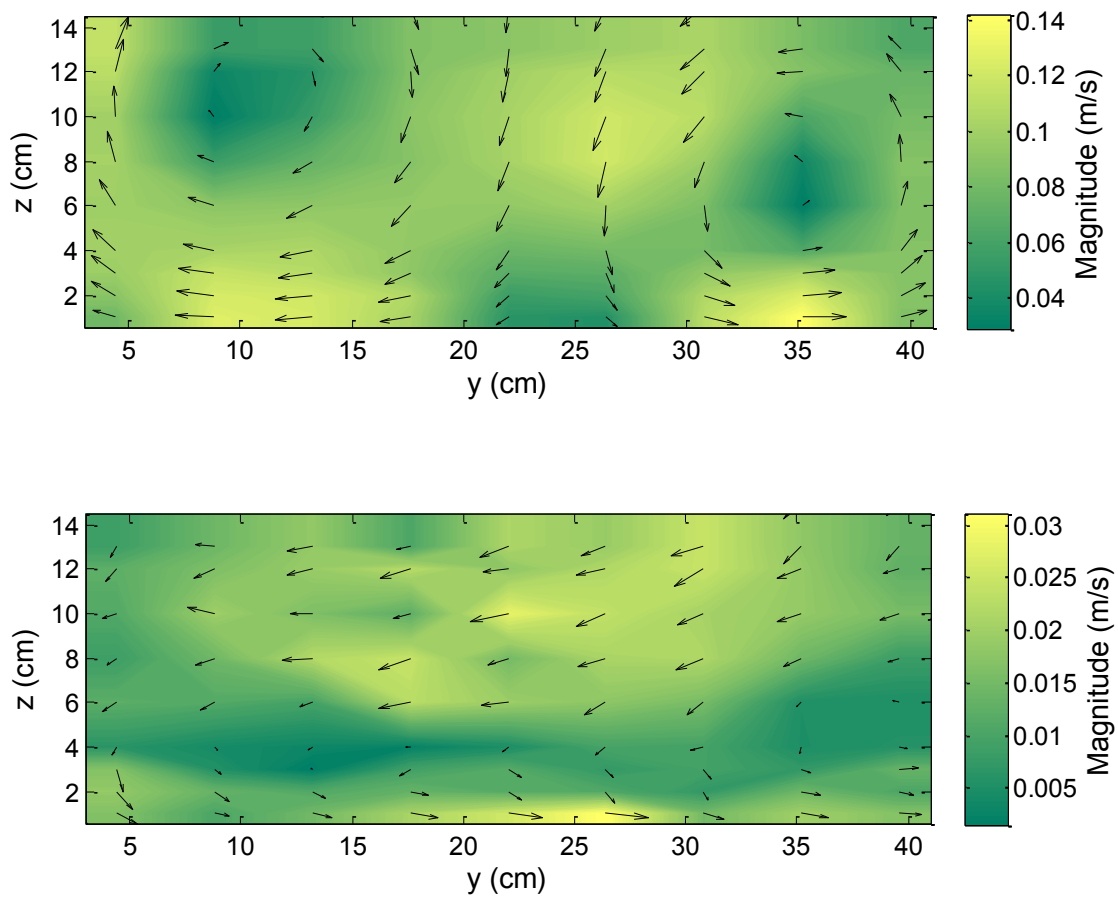
Figure 5-3.   Planar velocity vector fields obtained at 0.46 m downstream of the delta wing (top) and without delta wing (bottom) at the same location
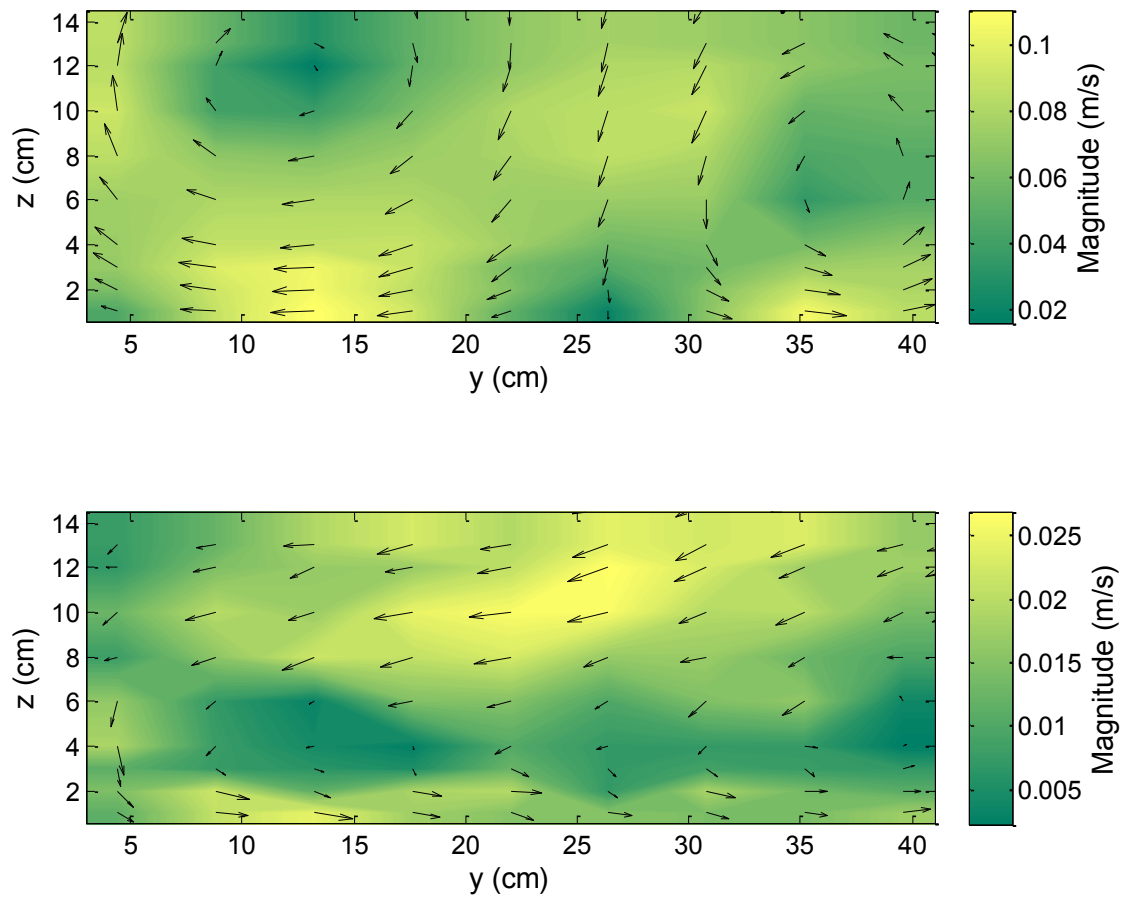
Figure 5-4.   Planar velocity vector fields obtained at 0.76 m downstream of the delta wing (top) and without delta wing (bottom) at the same location
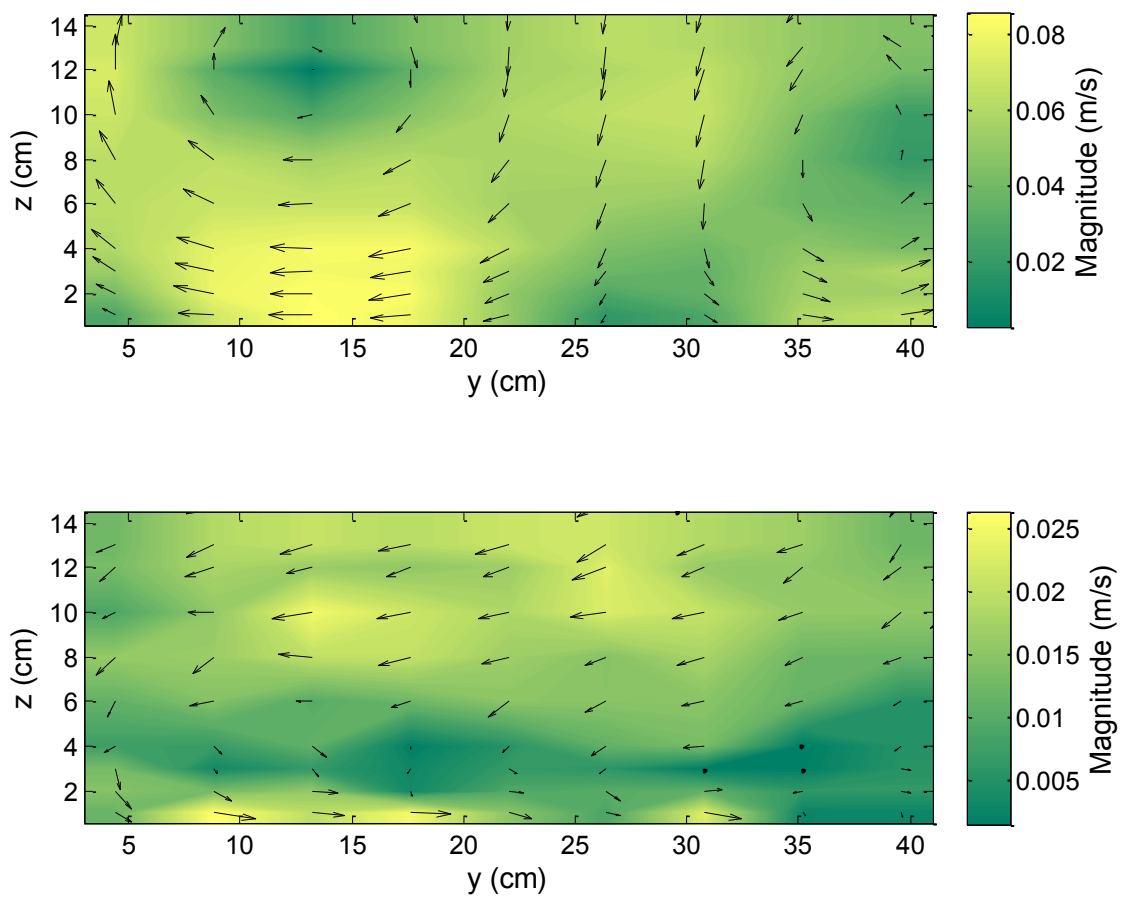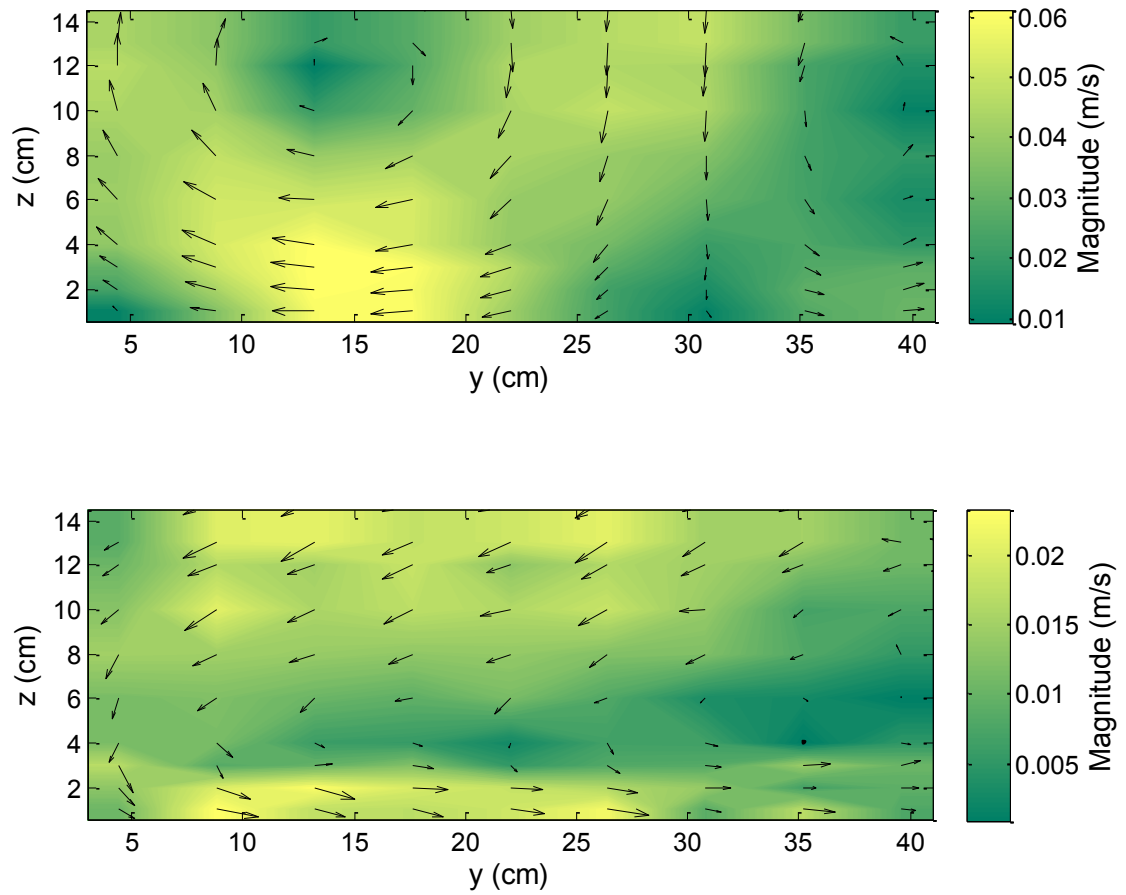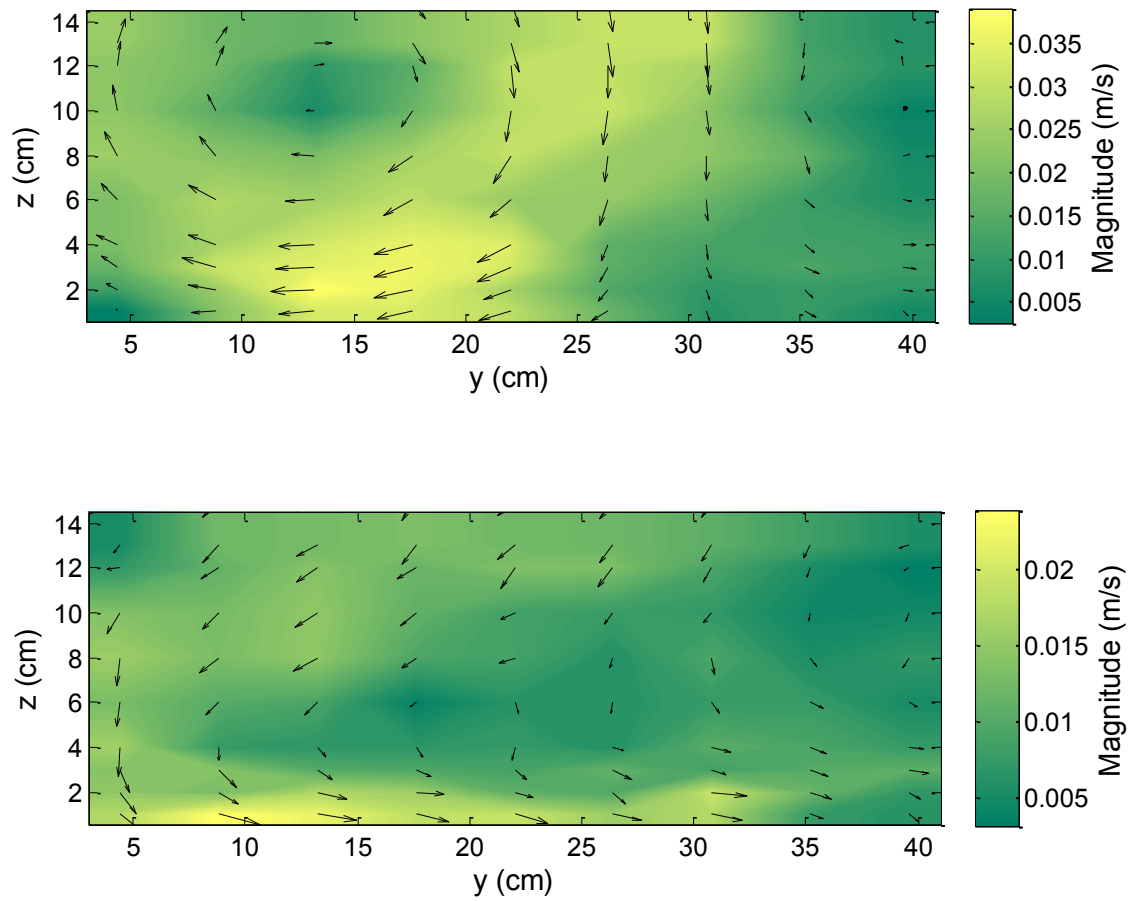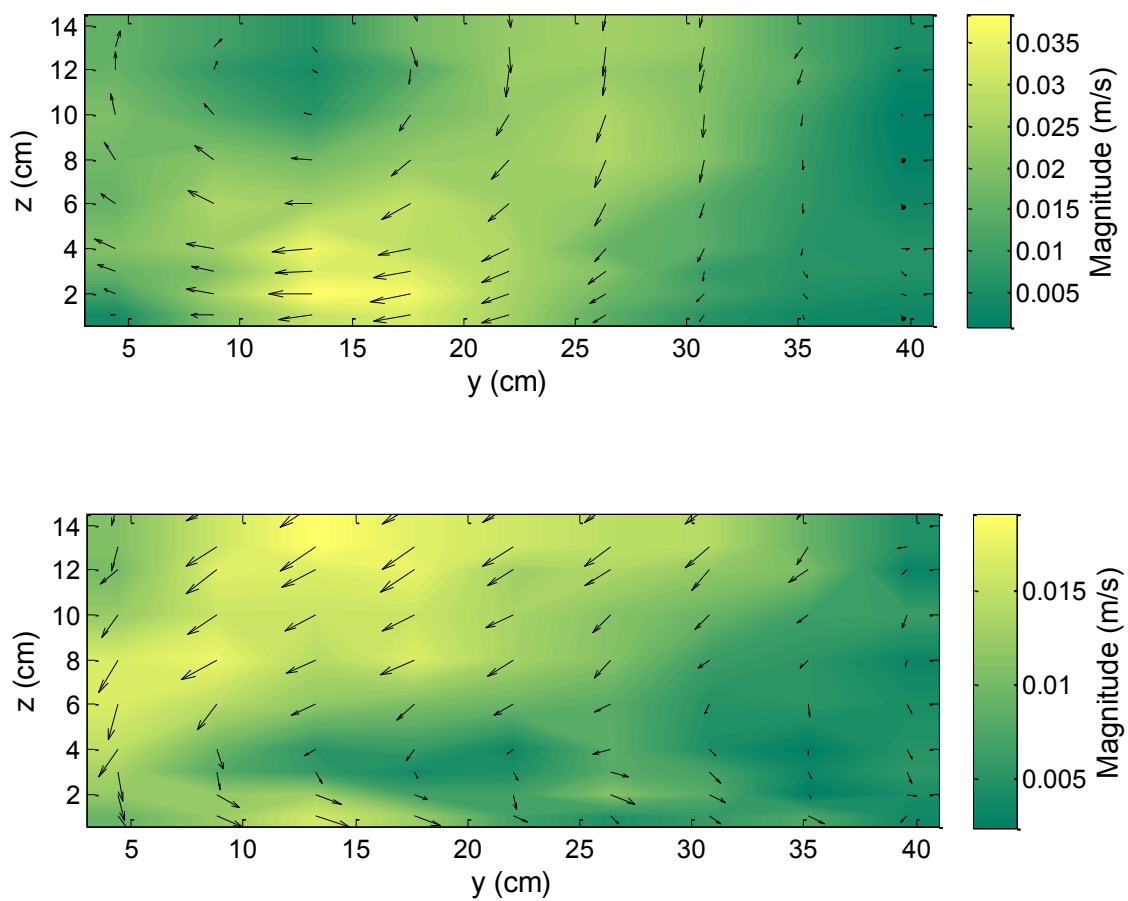
Figure 5-5.   Planar velocity vector fields obtained at 1.07 m downstream of the delta wing (top) and without delta wing (bottom) at the same location
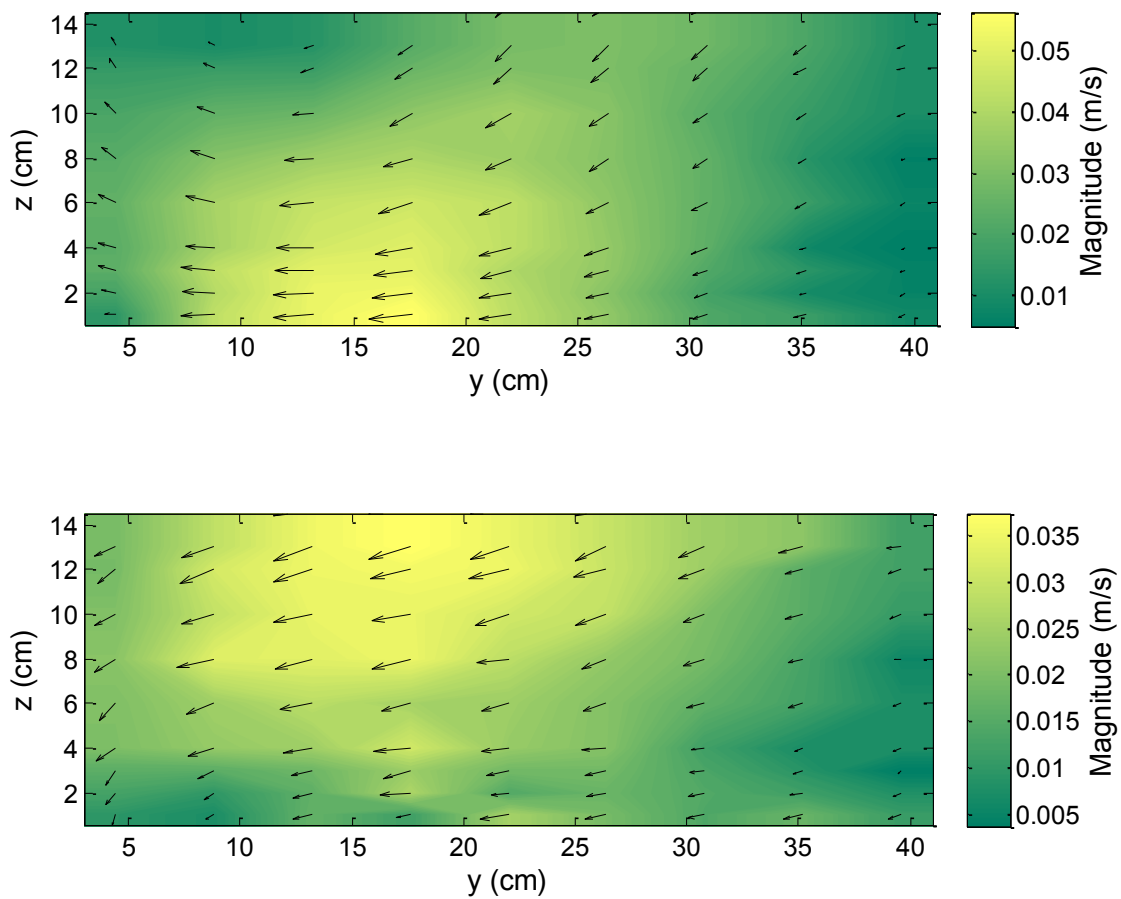
Figure 5-6.   Planar velocity vector fields obtained at 1.52 m downstream of the delta wing (top) and without delta wing (bottom) at the same location

Figure 5-7.   Planar velocity vector fields obtained at 2.29 m downstream of the delta wing (top) and without delta wing (bottom) at the same location

Figure 5-8.   Planar velocity vector fields obtained at 2.74 m downstream of the delta wing (top) and without delta wing (bottom) at the same location

Figure 5-9.   Planar velocity vector fields obtained at 2.99 m downstream of the delta wing (top) and without delta wing (bottom) at the same location
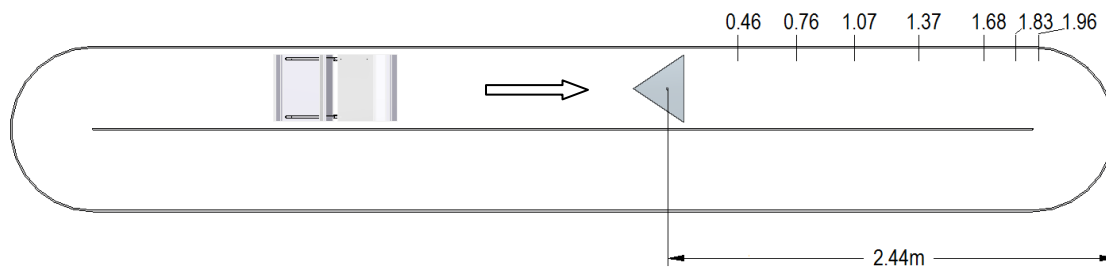
Figure 5-10.   Position of the delta wing in open channel relative to paddle wheel and measurement locations (in m) referenced from the centroid of the delta wing

Table 5-4.   Comparison of maximum vertical velocities for experiment set 2

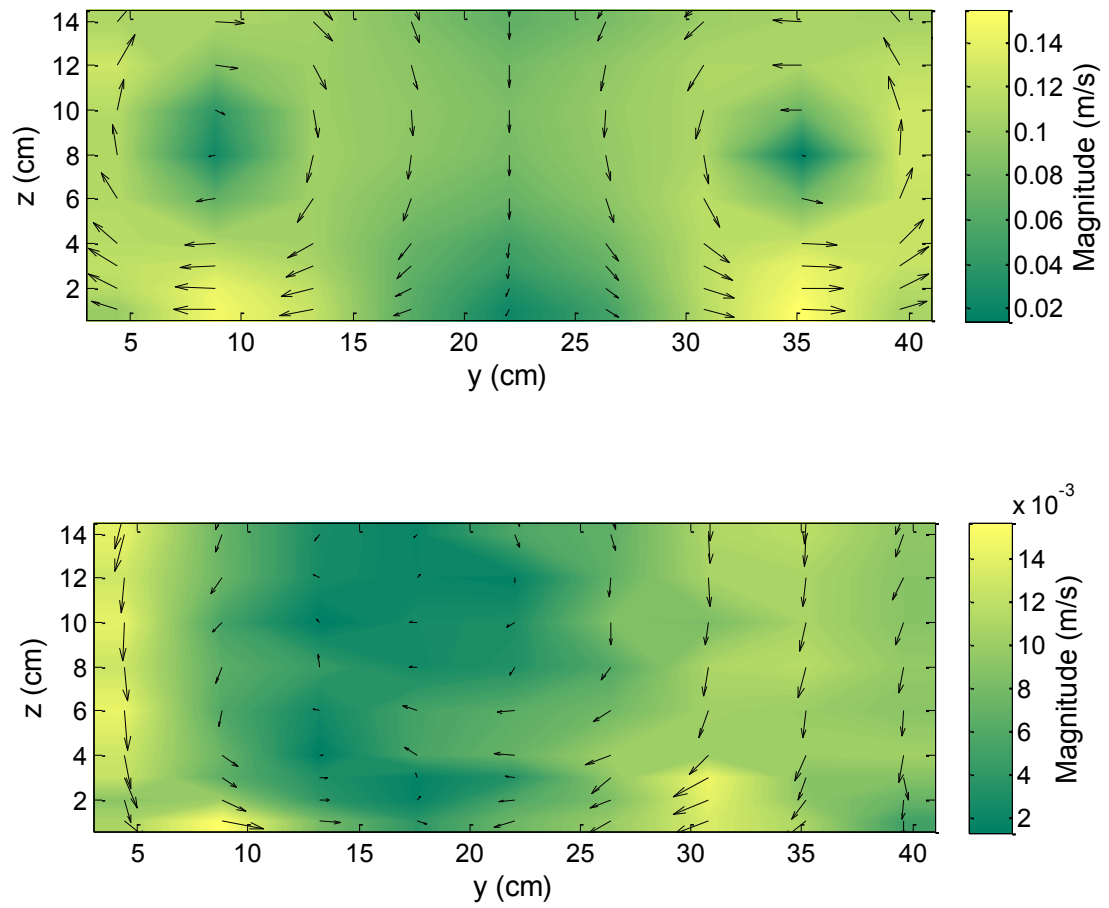| Distance (m)	Delta wing V_{max} (m/s)	Without delta wing V_{max} (m/s)
0.46	0.1281	0.0045
0.76	0.105	0.0021
1.07	0.0892	0.0006
1.37	0.0714	0.0004
1.68	0.0515	-0.0016
1.83	0.0436	0.0003
1.96	0.0441	0.003

Figure 5-11.   Planar velocity vector fields obtained at 0.46 m downstream of the delta wing (top) and without delta wing (bottom) at the same location
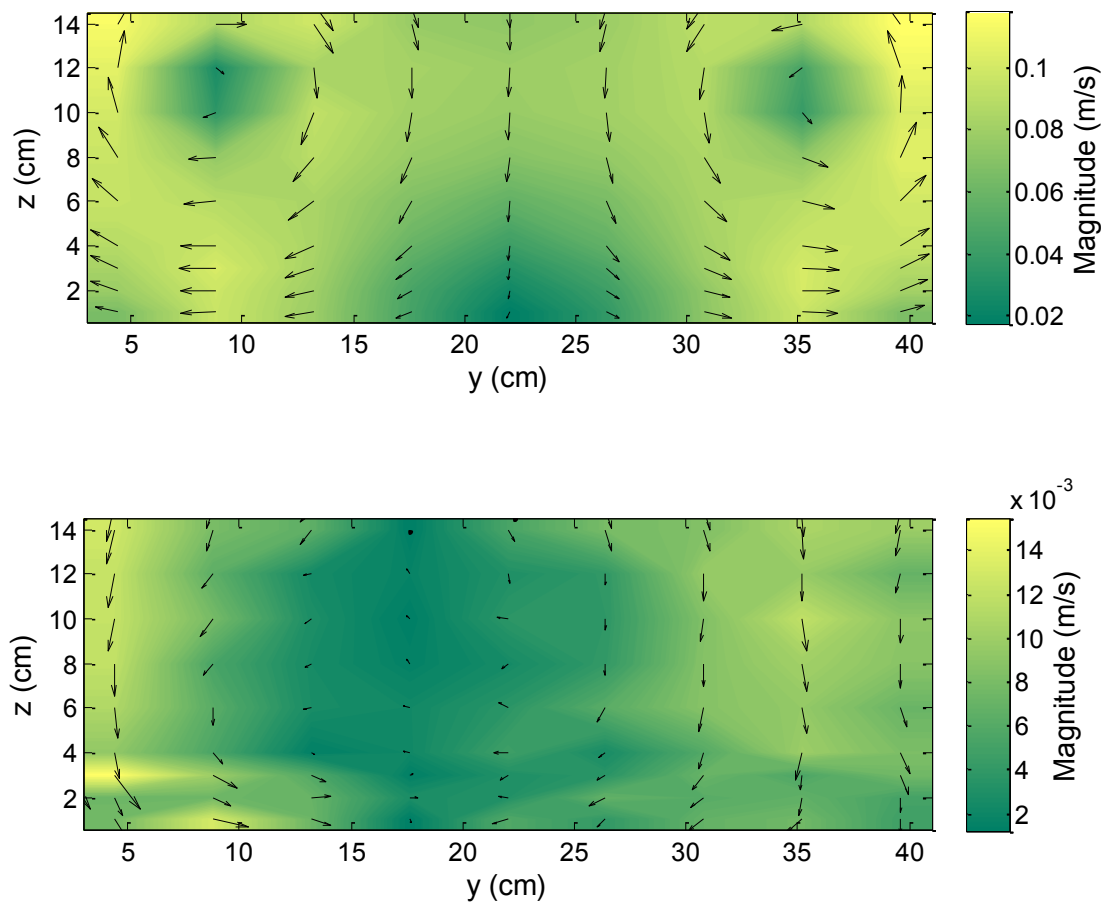
Figure 5-12.   Planar velocity vector fields obtained at 0.76 m downstream of the delta wing (top) and without delta wing (bottom) at the same location
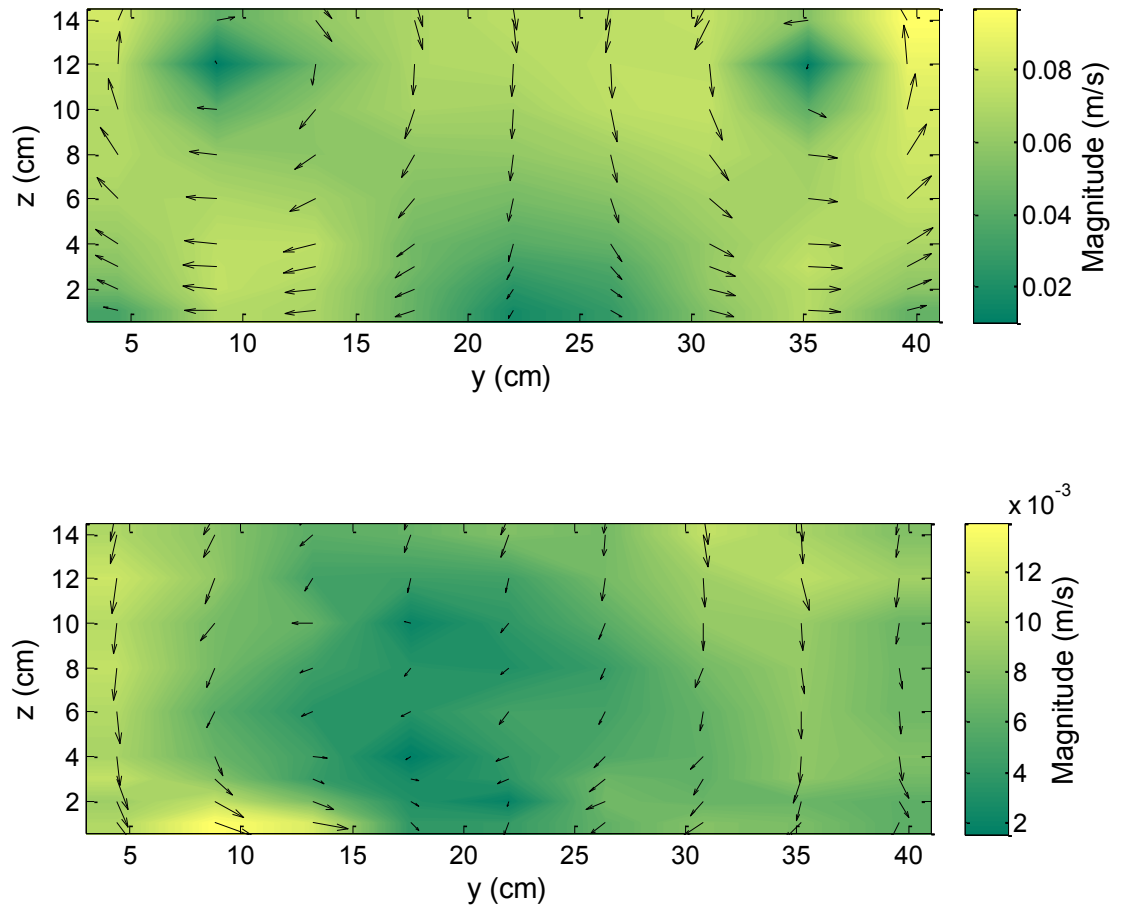
Figure 5-13.   Planar velocity vector fields obtained at 1.07 m downstream of the delta wing (top) and without delta wing (bottom) at the same location
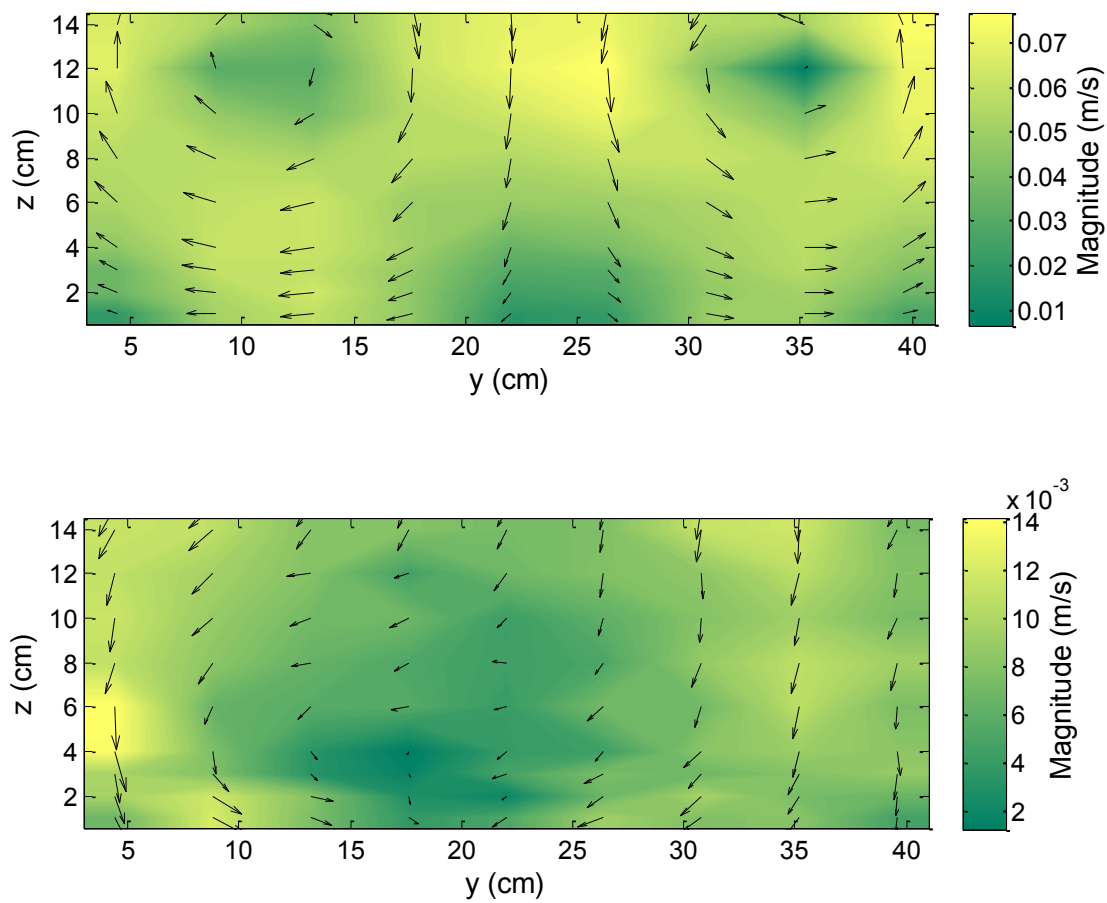
Figure 5-14.　Planar velocity vector fields obtained at 1.37 m downstream of the delta wing (top) and without delta wing (bottom) at the same location
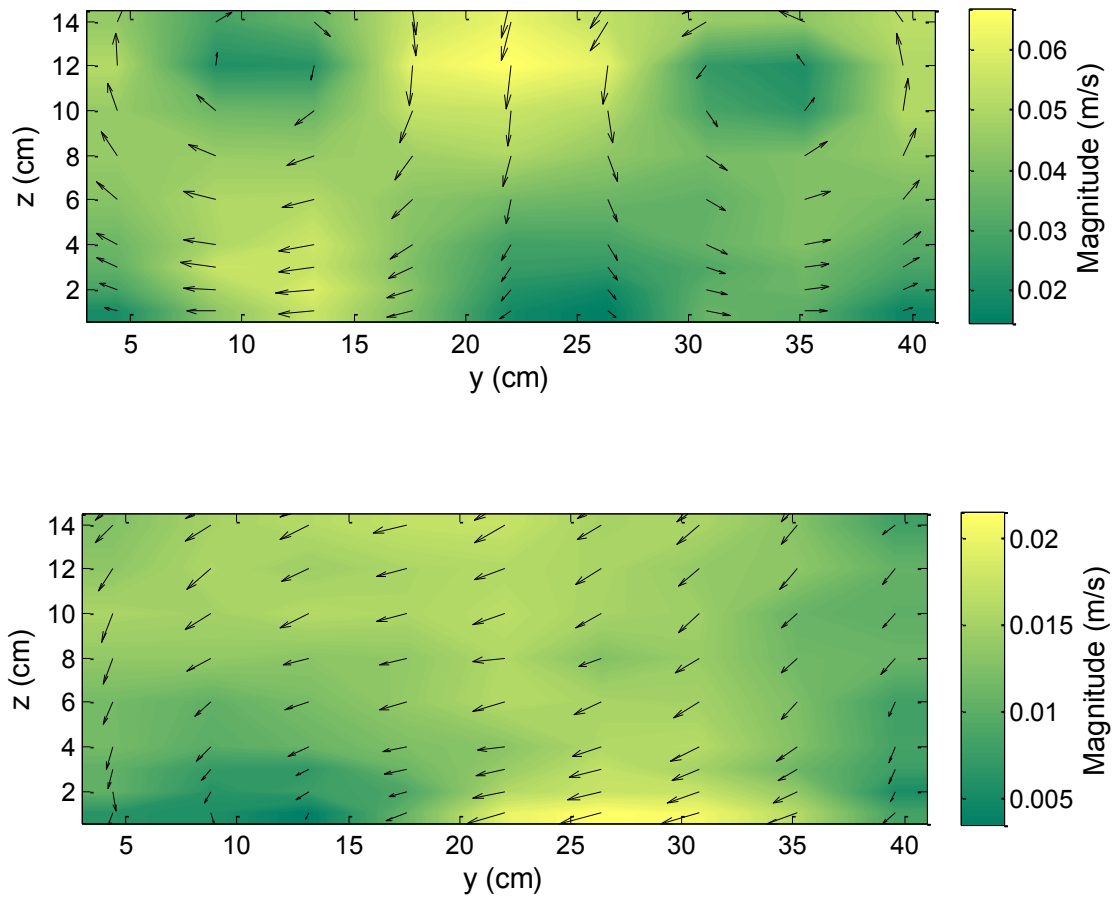
Figure 5-15.   Planar velocity vector fields obtained at 1.68 m downstream of the delta wing (top) and without delta wing (bottom) at the same location
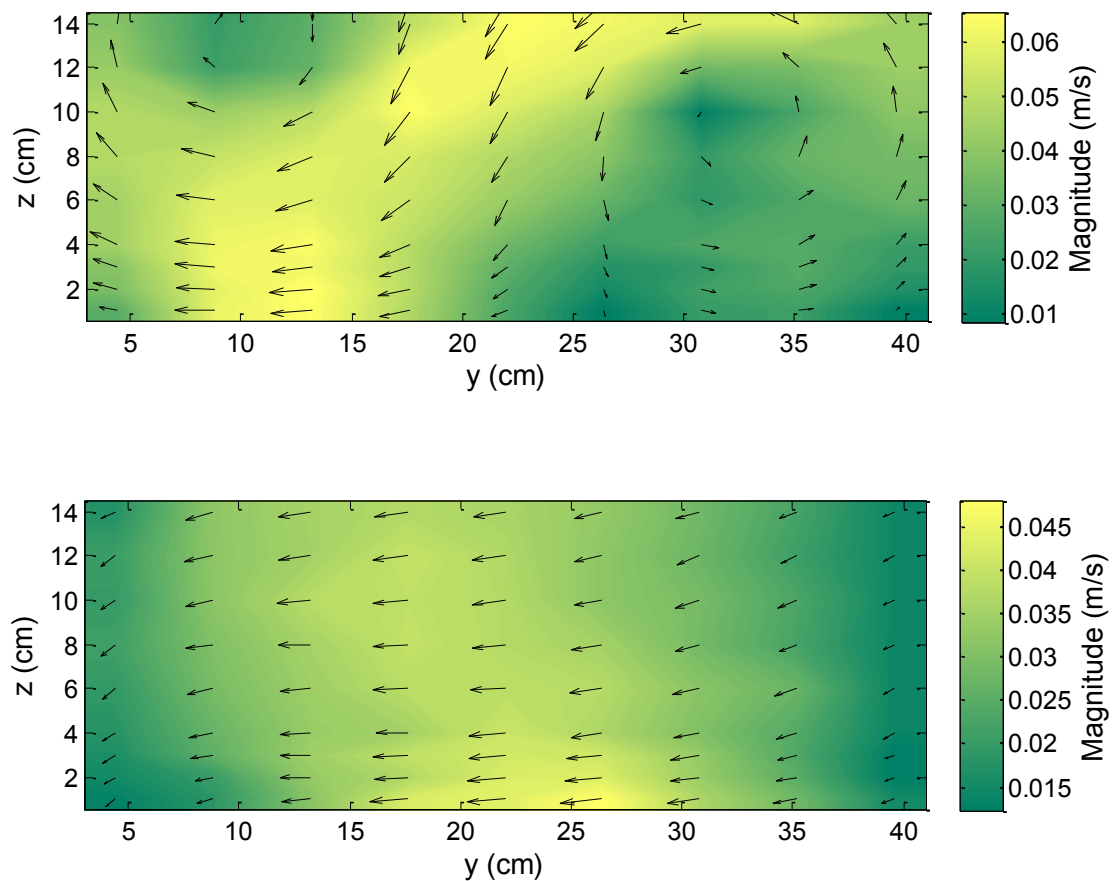
Figure 5-16. Planar velocity vector fields obtained at 1.83 m downstream of the delta wing (top) and without delta wing (bottom) at the same location
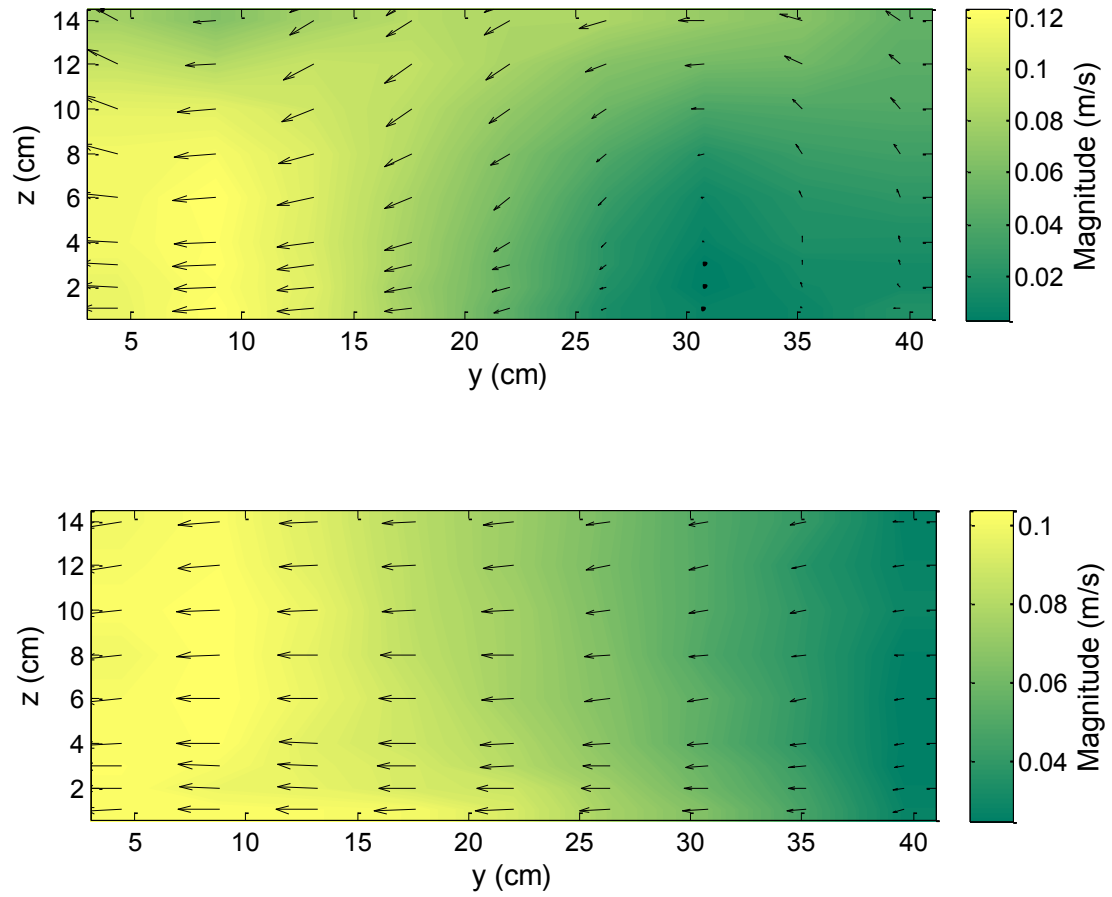
Figure 5-17.   Planar velocity vector fields obtained at 1.96 m downstream of the delta wing (top) and without delta wing (bottom) at the same location

5.2.3. Experiment Set 3

To study the effect of bends and the impact of vertical mixing, delta wing was placed close to the bend. Again the raceway with delta wing was operated at a paddle wheel speed of 11 RPM and without delta wing was operated at 11.5 RPM. The measurement locations are shown in Figure 5-18. Recirculation regions and dead zones were identified just after the 180° bends. Dead zones frequently develop after the bends because the change of direction can decrease the velocities near the divider. These dead zones lead to the settling of tracer particles (assume algae cells) in the raceway. It was theorized that several secondary flows takes place in the bend due to the inward flow near the bend and the outward flow near the surface. Stagnation regions in the raceway were also observed at some locations near to the divider indicating the poor hydraulics. These findings indicated that the hydraulics of the raceway ponds is critical to obtain even mixing. It was suggested that the use of flow deflectors around the 180° bends eliminates the cross flows, dead zones and straighten the flow in the open channel raceway [4].
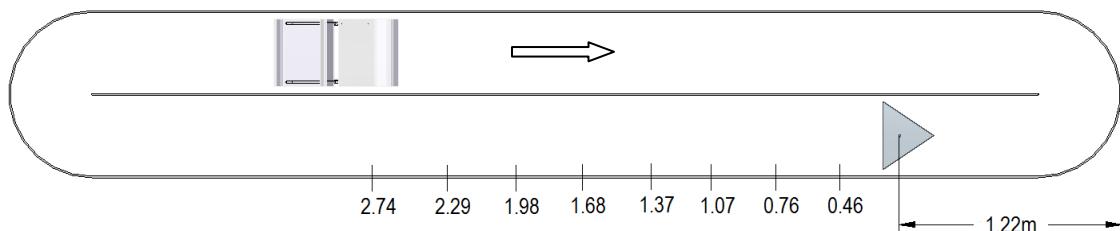

Figure 5-18.   Position of the delta wing in open channel and measurement locations (in m) referenced from the centroid of the delta wing

The maximum vertical velocities with and without delta wing in the raceway are shown in Table 5-5. A 5-fold increase in vertical velocities was observed for the raceway with delta wing. It was found that the maximum vertical velocities for the raceway without delta wing were high compared to the previous experiments probably due to the high velocity region immediately after the bend. Considering a small region, this indicates that the bends help in vertical motion of algae to some extent. Figures 5-19 to 5-26 show the planar velocity vector fields with and without delta wing in the raceway. It was clearly observed that the vortices broke down and started to dissipate further downstream of the delta wing. From a close observation of all the planar velocity vector fields obtained by ADV, it was found that the vortices generated by the delta wing in the raceway were sustained for a distance of around 3 m downstream of the delta wing.

Table 5-5. Comparison of maximum vertical velocities for experiment set 3

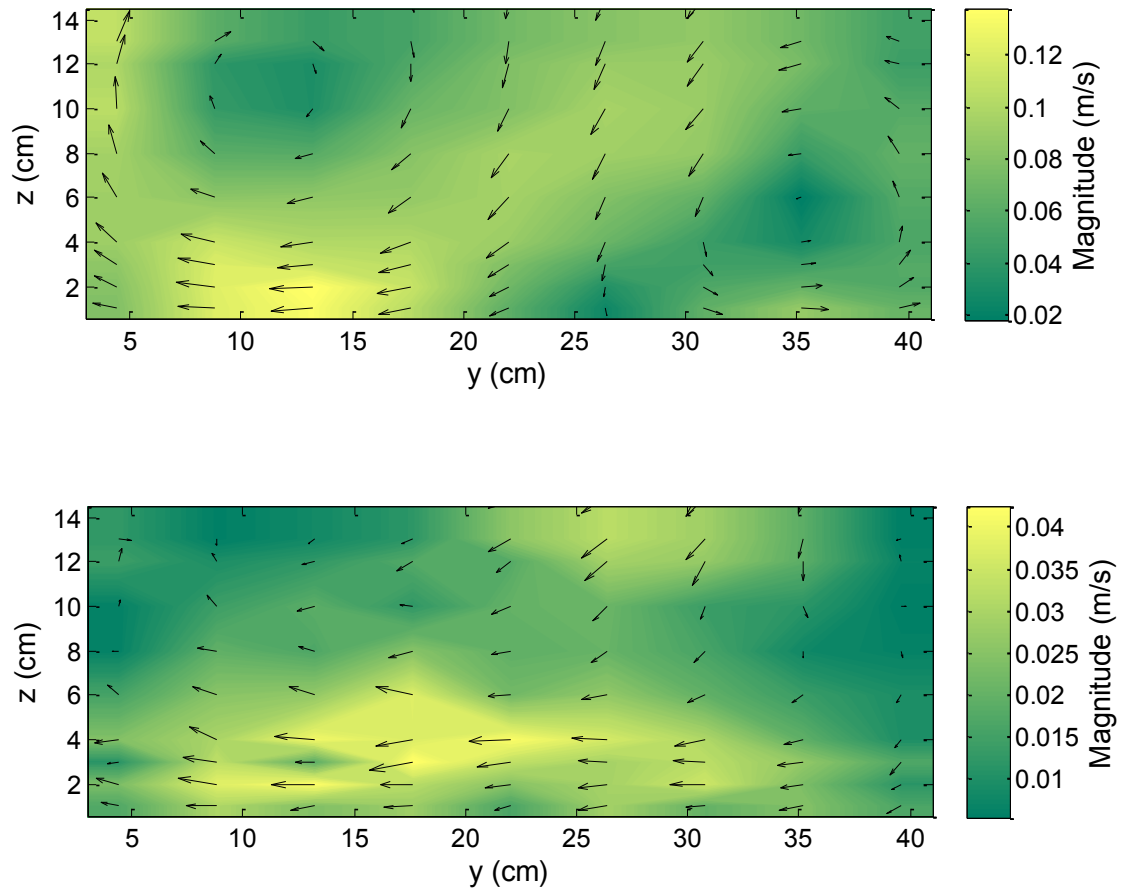| Distance (m)	Delta wing V_{max} (m/s)	Without delta wing V_{max} (m/s)
0.46	0.1056	0.0139
0.76	0.0663	0.0108
1.07	0.0482	0.0143
1.37	0.0312	0.0049
1.68	0.0201	0.0047
1.98	0.0142	0.0035
2.29	0.0112	0.0019
2.74	0.0056	0.0045

Figure 5-19.   Planar velocity vector fields obtained at 0.46 m downstream of the delta wing (top) and without delta wing (bottom) at the same location

Figure 5-20.   Planar velocity vector fields obtained at 0.76 m downstream of the delta wing (top) and without delta wing (bottom) at the same location

Figure 5-21. Planar velocity vector fields obtained at 1.07 m downstream of the delta wing (top) and without delta wing (bottom) at the same location
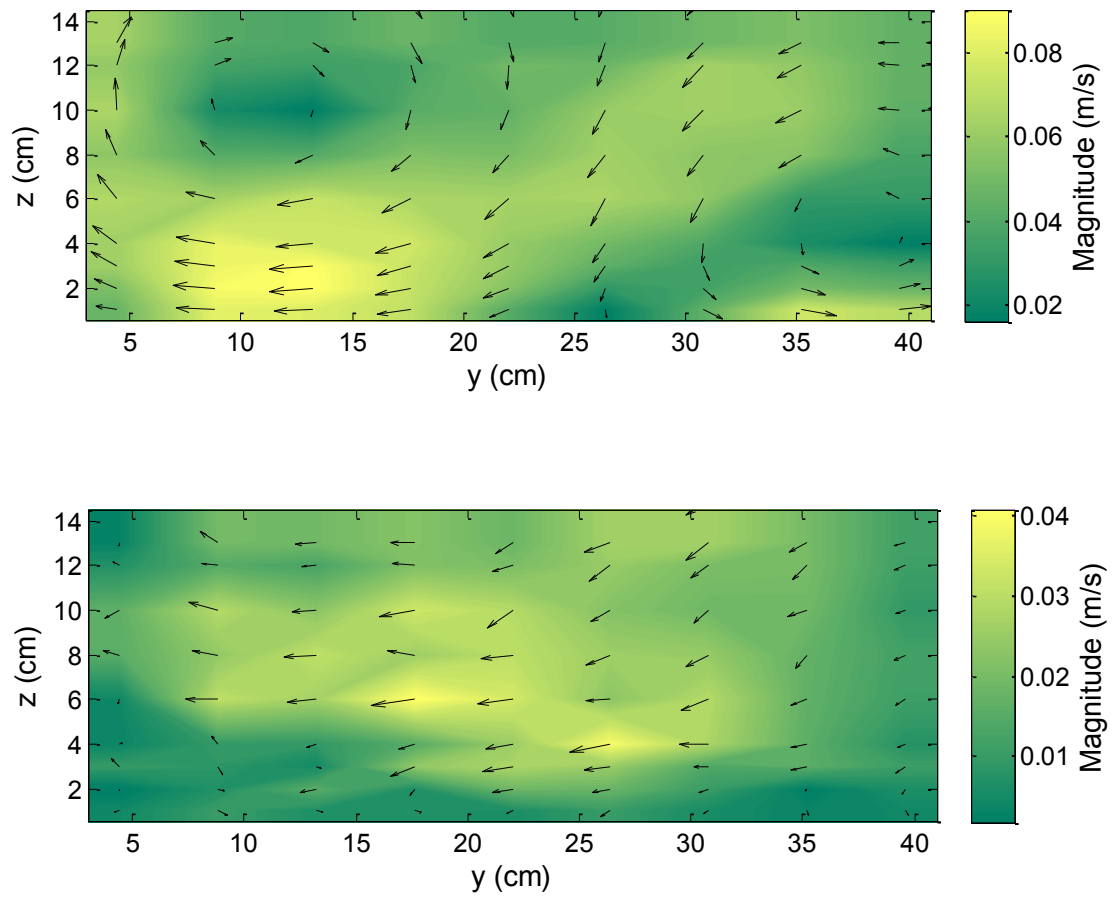
Figure 5-22.   Planar velocity vector fields obtained at 1.37 m downstream of the delta wing (top) and without delta wing (bottom) at the same location
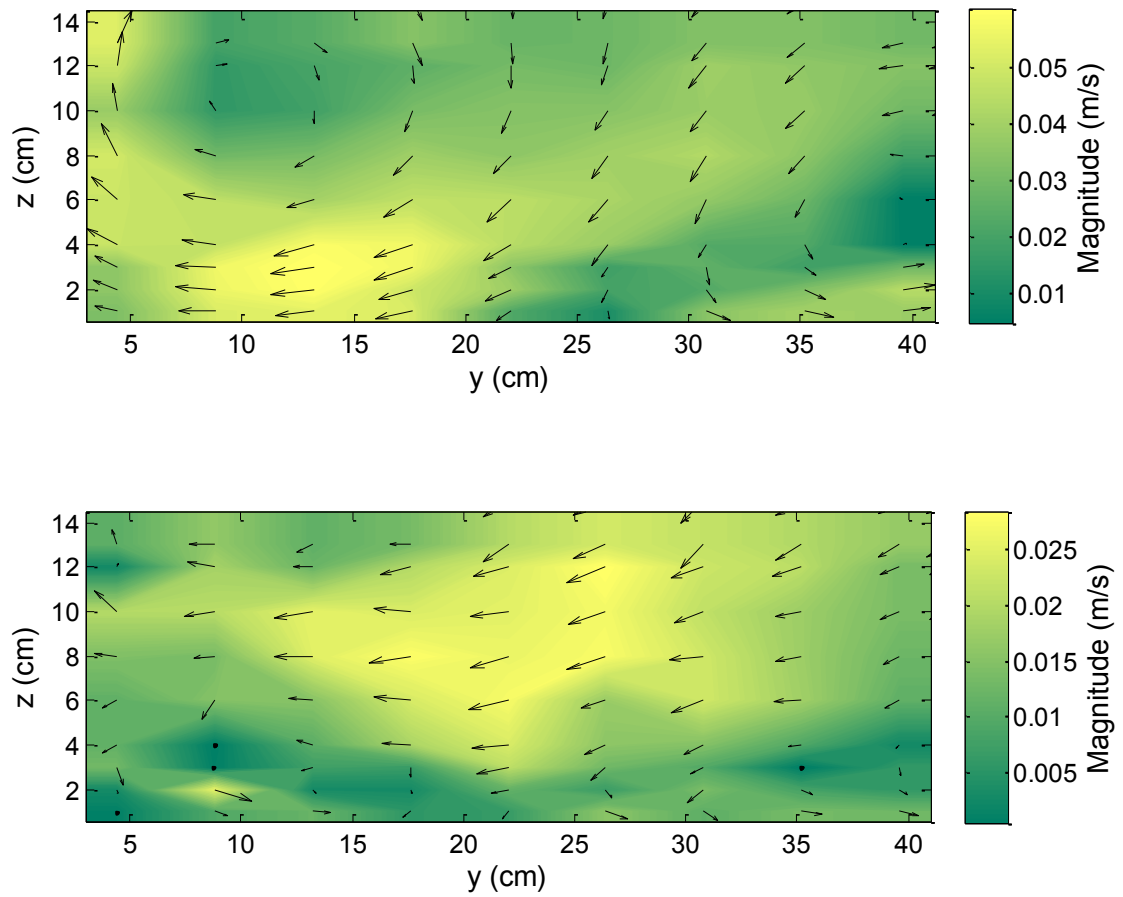
Figure 5-23. Planar velocity vector fields obtained at 1.68 m downstream of the delta wing (top) and without delta wing (bottom) at the same location
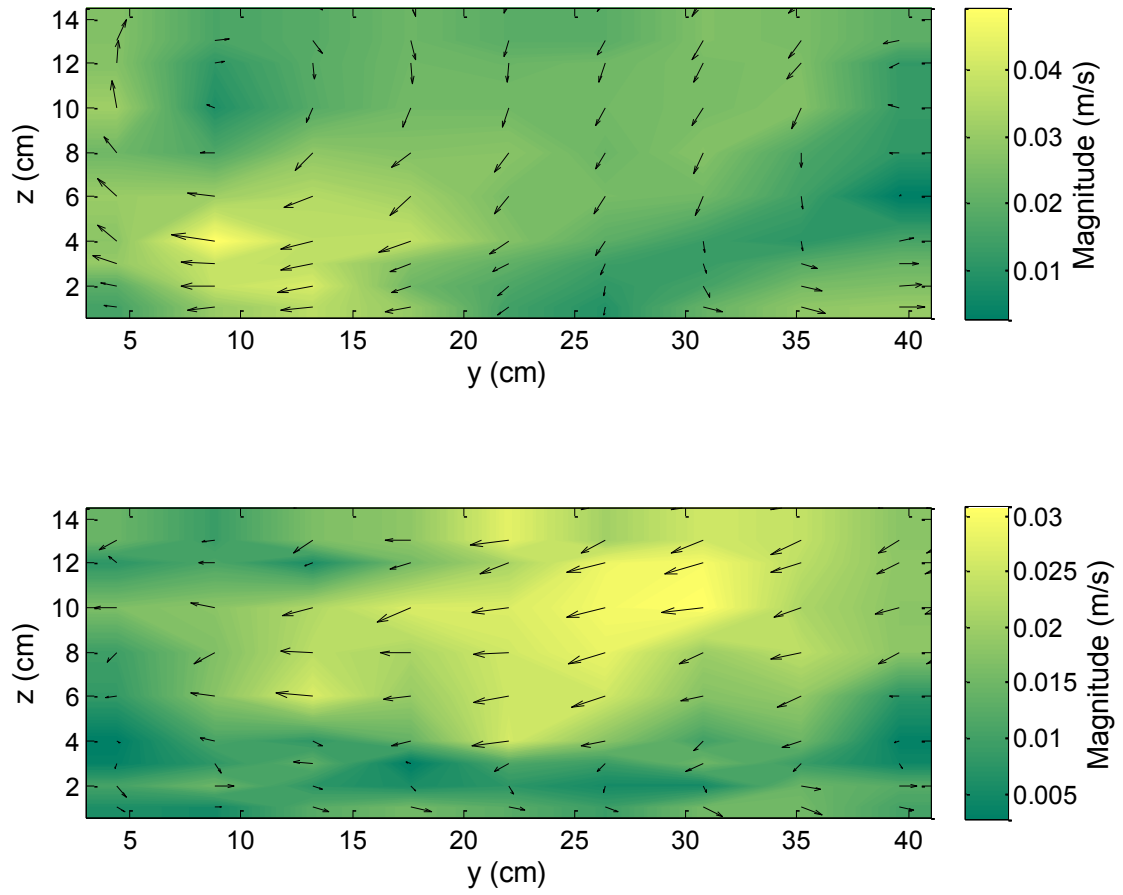
Figure 5-24.   Planar velocity vector fields obtained at 1.98 m downstream of the delta wing (top) and without delta wing (bottom) at the same location

Figure 5-25.   Planar velocity vector fields obtained at 2.29 m downstream of the delta wing (top) and without delta wing (bottom) at the same location

Figure 5-26.   Planar velocity vector fields obtained at 2.74 m downstream of the delta wing (top) and without delta wing (bottom) at the same location
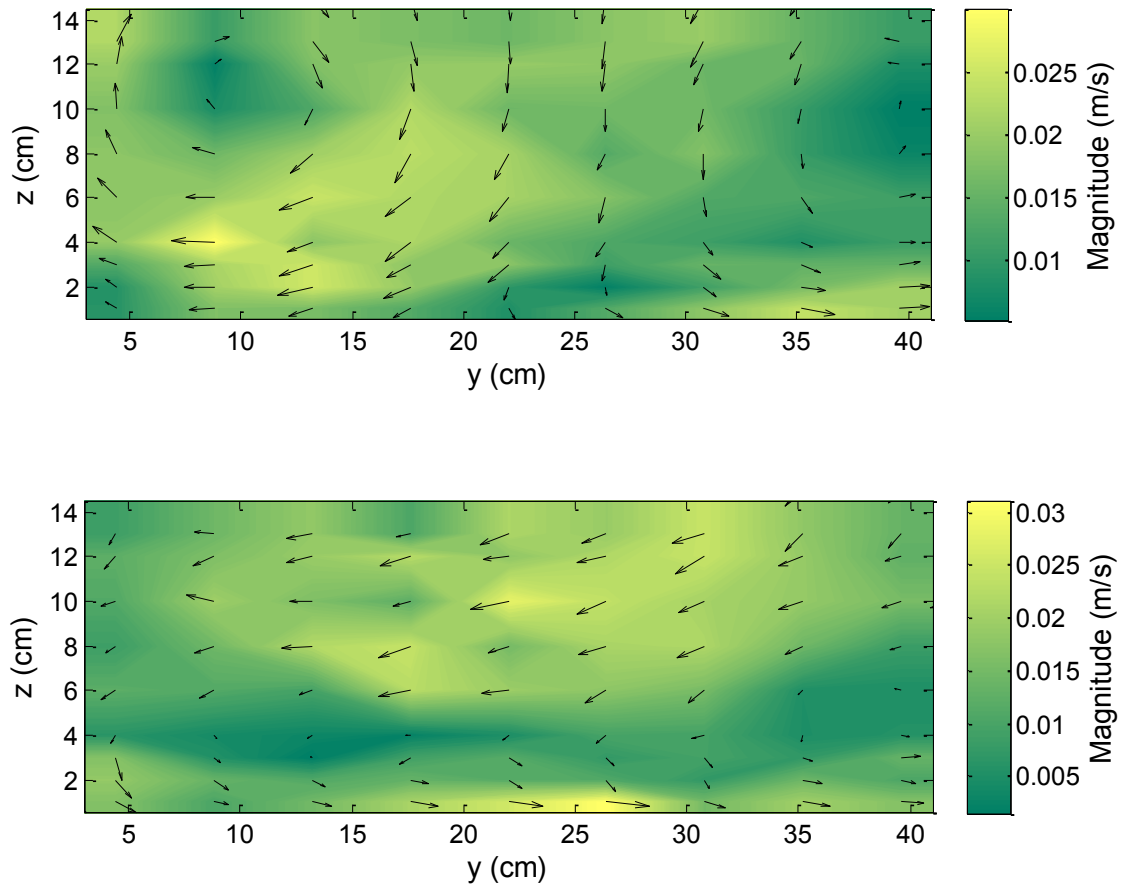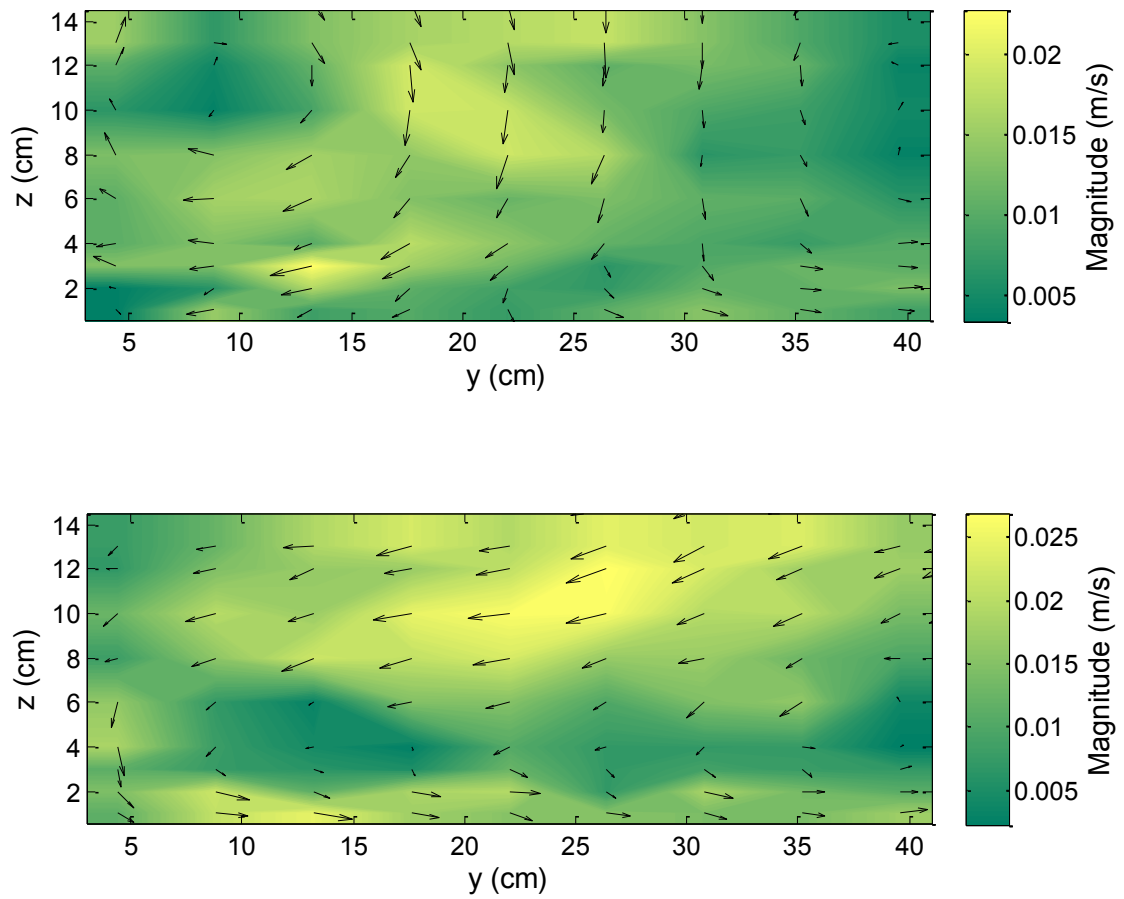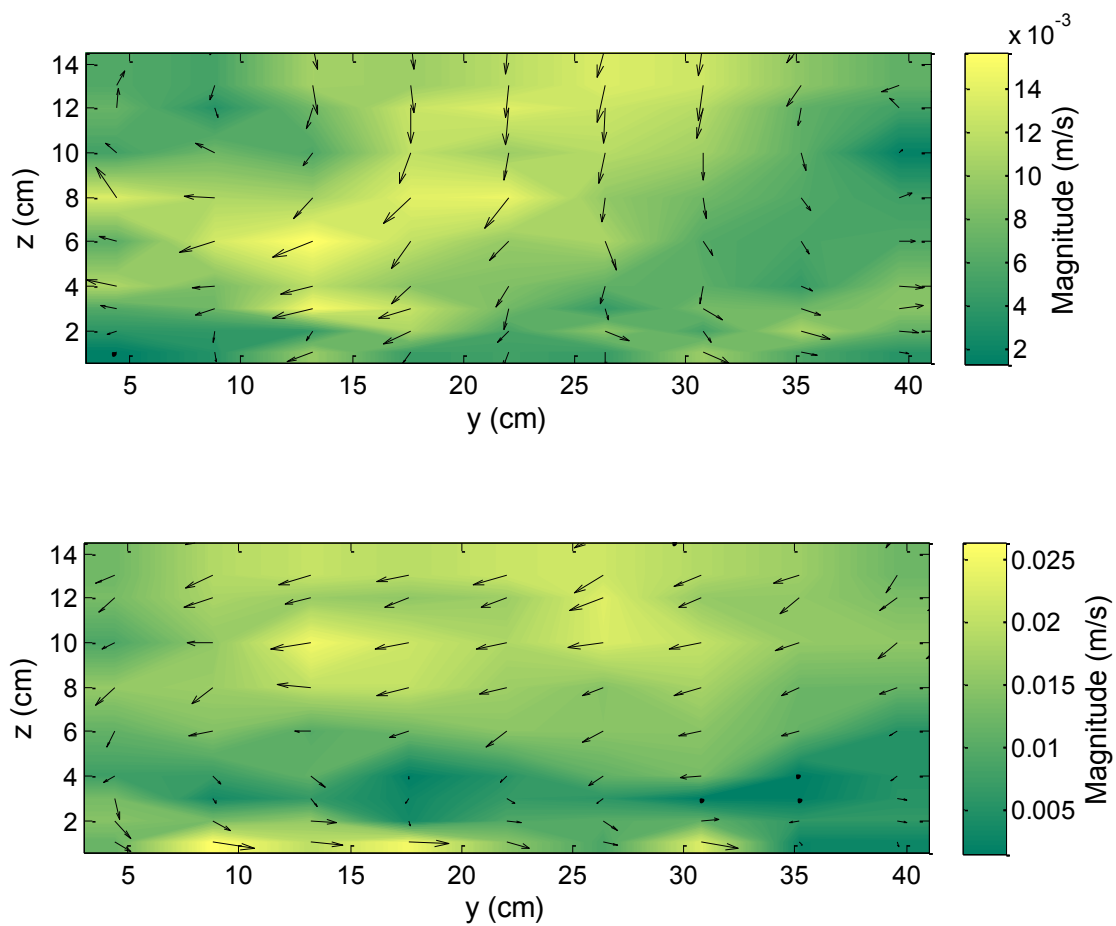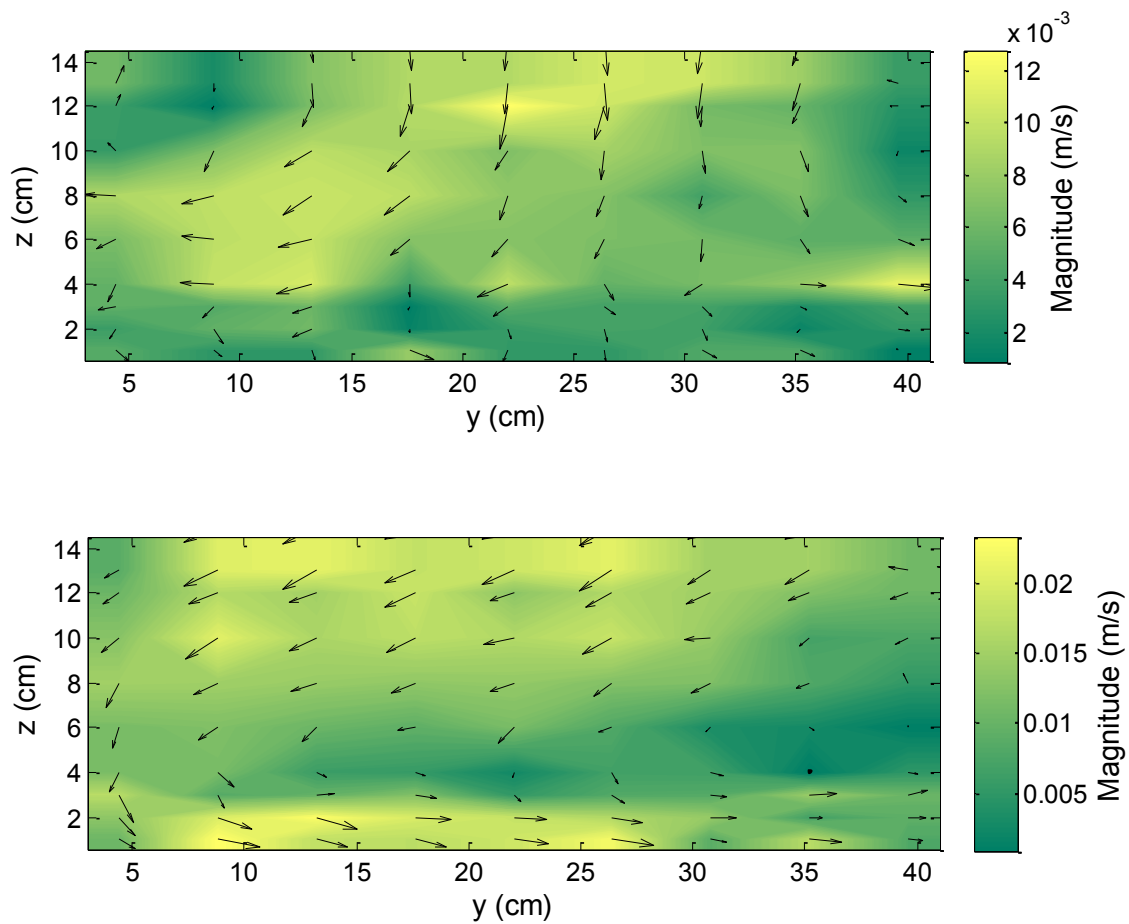
5.3. Quantification of Vertical Mixing

Although the comparisons of maximum vertical velocities and planar velocity vector fields revealed the impact of vertical mixing, effort was made to quantify this phenomenon using vertical mixing index and turbulence dissipation rates and scales. The obtained results were presented below.

5.3.1. Vertical Mixing Index Results

A parameter should be needed to quantify the vertical mixing behavior in the raceway. Vertical Mixing Index (VMI) was termed and used to compare the mixing relationships with and without delta wing in the raceway. The positive and negative vertical velocity components in the plane downstream of the delta wing cancel each other due to the formation of counter rotating vortices in the raceway. Hence, a normalized parameter for vertical mixing (in %) was defined using the following equations

$$W_A = \left(\sum_{i=1}^{p} |W_p| \right) \Big/ s \tag{5.1}$$

$$VMI = 100\% \frac{W_A}{U_A} \tag{5.2}$$

where p is the grid point, $|W_p|$ is the absolute value of the vertical velocity at each grid point, s is the number of grid points, VMI is the vertical mixing index, W_A is the average of the absolute value of vertical velocities at a section, and U_A is the average of the streamwise velocities at a section.

If the VMI is greater than 0%, this indicates the presence of vertical mixing and/or sinking of algae cells within the raceway. A VMI equal to 0% suggests that the

algae cells settle towards the bottom and form sediments. The VMI provides quantitative information of these two opposing processes *i.e.* rising and sinking of algae cells. The effects of mixing and sinking cannot be separated and that the VMI value can represent rising cells for the light source or cells sinking which have adapted to the dark cycles [34].

The VMI relationships with respect to distance referenced from the centroid of the delta wing are shown in Figure 5-27 to Figure 5-29. It was observed that the averaged VMI for the raceway without delta wing was around 2%. It was found that the expanded uncertainty for VMI was ±0.3% at a 95% level of confidence. An averaged VMI of 10%, 14.5%, and 7.5% were reported for the raceway with delta wing in the experiment sets 1, 2 and 3 respectively. The low VMI in the experiment set 3 was postulated due to the effect of secondary flows on the delta wing close to the bend. An exponential decay of VMI was observed for the delta wing case in all the set of experiments. As seen from the plots, the VMI decreased with the downstream distance of the delta wing in the raceway and approached towards the condition without delta wing at a distance of around 3 m for experiment set 1 and 2.5 m for experiment set 3. Due the effects of 180° bends, it was considered that the experimental raceway was not long enough to investigate the sustainability of the longitudinal streamwise vortices downstream of the delta wing.

The VMI results were promising for the raceway with delta wing showing the importance of vertical mixing or circulation of the algae cells.
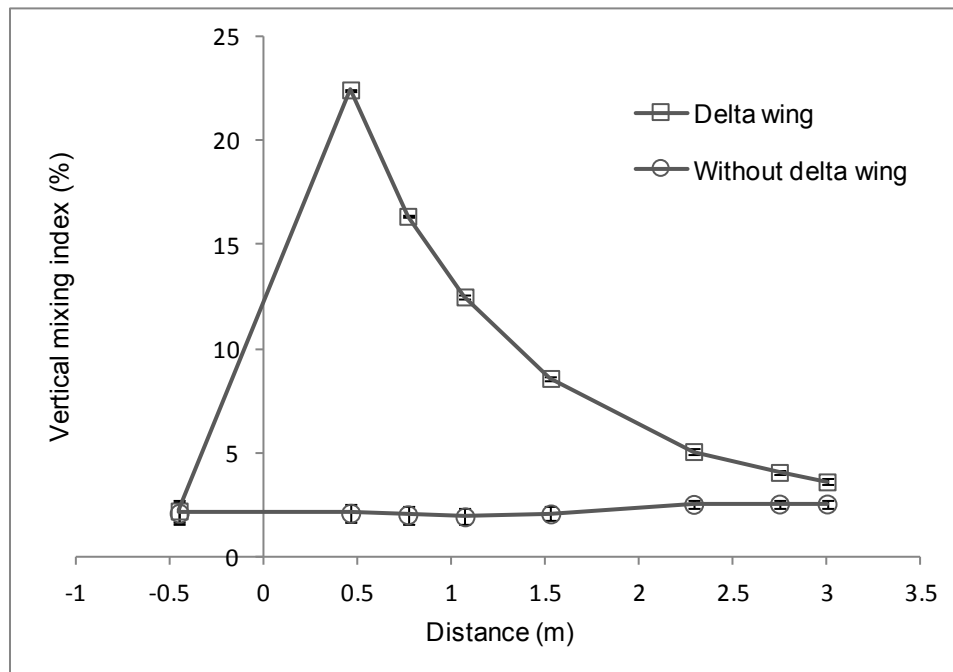
72

Figure 5-27.   Comparison of vertical mixing index for experiment set 1
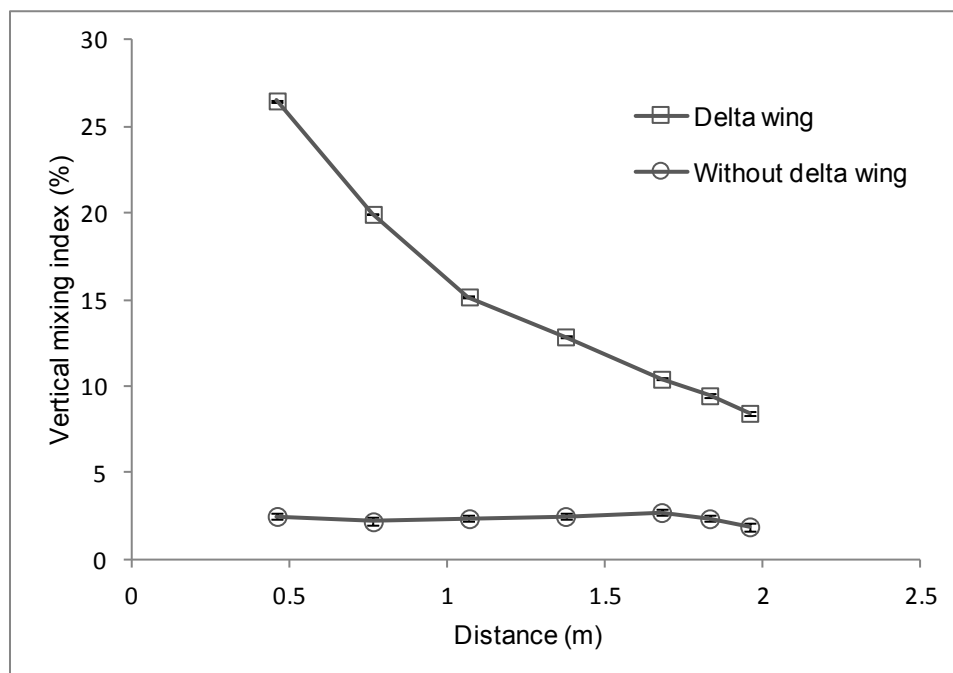

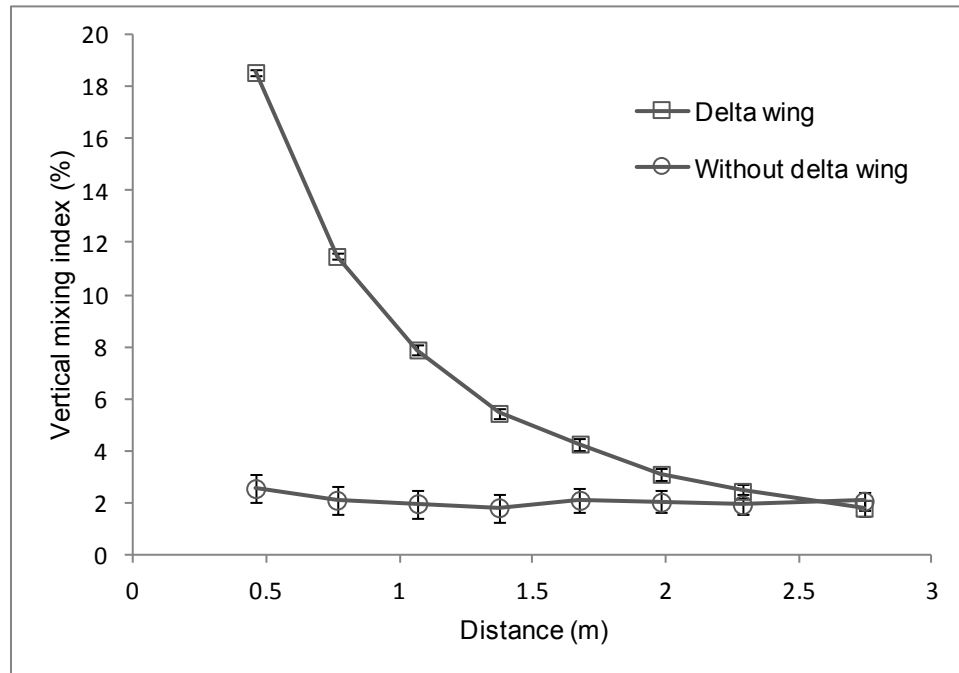Figure 5-28.   Comparison of vertical mixing index for experiment set 2

Figure 5-29.   Comparison of vertical mixing index for experiment set 3

5.3.2.   Turbulence Dissipation Rates and Scales

The results obtained so far supported the vertical mixing intensity due to the presence of large-scale fluid motions or large-scale eddies (vortices) in the raceway. In order to study small-scale turbulence in the raceway, turbulence dissipation rates (ε) were estimated to compare with the published literature. The power spectral density-frequency plots were computed from each velocity record on the grid and a -5/3 slope was fitted to identify the inertial subrange using a power law on the log-log plot. The vertical velocity component was chosen, since the noise level rarely exceeds the turbulent fluctuations when compared to the other two components. A typical example of the frequency based velocity spectra obtained at a point in the plane with and without delta wing are shown in Figure 5-30 and Figure 5-31, respectively.
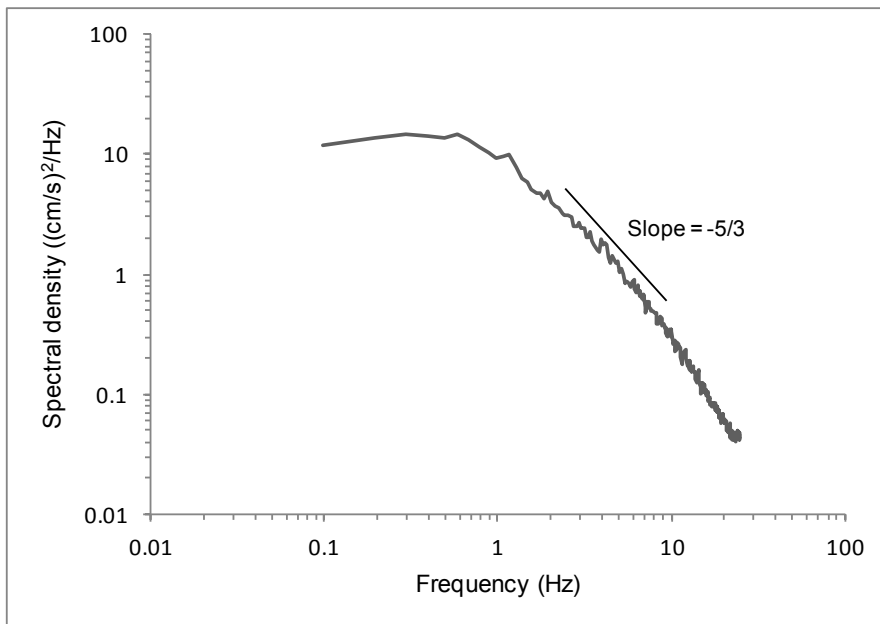
Figure 5-30.   Power spectral density log-log plot of the vertical fluctuating velocity component obtained at a point with delta wing
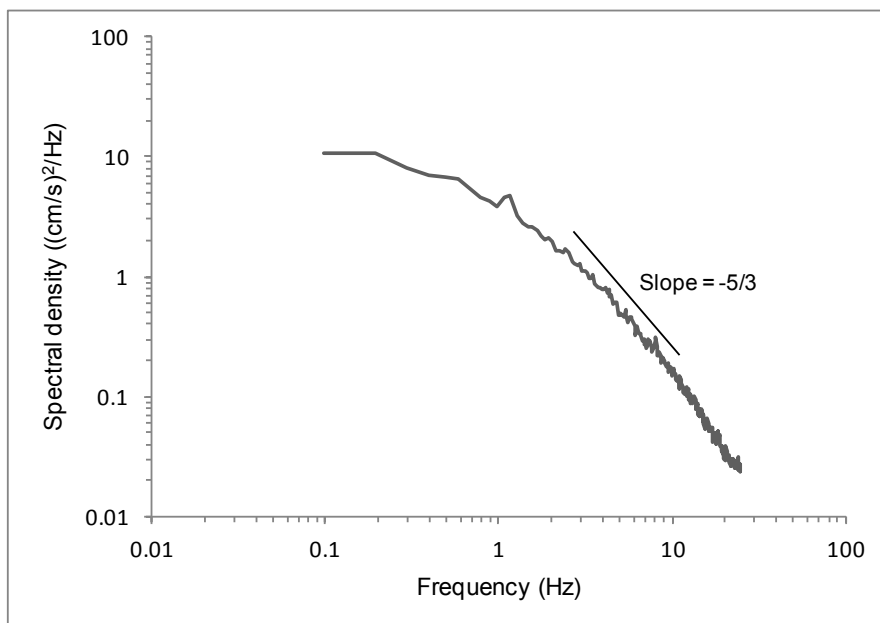

Figure 5-31.   Power spectral density log-log plot of the vertical fluctuating velocity component obtained at the same point without delta wing

In both examples, the spectra with delta wing show higher energy levels than the spectra without delta wing in the raceway. To compare agreement in the inertial subrange with the Kolmogorov -5/3 law, lines at a -5/3 slope are clearly marked on the spectral plots (typically between the frequencies of 2 and 10 Hz). Turbulence dissipation rates were estimated from the magnitude of the frequency spectra in the inertial subrange. Power spectral density $S(f)$ of the measured velocity time series data that deviate significantly from the -5/3 slope was excluded from the analysis. Turbulence dissipation rate at each plane or section was obtained from averaging the estimated turbulence rates at each grid point.

The averaged turbulence dissipation rates were plotted against the downstream distance of the delta wing for experiment set 1 and 2, as shown in Figure 5-32 and Figure 5-33, respectively. The turbulence dissipation rates with delta wing in the raceway were higher by 7-fold and 2-fold compared to the raceway without delta wing for experiment set 1 and 2, respectively. Dissipation rates were higher close to the delta wing due to strong vortices. As the vortices dissipate downstream of the delta wing an exponential decay of turbulence dissipation rate was clearly observed. It was also observed in Figure 5-32 that the turbulence dissipation rate of the delta wing in the raceway decreased and approached towards the condition without delta wing at a distance of around 3 m. Turbulence dissipation rates were not estimated for the experiment set 3 due to the violation of Taylor's frozen turbulence hypothesis ($u'/U \ll 1$) at the recirculation or dead zones near the bend.
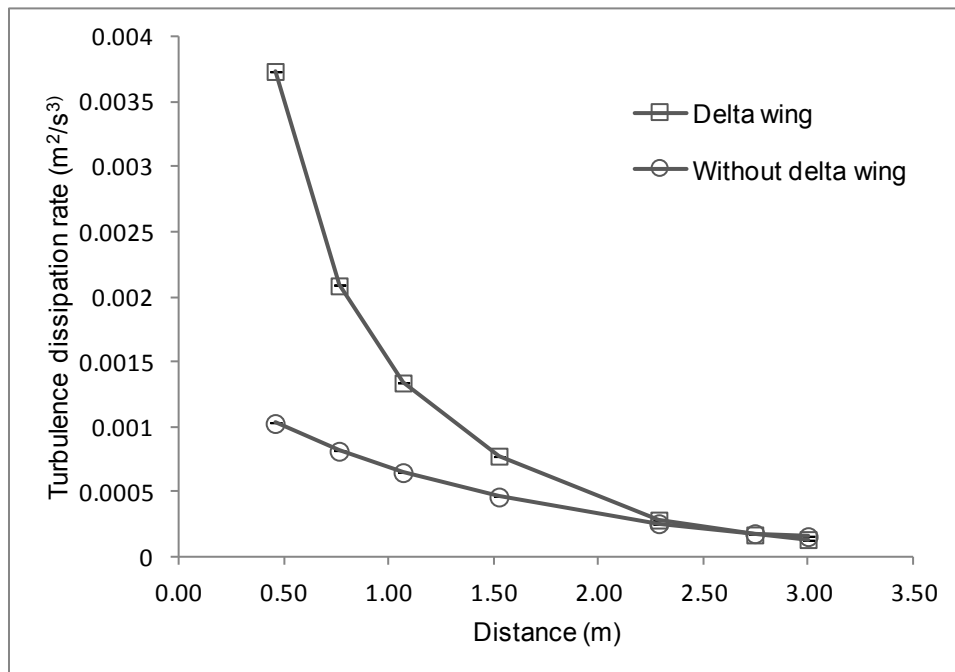
Figure 5-32.   Comparison of averaged turbulence dissipation rates for experiment set 1
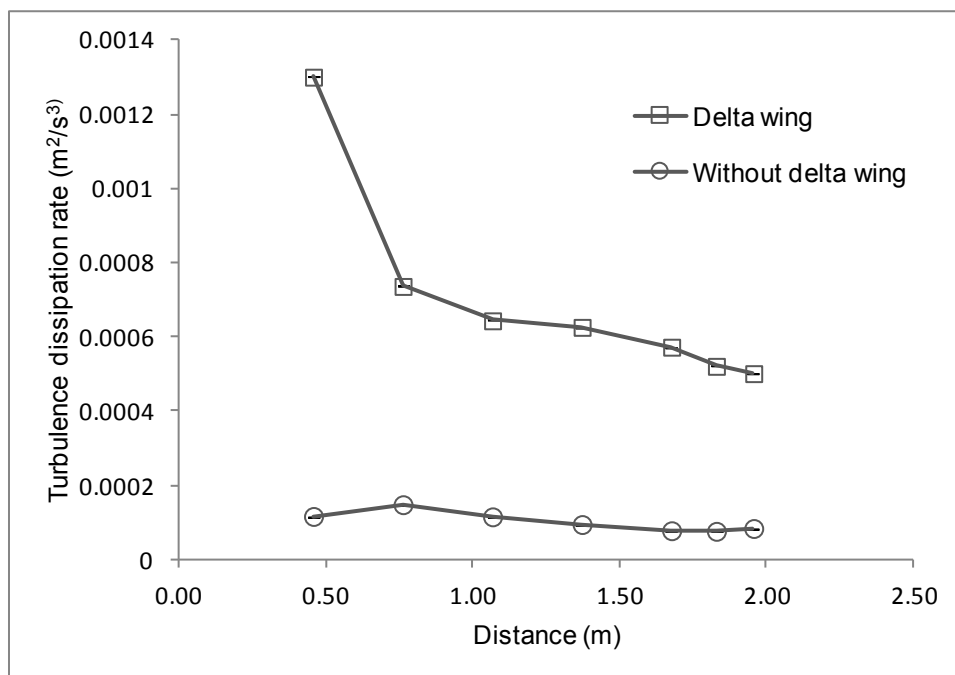

Figure 5-33.   Comparison of averaged turbulence dissipation rates for experiment set 2

The turbulence dissipation rates estimated in this research were checked with the published data in open channel turbulent flow measured by ADV and were in agreement with each other [31]. The averaged turbulence dissipation rates and Kolmogorov length scales at the measurement locations of experiment set 1 and 2 are shown in Table 5-6 and Table 5-7 respectively. The Kolmogorov length scale determines the size of the smallest turbulent eddy in the fluid. The Kolmogorov length scales with delta wing and without delta wing in the raceway were around 120 to 340 μm. Algae typically range in size from 10 to 50 μm. Therefore, algae cells are smaller than the size of the smallest turbulent eddies. It was hypothesized that these small-scale fluid motions can enhance the exchange rate between the algae cells and its environment.

Table 5-6.   Averaged turbulence dissipation rates and Kolmogorov length scales for experiment set 1

Distance (m)	Delta wing ε (m^2/s^3)	Kolmogorov length scale η (μm)	Without delta wing ε (m^2/s^3)	Kolmogorov length scale η (μm)
0.46	3.7×10^{-3}	128	10^{-3}	177
0.76	2.1×10^{-3}	149	8.1×10^{-4}	188
1.07	1.3×10^{-3}	166	6.5×10^{-4}	199
1.52	7.8×10^{-4}	190	4.6×10^{-4}	217
2.29	2.8×10^{-4}	245	2.5×10^{-4}	251
2.74	1.7×10^{-4}	279	1.8×10^{-4}	275
2.99	1.3×10^{-4}	296	1.5×10^{-4}	284
Average	1.2×10^{-3}	207	5×10^{-4}	227

Table 5-7. Averaged turbulence dissipation rates and Kolmogorov length scales for experiment set 2

Distance (m)	Delta wing ε (m^2/s^3)	Kolmogorov length scale η (μm)	Without delta wing ε (m^2/s^3)	Kolmogorov length scale η (μm)
0.46	1.3×10^{-3}	167	1.2×10^{-4}	306
0.76	7.4×10^{-4}	193	1.5×10^{-4}	288
1.07	6.4×10^{-4}	199	1.2×10^{-4}	306
1.37	6.3×10^{-4}	201	9.5×10^{-5}	322
1.68	5.7×10^{-4}	205	7.8×10^{-5}	338
1.83	5.2×10^{-4}	210	7.6×10^{-5}	340
1.96	5×10^{-4}	212	8.4×10^{-5}	332
Average	7×10^{-4}	198	10^{-4}	319

The turbulence dissipation rates obtained for the raceway were compared with the literature and are shown in Table 5-8. The turbulence dissipation rates reported for the raceway with and without the delta wing are higher than the dissipation rates presented in the literature review and published research. However, it is clear from the literature review that the small-scale turbulence effect on algae growth is more related to the methods of turbulent generation and the type of algae species selected.

Table 5-8. Comparison between the turbulence dissipation rates reported in the literature and the present studies

Reference	Size (μm)	Setup	ε (m^2/s^3)	η (μm)	Algae growth
Thomas and Gibson [10]	30-35	Couette cylinder	1.8×10^{-5}	487	Decrease
Hondzo and Lyn [14]	10-30	Oscillating grid	1.37×10^{-4}	293	Decrease
Sullivan and Swift [15]	30	Oscillating rod	10^{-4}	317	Increase
Sullivan et al. [16]	30	Oscillating rod	10^{-3}	178	Decrease
Warnaars and Hondzo [17]	10	Reactor	10^{-7}	1784	Increase
Voleti Thesis - Tracer particles, no algae	10	Raceway with delta wing	1.2×10^{-3}	207	–
Voleti Thesis - Tracer particles, no algae	10	Raceway without delta wing	5×10^{-4}	227	–

CHAPTER 6

CONCLUSIONS AND RECOMMENDATIONS

An extensive literature review was performed to show the effect of small-scale turbulence on algae growth. The literature review determined that no experimental work had been done previously on the quantification of vertical mixing, turbulence dissipation rates and scales in the algal raceway ponds. Experiments were designed and conducted along the entire length of the open channel raceway to study mixing characteristics with and without delta wing. The main conclusions of this research are as follows:

- All the velocity measurements were performed using an ADV tool. The expanded uncertainty of the mean velocities measured by ADV was within the range of 2 to 5%. A comparison was made between ADV and PIV tools to know the measurement accuracy of data collected in the raceway. The mean and RMS velocities measured by the two techniques were within 4% and 9% respectively.

- The delta wing in the raceway has shown a great influence of vertical mixing compared to the normal raceway without delta wing. This was shown by the planar velocity vector fields and the maximum vertical velocities measured for both cases.

- The vertical mixing index of the raceway with delta wing was significantly high compared to the raceway without delta wing. The longitudinal streamwise vortices generated by the delta wings were sustained for a distance of around 3 m downstream of the delta wing. Since the conditions were normal after 3 m downstream of the delta wing, the results indicate that a series of delta wings positioned at approximately 3 m

intervals would be sufficient to promote the notable mixing and turbulence conditions.

- The turbulence dissipation rates were estimated for the raceway with and without delta wing. The averaged turbulence dissipation rates are higher compared to the published literature. Care should be taken specifically in the selection of algae cells for cultivation in the algae raceway.

- Delta wings were economically identified as a viable means of enhancing vertical mixing in the open channel raceway. The use of delta wings appears to be an effective and inexpensive way to move the algae cells between the surface and bottom of algal raceway pond thereby increasing light utilization efficiency.

- It was suggested that one delta wing in the open channel was not sufficient to increase vertical mixing of the outdoor raceway. An array of delta wings will be necessary in the raceway to satisfy the desired mixing conditions. To account for the impact of power consumption by the paddle wheel, the water circulation velocity should be lowered with the addition of delta wings.

Important parameters of the delta wing vortex formations include channel width, water depth, delta wing shape, velocity, and angle of attack. There is more scope to test these parameters for the optimization of delta wing in future. The raceway with and without delta wings should be tested with various algae strains for productivity. If mixing does have an influence on the algal productivity, then it would be an important factor to consider when algal production systems are designed or managed.

REFERENCES

[1]   Chisti, Y., 2008, "Biodesel from Microalgae Beats Bioethanol," Trends Biotechnol., 26(3), pp. 126-131.

[2]   Persoone, G., Morales, J., Verlet, H., and DePauw, N., 1980, "Air-lift Pumps and the Effect of Mixing on Algal Growth," Algae Biomass, G. Shelef, and Soeder, C. J., ed., Elsevier/North-Holland Biomedical Press, Amsterdam, The Netherlands, pp. 505-522.

[3]   Ketheesan, B., and Nirmalakhandan, N., 2011, "Development of a New Airlift-driven Raceway Reactor for Algal Cultivation," Appl. Energ., 88(10), pp. 3370-3376.

[4]   Sheehan, J., Dunahay, T.G., Benemann, J.R., Roessler, P.G., and Weissman, J.C., 1998, "A Look Back at the U.S. Department of Energy's Aquatic Species Program: Biodiesel from Algae," Technical Report No. NREL/TP-580-24190, National Renewable Energy Laboratory (NREL), Golden, Colorado, USA.

[5]   Weissman, J. C., and Goebel, R.P., 1985, "Design and Analysis of Microalgal Open Pond Systems for the Purpose of Producing Fuels," Technical Report No. SERI/STR-231-2840, Microbial Products, Inc., Fairfield, California, USA.

[6]   Weissman, J. C., Tillet, D.M., and Goebel, R.P., 1989, "Design and Optimization of an Outdoor Microalgae Test Facility," Final Technical Report No. SERI/STR-232-3569, Microbial Products, Inc., Vacafille, California, USA.

[7]   Laws, E. A., Terry, K. L., Wickman, J., and Chalup, M. S., 1983, "A Simple Algal Production System Designed to Utilize the Flashing Light Effect," Biotechnol. Bioengin., 25(10), pp. 2319-2335.

[8]   Grobbelaar, J. U., 1991, "The Influence of Light/Dark Cycles in Mixed Algal Cultures on their Productivity," Bioresource Technol., 38(2-3), pp. 189-194.

[9]   Ogbonna, J. C., Yada, H., and Tanaka, H., 1995, "Effect of Cell Movement by Random Mixing between the Surface and Bottom of Photobioreactors on Algal Productivity," J. Ferment. and Bioengin., 79(2), pp. 152-157.

[10]   Thomas, W. H., and Gibson, C.H., 1990, "Effects of Small-Scale Turbulence on Microalgae," J. Appl. Phycol., 2, pp. 71-77.

[11] Al-Homoud, A., and Honzdo, M., 2007, "Energy Dissipation Estimates in Oscillating Grid Setup: LDV and PIV Measurements," Environ. Fluid Mech., 7(2), pp. 143-158.

[12] Berdalet, E., and Estrada, M., 2006, "Effects of Small-Scale Turbulence on the Physiological Functioning of Marine Microalgae," Algal Cultures, Analogues of Blooms and Applications, D. V. Subba Rao, ed., Science Publishers, Inc., Enfield, USA, pp. 459-500.

[13] Berdalet, E., Peters, F., Koumandou, V.L., Roldan, C., Guadayol, O., and Estrada, M., 2007, "Species-Specific Physiological Response of Dinoflagellates to Quantified Small-Scale Turbulence," J. Phycol., 43(5), pp. 965-977.

[14] Hondzo, M., and Lyn, D., 1999, "Quantified Small-Scale Turbulence Inhibits the Growth of a Green Alga," Freshwater Biol., 41(1), pp. 51-61.

[15] Sullivan, J. M., and Swift, E., 2003, "Effects of Small-Scale Turbulence on Net Growth Rate and Size of Ten Species of Marine Dinoflagellates," J. Phycol., 39(1), pp. 83-94.

[16] Sullivan, J. M., Swift, E., Donaghay, P.L., and Rines, J.E.B., 2003, "Small-Scale Turbulence Affects the Division Rate and Morphology of Two Red-tide Dinoflagellates," Harmful Algae, 2(3), pp. 183-199.

[17] Warnaars, T. A., and Hondzo, M., 2006, "Small-Scale Fluid Motion Mediates Growth and Nutrient Uptake of *Selenastrum Capricornutum*," Freshwater Biol., 51(6), pp. 999-1015.

[18] Marshall, J. S., and Huang, Y., 2010, "Simulation of Light-limited Algae Growth in Homogenous Turbulence," Chem. Eng. Sci., 65(12), pp. 3865-3875.

[19] Richmond, A., and Vonshak, A., 1978, "Spirulina Culture in Israel," Arch. Hydrobiol., 11, pp. 274-280.

[20] Weissman, J. C., Goebel, R.P., and Benemann, J.R., 1988, "Photobioreactor Design: Mixing, Carbon Utilization, and Oxygen Accumulation," Biotechnol. and Bioengin., 31, pp. 336-344.

[21] Cheng, E. D. H., and Dugan, G. L., 1995, "Low-Energy Mixing in Algal Culture Raceways," J. Energ. Eng., 121(3), pp. 100-107.

[22] SonTek, 2001, "SonTek ADVField/Hydra Acoustic Doppler Velocimeter (Field) Technical Documentation," SonTek, San Diego, USA.

[23]   SonTek - a Xylem brand, www.sontek.com/microadv.php.

[24]   Helmi, A. M., and El-Gamanl, M.H., 2011, "Experimental and Numerical Investigations of Flow Through Free Double Baffle Gates," Water SA, 37(2), pp. 245-254.

[25]   Muste, M., Yu, K., Pratt, T., and Abraham, D., 2004, "Practical Aspects of ADCP Data Use for Quantification of Mean River Flow Characteristics; Part II: Fixed-vessel Measurements," Flow Meas. Instrum., 15(1), pp. 17-28.

[26]   Wahl, T. L., 2000, "Analyzing ADV Data Using WinADV," Proc. Joint Conference on Water Resources Engineering and Water Resources Planning & Management, ASCE, Minneapolis, Minnesota, USA, pp. 1-10.

[27]   Goring, D. G., and Nikora, V.I., 2002, "Despiking Acoustic Doppler Velocimeter Data," J. Hydraul. Eng., 128(1), pp. 117-126.

[28]   Wahl, T. L., 2002, "Discussion of "Despiking Acoustic Doppler Velocimeter Data" by Derek G. Goring and Vladimir I. Nikora," J. Hydraul. Eng., 128(1), pp. 117-126.

[29]   Meile, T., Cesare, D.G., Blanckaert, K., and Schleiss, A.J., 2008, "Improvement of Acoustic Doppler Velocimetry in Steady and Unsteady Turbulent Open-channel flows by Means of Seeding with Hydrogen Bubbles," Flow Meas. and Instrum., 19(3), pp. 215-221.

[30]   Coleman, H. W., and Steele, W.G., 2009, Experimentation, Validation, and Uncertainty Analysis for Engineers, John Wiley & Sons, New Jersey, Chap. 3-5.

[31]   Rusello, P. J., and Cowen, E.A., 2011, "Turbulent Dissipation Estimates from Pulse Coherent Doppler Instruments," Proc. 10th Current, Waves and Turbulence Measurements, IEEE/OES, Monterey, California, USA, pp. 167-172.

[32]   Ogston, A. S., Sternberg, C.R., and Asher, W.E., 1995, "Estimation of Turbulence-Dissipation Rates and Gas-Transfer Velocities in a Surf Pool: Analysis of the Results from WABEX-93," Final Technical Report No. N00014-90-J-1189, University of Washington, Seattle.

[33]   Petersen, J. E., Kemp, W.M., Kennedy, V.S., Dennison, W.C., and Kangas, P., 2010, "Designing Experimental Ecosystem Studies," Enclosed Experimental Ecosystems and Scale, Springer US, New York, pp. 43-131.

[34]   Griffith, G. P., Vennell, R., and Williams, M.J.M., 2010, "An Algal Photoprotection Index and Vertical Mixing in the Southern Ocean," J. Plankton Res., 32(4), pp. 515-527.

[35]   White, F. M., 2010, "Flow Past Immersed Bodies," Fluid Mechanics, 7, ed., McGraw Hill, New York, Chap. 7.

APPENDICES

Appendix A

RACEWAY ENERGY MODEL

A theoretical raceway energy model was developed for the experimental raceway using MathCAD and the results are presented in this appendix. This model includes the drag losses, frictional head losses and kinetic head losses associated with the delta wing, straight channel and bends respectively. The energy model was developed to operate the paddlewheel-driven raceway at different velocities, depths, roughness factors, and paddle wheel drive system efficiencies.

The drag of the delta wing (equilateral triangle) in the experimental raceway was unknown and assumed as 1.6 (Re $\geq 10^4$) [35]. The calculated paddle wheel drive system efficiency for the experimental raceway was only 5% due to the part-load efficiencies of the motor and gear reducer. However, the efficiency varies between raceway to raceway in the field applications. A 50% paddle wheel drive system efficiency was assumed for this general analysis. Initially, power consumed by the raceway with delta wing was compared with the normal raceway. The raceway with delta wing was only considered later to observe the factors that influence power requirements. The energy consumption or intake plays an important role in the algal production systems.

RACEWAY ENERGY MODEL - THEORETICAL APPROACH

Hydraulic power calculations:

Manning's roughness coefficient

$$n := 0.01 \frac{s}{m^{\frac{1}{3}}}$$

Kinetic loss coefficient for 180^0 bends

$$K := 2$$

Gravitational acceleration

$$g = 9.807 \frac{m}{s^2}$$

Density of the water

$$\rho := 998.2 \frac{kg}{m^3}$$

Water depth in the raceway

$$d := 0.2032m$$

Width of the open channel

$$b := 0.4413m$$

Hydraulic radius of the open channel

$$R := \frac{d \cdot b}{b + 2 \cdot d}$$

Total straight channel length of the open channel

$$L := 10.3632m$$

Frictional head loss along the length of the raceway

$$h_L(U) := \frac{U^2 \cdot n^2 \cdot L}{R^{\frac{4}{3}}}$$

Kinetic head loss due to the 180^0 bends

$$h_b(U) := \frac{K \cdot U^2}{2 \cdot g}$$

Total head loss in the raceway

$$h(U) := h_L(U) + 2 \cdot h_b(U)$$

Volume flow rate of liquid in channel

$$Q(U) := b \cdot d \cdot U$$

Paddle wheel drive system efficiency

$$\eta := 0.5 \qquad \text{(Vary from raceway to raceway - assuming 50\% efficient)}$$

Hydraulic power required for maintain flow in the raceway

$$P_H(U) := \frac{\rho \cdot g \cdot h(U) \cdot Q(U)}{\eta}$$

Delta wing drag power calculations:

Length of the delta wing (equilateral triangle)

$$a := 0.3683 \text{m}$$

Reference area for the delta wing (frontal area)

$$A := \frac{\sqrt{3}}{4} \cdot a^2$$

Coefficient of drag based on frontal area for an equilateral triangle

$$C_D := 1.6 \qquad \text{(F.M. White, Chapter 7, Flow past immersed bodies)}$$

Number of delta wings in the raceway

$$N_d := 1$$

Power expended by delta wing due to drag

$$P_D(U) := N_d \cdot \left(\frac{1}{2} \cdot C_D \rho \cdot A \cdot U^3 \right)$$

Total power required for operating the raceway without delta wing

$$P_R(U) := P_H(U)$$

Total power required for operating the raceway with delta wing

$$P_{RD}(U) := P_H(U) + P_D(U)$$
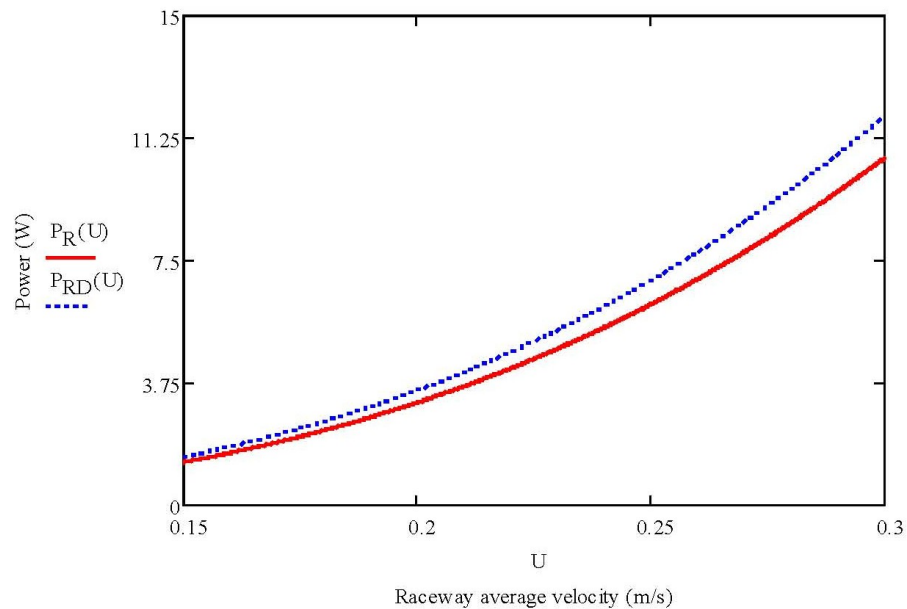
$$P_R\left(0.2\frac{m}{s}\right) = 3.155\,W \qquad P_R\left(0.25\frac{m}{s}\right) = 6.163\,W \qquad P_R\left(0.30\frac{m}{s}\right) = 10.649\,W$$

$$P_{RD}\left(0.2\frac{m}{s}\right) = 3.531\,W \qquad P_{RD}\left(0.25\frac{m}{s}\right) = 6.896\,W \qquad P_{RD}\left(0.30\frac{m}{s}\right) = 11.915\,W$$

Figure A-1.   Total calculated power versus average velocity in the raceway

It can be seen from Figure A-1 that the power varies as the cube of the flow velocity. Due to drag of the delta wing, the raceway with delta wing was consuming 12% more power than the normal raceway. However, the power can be lowered by decreasing the water circulation velocity in the desire vertical mixing scenario.
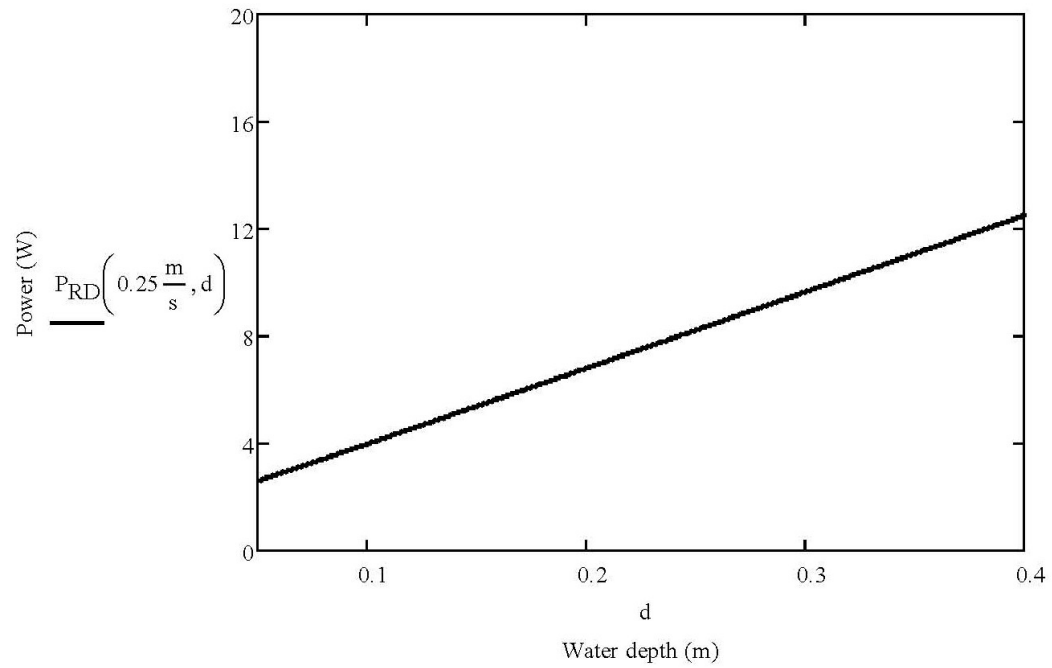
$$P_{RD}\left(0.25\frac{m}{s},0.2m\right) = 6.805\,W \qquad P_{RD}\left(0.25\frac{m}{s},0.3m\right) = 9.649\,W$$

$$P_{RD}\left(0.25\frac{m}{s},0.4m\right) = 12.499\,W$$

Figure A-2.   Total calculated power versus culture depth of the raceway

It was observed from Figure A-2 that the power consumption of the raceway increases linearly as the culture depth increases.
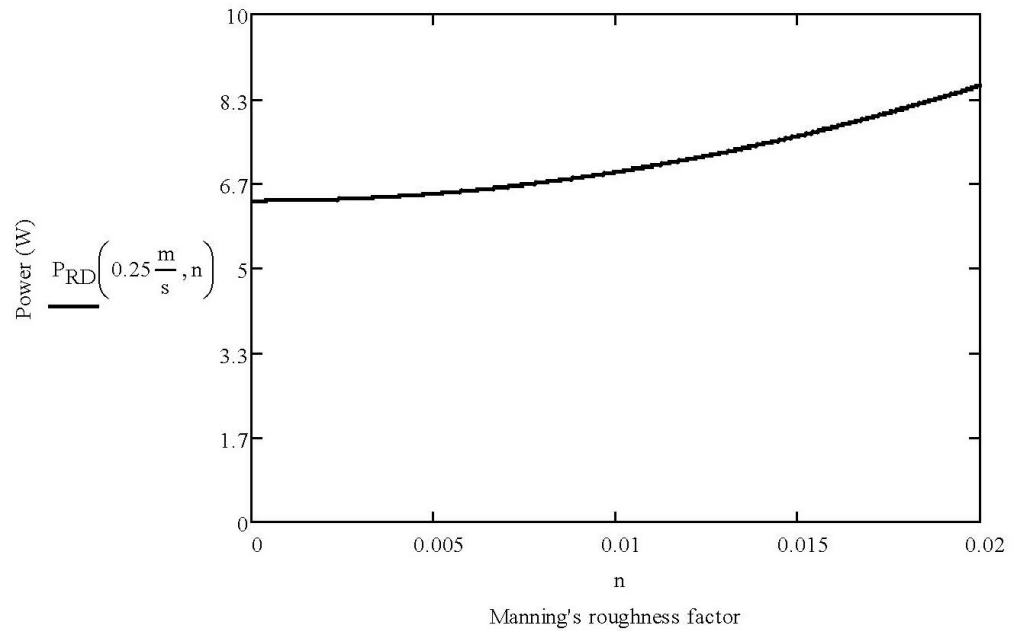
$$P_{RD}\left(0.25\frac{m}{s},0.01\frac{s}{m^{\frac{1}{3}}}\right) = 6.896\,W \qquad P_{RD}\left(0.25\frac{m}{s},0.015\frac{s}{m^{\frac{1}{3}}}\right) = 7.606\,W$$

$$P_{RD}\left(0.25\frac{m}{s},0.02\frac{s}{m^{\frac{1}{3}}}\right) = 8.6\,W$$

Figure A-3.   Total calculated power versus roughness factor

The effect of roughness factor on the raceway power consumption is shown in Figure A-3. The roughness factors shown in the plot are common for the algae raceway ponds. The head loss in the open channel depends on the roughness factor and this leads to an increase in power consumption.
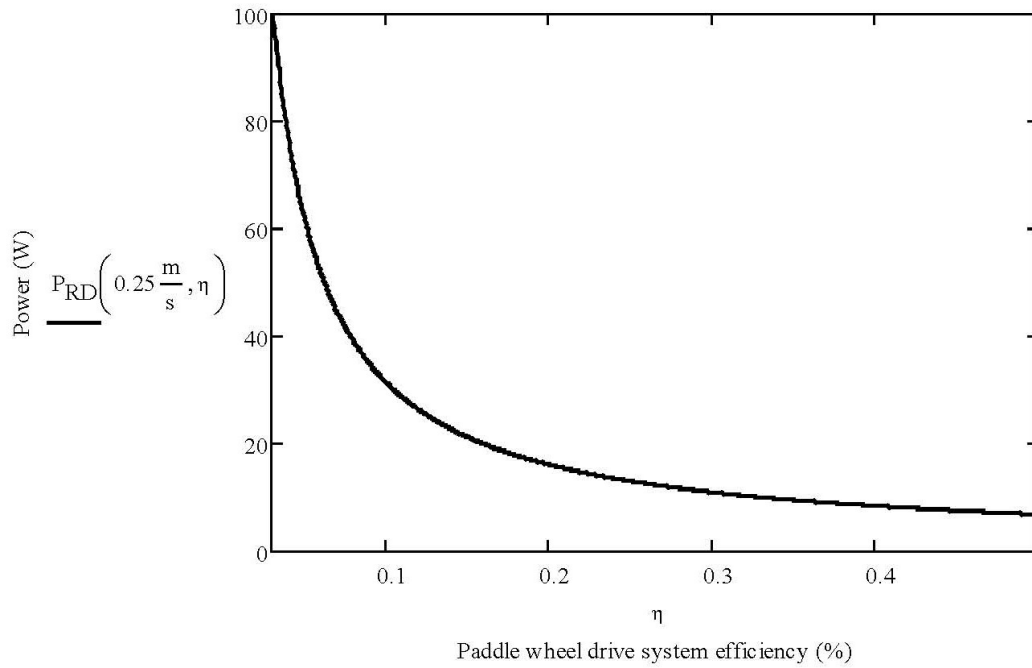
$$P_{RD}\left(0.25\frac{m}{s},0.1\right) = 31.546\,W \qquad P_{RD}\left(0.25\frac{m}{s},0.2\right) = 16.139\,W$$

$$P_{RD}\left(0.25\frac{m}{s},0.3\right) = 11.004\,W \qquad P_{RD}\left(0.25\frac{m}{s},0.4\right) = 8.436\,W$$

Figure A-4. Total calculated power versus paddle wheel drive system efficiency

The paddle wheel drive system efficiency plays an important role in driving the fluid in raceway and the effect can be seen in Figure A-4. Power consumption of the raceway exponentially decreases as the paddle wheel drive system efficiency increases.

Appendix B

ADV-PIV CONTOUR PLOTS

The contour plots of the mean velocity, turbulence, and other quantities measured using ADV and PIV tools at the same flow conditions with and without delta wing in the raceway are shown in this appendix.
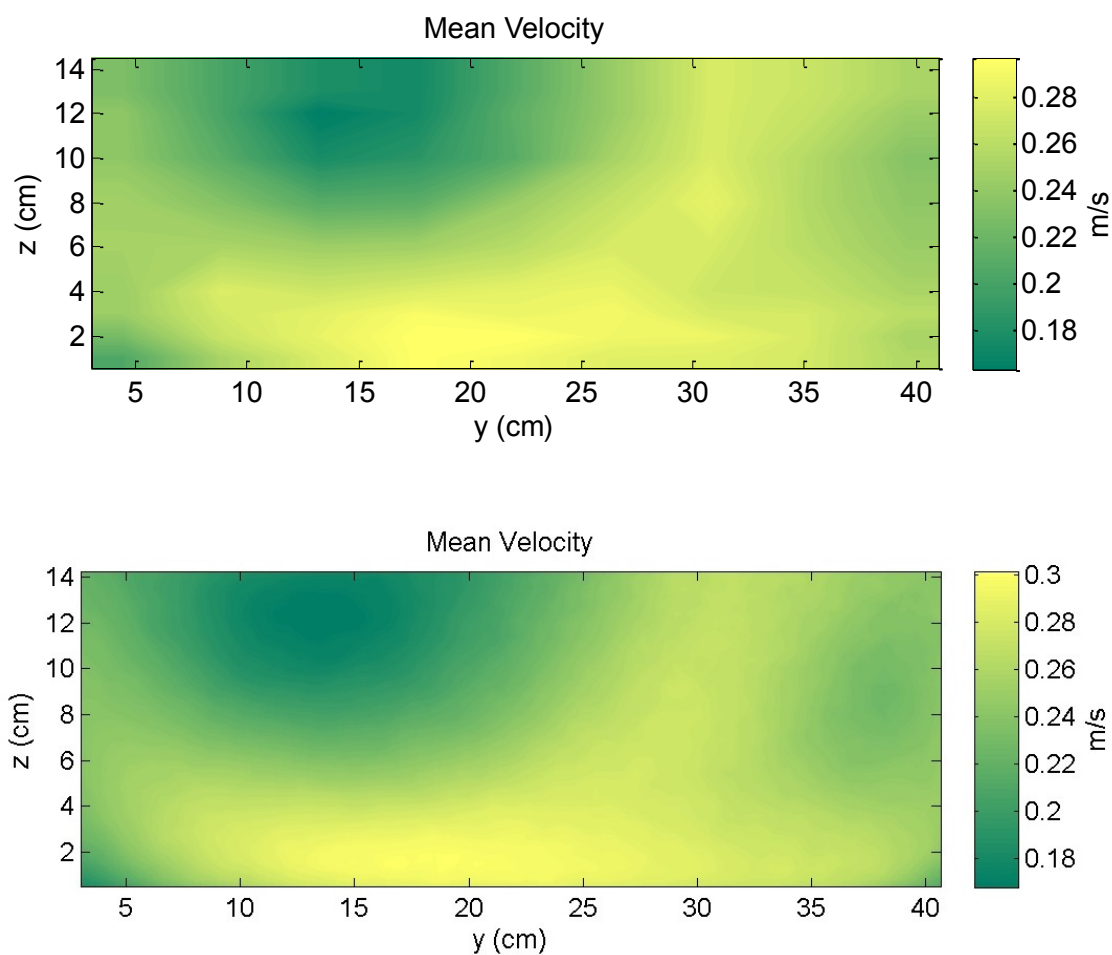
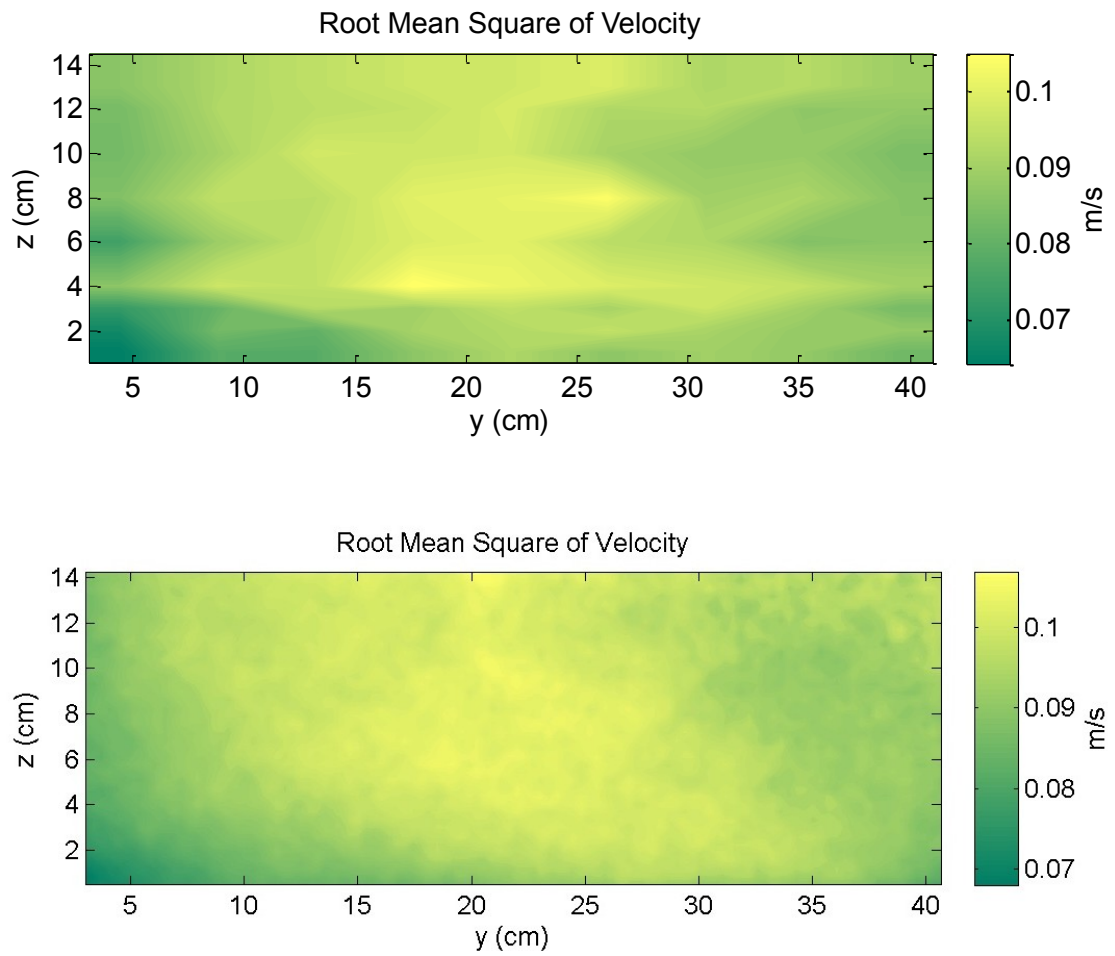

Figure B-1.   Contour plots of the mean velocity measured using ADV (top) and PIV (bottom) with delta wing
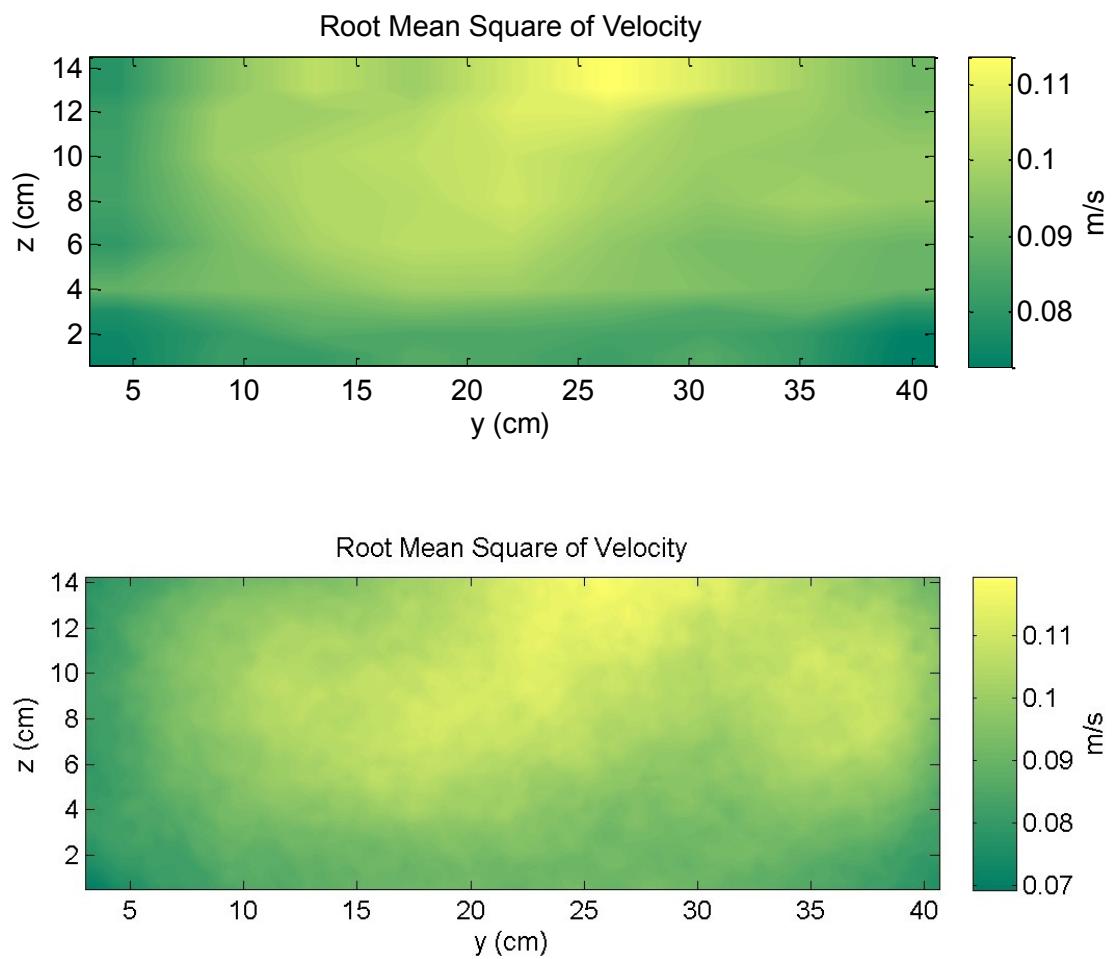
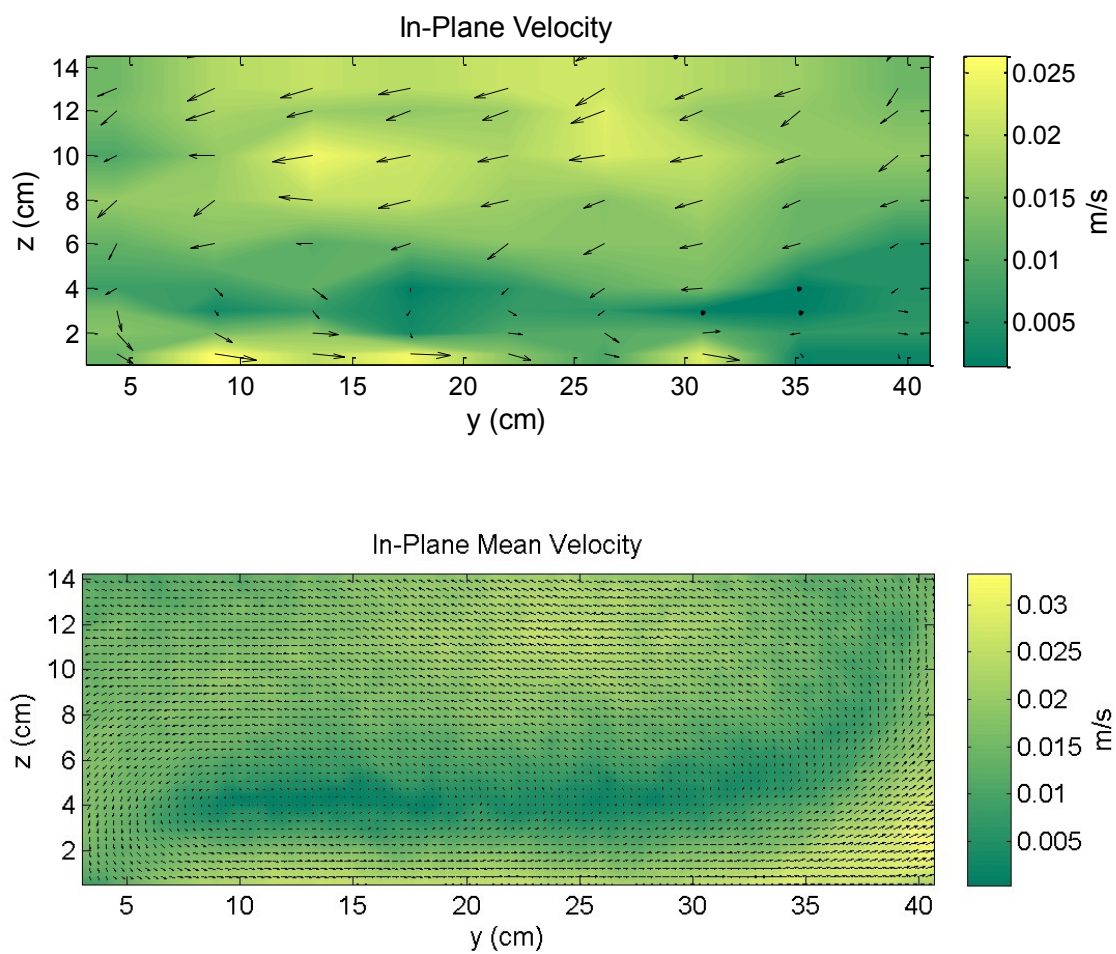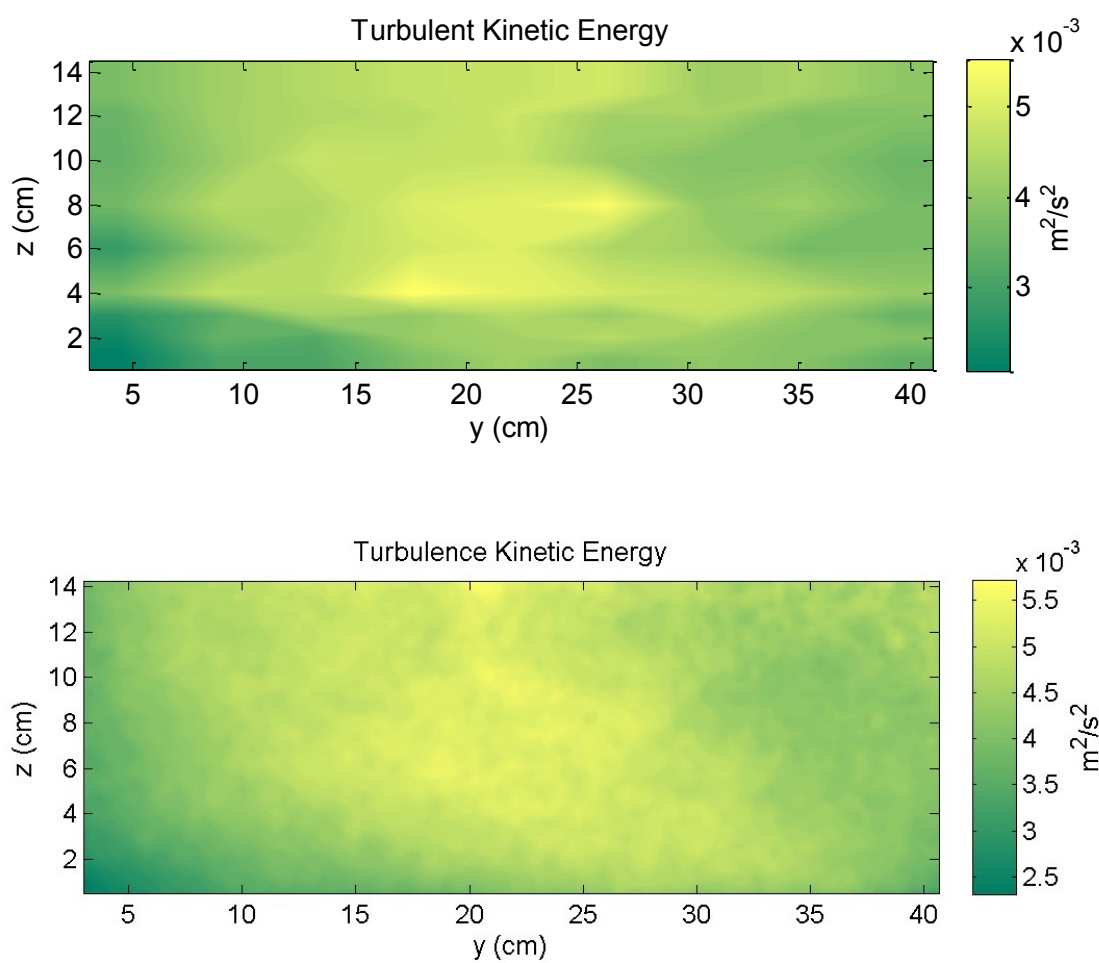Figure B-2.   Contour plots of the root mean square velocity measured using ADV (top) and PIV (bottom) with delta wing
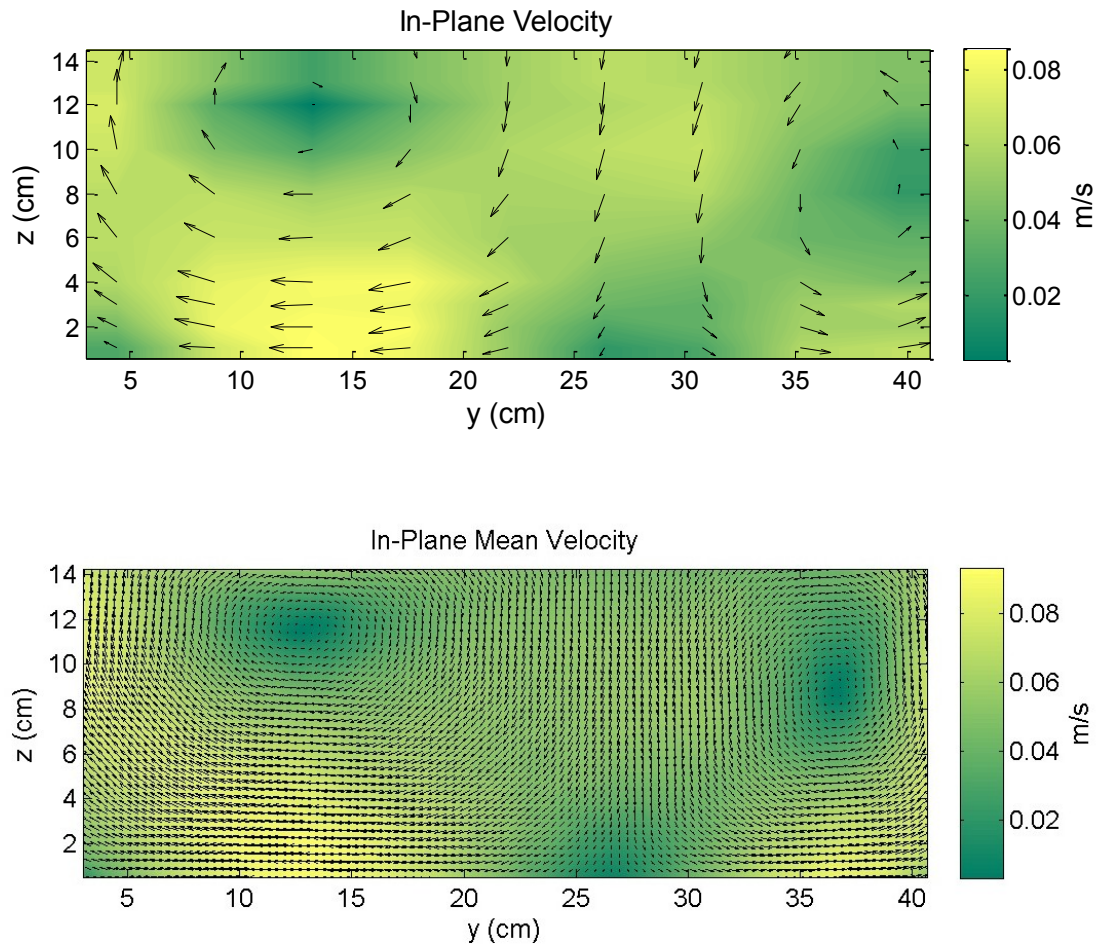
Figure B-3. Contour plots of the in-plane velocity measured using ADV (top) and PIV (bottom) with delta wing
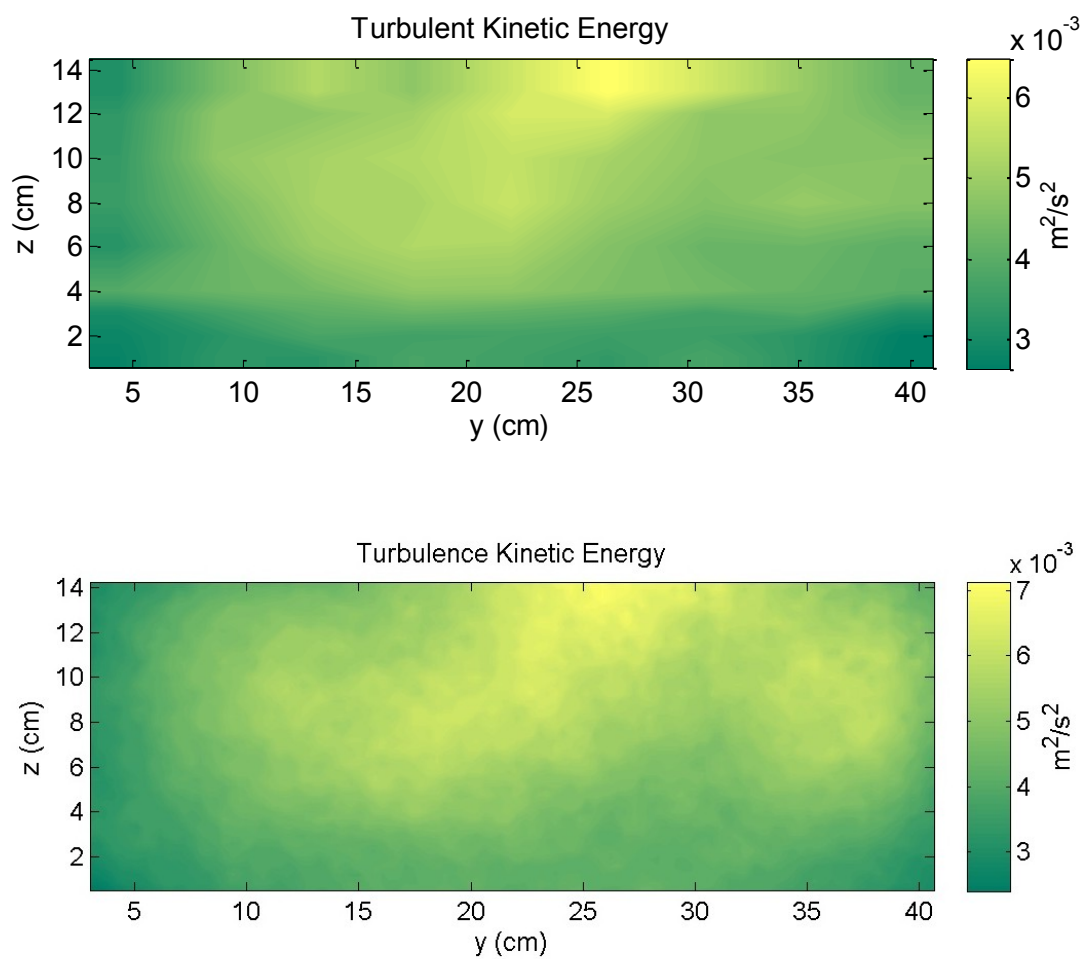
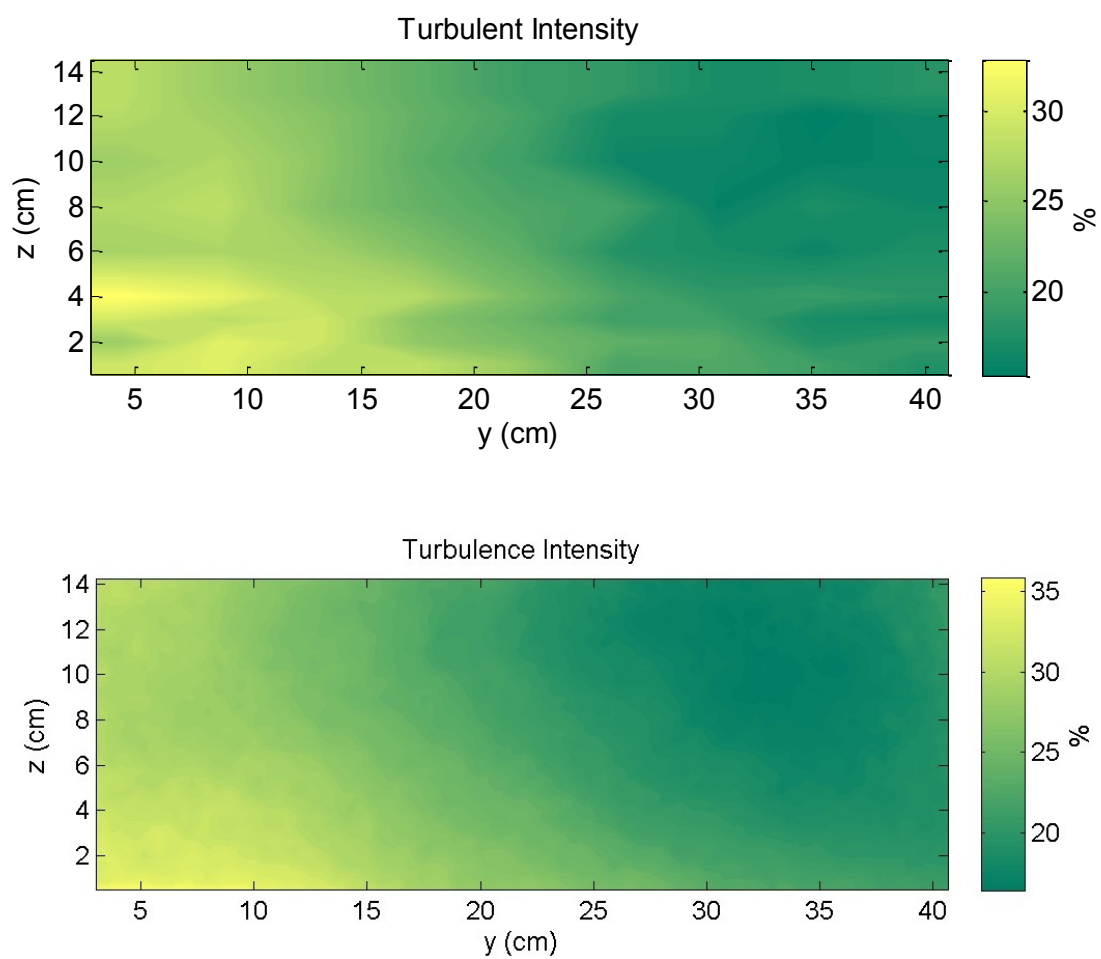Figure B-4.   Contour plots of the turbulence kinetic energy measured using ADV (top) and PIV (bottom) with delta wing
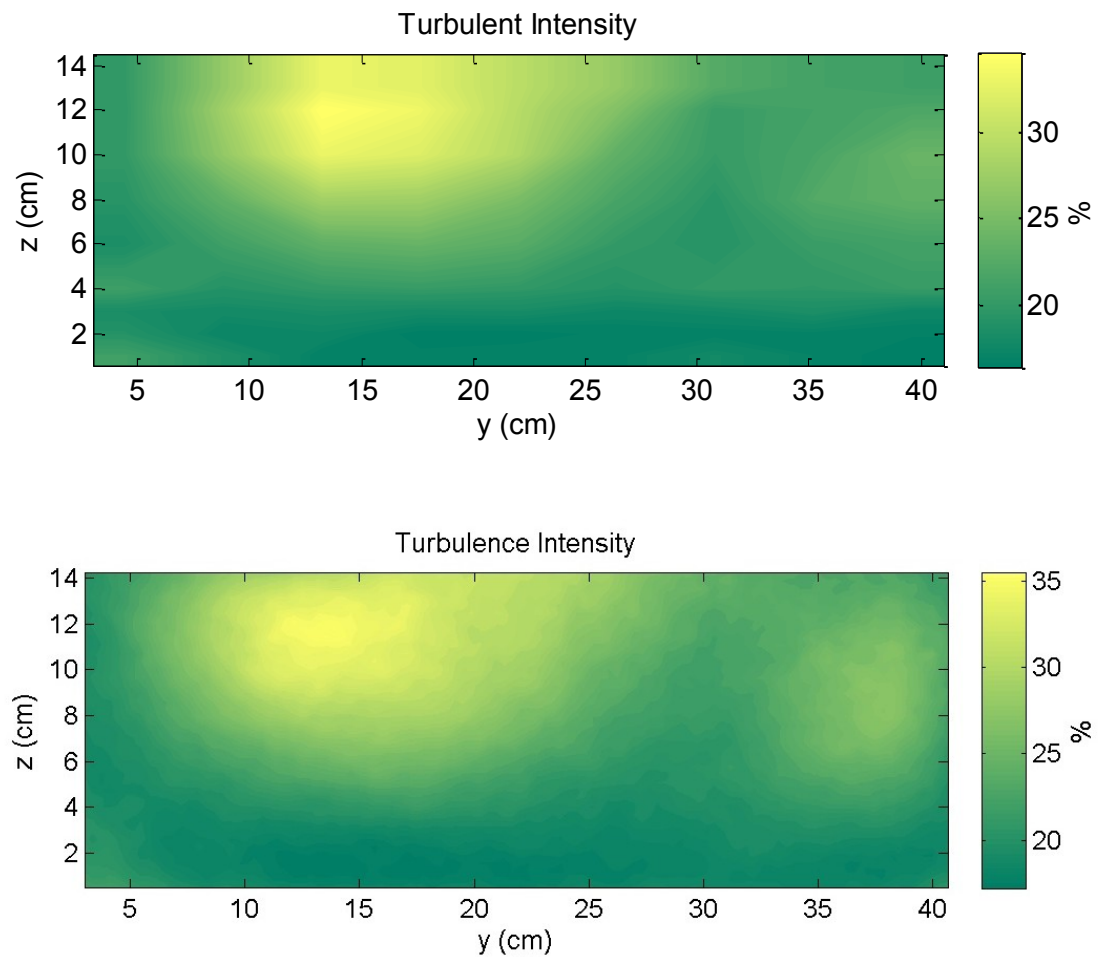
Figure B-5.   Contour plots of the turbulence intensity measured using ADV (top) and PIV (bottom) with delta wing
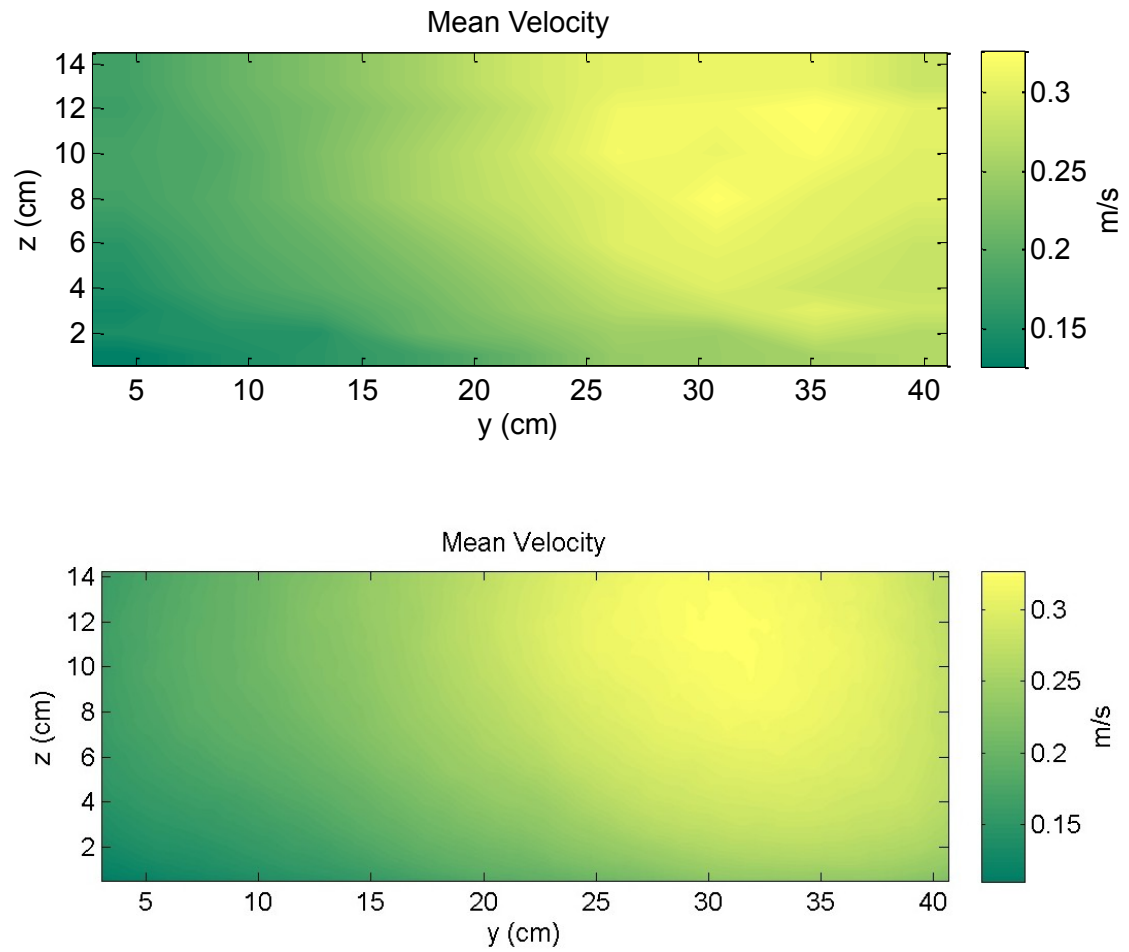
Figure B-6. Contour plots of the mean velocity measured using ADV (top) and PIV (bottom) without delta wing

Figure B-7.   Contour plots of the root mean square velocity measured using ADV (top) and PIV (bottom) without delta wing

Figure B-8.   Contour plots of the in-pane velocity measured using ADV (top) and PIV (bottom) without delta wing

Figure B-9.   Contour plots of the turbulence kinetic energy measured using ADV (top) and PIV (bottom) without delta wing

Figure B-10.   Contour plots of the turbulence intensity measured using ADV (top) and PIV (bottom) without delta wing

Appendix C

COPYRIGHT PERMISSION

Permissions to use Figure 3-1, Figure 4-5, Figure 4-6, and Figure 4-15 in this thesis were requested and provided in this appendix.

SPRINGER LICENSE
TERMS AND CONDITIONS

Apr 10, 2012

This is a License Agreement between Ram Sudheer Voleti ("You") and Springer ("Springer") provided by Copyright Clearance Center ("CCC"). The license consists of your order details, the terms and conditions provided by Springer, and the payment terms and conditions.

All payments must be made in full to CCC. For payment instructions, please see information listed at the bottom of this form.

License Number	2885201316456
License date	Apr 10, 2012
Licensed content publisher	Springer
Licensed content publication	Springer eBook
Licensed content title	Designing Experimental Ecosystem Studies
Licensed content author	J.E. Petersen
Licensed content date	Jan 23, 2010
Type of Use	Thesis/Dissertation
Portion	Figures
Author of this Springer article	No
Order reference number	
Title of your thesis / dissertation	Experimental Studies of Vertical Mixing in an Open Channel Raceway for Algae Production
Expected completion date	May 2012
Estimated size(pages)	120
Total	0.00 USD

Terms and Conditions

Introduction
The publisher for this copyrighted material is Springer Science + Business Media. By clicking "accept" in connection with completing this licensing transaction, you agree that the following terms and conditions apply to this transaction (along with the Billing and Payment terms and conditions established by Copyright Clearance Center, Inc. ("CCC"), at the time that you opened your Rightslink account and that are available at any time at http://myaccount.copyright.com).

Limited License
With reference to your request to reprint in your thesis material on which Springer Science and Business Media control the copyright, permission is granted, free of charge, for the use indicated in your enquiry.

Licenses are for one-time use only with a maximum distribution equal to the number that you

April 18, 2012

Ram Sudheer Voleti
944N, 700E, #2
Logan, UT
Phone: (435) 213-6121
E-mail: ramsudheer.voleti@gmail.com

Dear Joel Edelman:

I am in the process of preparing my thesis in the Department of Mechanical and Aerospace Engineering at Utah State University. I hope to complete in the Spring of 2012.

I am requesting your permission to include the attached material as shown. I will include acknowledgments and/or appropriate citations to the "SonTek – a xylem brand., MicroADV / ADV documentation" work as shown and copyright and reprint rights information in a special appendix. The bibliographical citation will appear at the end of the manuscript as shown. Please advise me of any changes you require.

Please indicate your approval of this request by signing in the space provided, attaching any other form or instruction necessary to confirm permission. If you charge a reprint fee for use of your material, please indicate that as well. If you have any questions, please call me at the number above.

I hope you will be able to reply immediately. If you are not the copyright holder, please forward my request to the appropriate person or institution.

Thank you for your cooperation,

Ram Sudheer Voleti

_____

I hereby give permission to Ram Sudheer Voleti to reprint the following material in his thesis.

SonTek, 2001, "SonTek ADVField/Hydra Acoustic Doppler Velocimeter (Field) Technical Documentation," SonTek, San Diego, USA.

SonTek – a xylem brand. www.sontek.com/microadv.php.

Signature: **Christina Iarossi**

Date: _____

Fee _____

Digitally signed by Christina Iarossi
DN: cn=Christina Iarossi, o=SonTek/
YSI, ou=Sales and Marketing,
email=ciarossi@sontek.com, c=US
Date: 2012.04.19 09:35:50 -07'00'